RELATIONSHIPS BETWEEN MATERIAL PROPERTIES AND MICROSTRUCTURE-MECHANICAL ATTRIBUTES OF EXTRUDED BIOPOLYMERIC FOAMS

by

RODERICK NAZARIO MALCABA AGBISIT

B.S., University of the Philippines Los Baños, 1992
M.S., Kansas State University, 1999

AN ABSTRACT OF A DISSERTATION

submitted in partial fulfillment of the requirements for the degree

DOCTOR OF PHILOSOPHY

Department Of Grain Science and Industry
College of Agriculture

KANSAS STATE UNIVERSITY
Manhattan, Kansas

2007

ABSTRACT

Material formulation and extrusion process parameters affect the foaming process in terms of expansion, cell nucleation, and resultant foam microstructure, which, in turn, control mechanical properties. This study utilizes non-invasive x-ray microtomography (XMT), in combination with mechanical testing and novel phase transition analysis techniques, to understand these complex relationships. The first part of this study provided significant insight into the deformation mechanism of extruded cornstarch foams. Microstructure features, including average cell diameter (2.07-6.32 mm), wall thickness (0.13-0.25 mm) and number density (18-146 cm^{-3}), were measured. Microstructure had moderate to high correlations ($|r|$ = 0.48 - 0.81) with mechanical properties, including compression modulus (2.2-7.8 MPa), crushing stress (42-240 kPa), number of spatial ruptures (2.6-3.6 mm^{-1}), average crushing force (22-67 N) and crispness work (6.4-22 N-mm). The second part of this study investigated the effects of formulation, using model systems comprising of cornstarch, whey protein isolate (WPI) and sucrose, on phase transition behavior, and physical, microstructure and mechanical properties of extrudates. Increase in WPI led to greater specific mechanical energy (SME) and higher extrudate expansion. WPI had a foaming effect, which increased the cell number density accompanied by decrease in average cell diameter. Increase in sucrose led to lesser SME and lower expansion of extrudates. Contrary to expectations, phase transition properties (softening temperature, T_s, and flow temperature, T_f) were not good indicators of SME. The concluding part of this study investigated glass transition and rheological properties of cornstarch at different moisture contents (18-30% wet basis) using differential scanning calorimetry (DSC), phase transition analysis (PTA) and on-line slit-die rheometry. Glass transition temperature (T_g) (31.20 - 57.55 °C) of extrudates decreased as moisture content increased. T_s (42.5 - 85.6°C) and T_f (109 - 136°C) also followed the same trend, and exhibited high correlations (r = 0.89 and 0.86, respectively) with T_g. These parameters were good estimates of phase transition properties of the complex and heterogeneous formulations. As expected, on-line rheological parameters, including flow behavior index, n (0.0438 - 0.304) and consistency coefficient, K (10,500 -

45,700 Pa-s^{n-1}), were functions of in-barrel moisture, and were related to phase transition properties using WLF kinetics.

RELATIONSHIPS BETWEEN MATERIAL PROPERTIES AND MICROSTRUCTURE-MECHANICAL ATTRIBUTES OF EXTRUDED BIOPOLYMERIC FOAMS

by

RODERICK NAZARIO MALCABA AGBISIT

B.S., University of the Philippines Los Baños, 1992
M.S., Kansas State University, 1999

A DISSERTATION

submitted in partial fulfillment of the requirements for the degree

DOCTOR OF PHILOSOPHY

Department of Grain Science and Industry
College of Agriculture

KANSAS STATE UNIVERSITY
Manhattan, Kansas

2007

Approved by:

Major Professor
Dr. Sajid H. Alavi

Copyright

ABSTRACT

Material formulation and extrusion process parameters affect the foaming process in terms of expansion, cell nucleation, and resultant foam microstructure, which, in turn, control mechanical properties. This study utilizes non-invasive x-ray microtomography (XMT), in combination with mechanical testing and novel phase transition analysis techniques, to understand these complex relationships. The first part of this study provided significant insight into the deformation mechanism of extruded cornstarch foams. Microstructure features, including average cell diameter (2.07-6.32 mm), wall thickness (0.13-0.25 mm) and number density (18-146 cm^{-3}), were measured. Microstructure had moderate to high correlations ($|r|$ = 0.48 - 0.81) with mechanical properties, including compression modulus (2.2-7.8 MPa), crushing stress (42-240 kPa), number of spatial ruptures (2.6-3.6 mm^{-1}), average crushing force (22-67 N) and crispness work (6.4-22 N-mm). The second part of this study investigated the effects of formulation, using model systems comprising of cornstarch, whey protein isolate (WPI) and sucrose, on phase transition behavior, and physical, microstructure and mechanical properties of extrudates. Increase in WPI led to greater specific mechanical energy (SME) and higher extrudate expansion. WPI had a foaming effect, which increased the cell number density accompanied by decrease in average cell diameter. Increase in sucrose led to lesser SME and lower expansion of extrudates. Contrary to expectations, phase transition properties (softening temperature, T_s, and flow temperature, T_f) were not good indicators of SME. The concluding part of this study investigated glass transition and rheological properties of cornstarch at different moisture contents (18-30% wet basis) using differential scanning calorimetry (DSC), phase transition analysis (PTA) and on-line slit-die rheometry. Glass transition temperature (T_g) (31.20 - 57.55 °C) of extrudates decreased as moisture content increased. T_s (42.5 - 85.6°C) and T_f (109 - 136°C) also followed the same trend, and exhibited high correlations (r = 0.89 and 0.86, respectively) with T_g. These parameters were good estimates of phase transition properties of the complex and heterogeneous formulations. As expected, on-line rheological parameters, including flow behavior index, n (0.0438 - 0.304) and consistency coefficient, K (10,500 -

45,700 Pa-s^{n-1}), were functions of in-barrel moisture, and were related to phase transition properties using WLF kinetics.

Table of Contents

List of Figures

List of Tables

List of Appendices

CHAPTER 1 - OVERVIEW OF THE STUDY

Foams and Foam Formation

Foams are two-phase systems wherein gas cells are enclosed by a liquid (or a solid, in the case of gelation or solidification of the liquid portion) (Weaire and Hutzler 1999). Foams exist as polyhedric or spherical collection of bubbles (Prins 1988). The volume ratio (gas to liquid) in a polyhedric foam is very large so that bubbles deform as they press against each other, creating a 'honeycomb-like' structure (e.g. beer foam). In some instances, the volume ratio is smaller allowing individual bubbles to retain their spherical shape (e.g. ice cream and choco-mousse). Foams are useful in a variety of ways. They are used for (1) producing lighter structures (low density) and saving on material cost, (2) improving insulation properties (low thermal conductivity), (3) preventing fracture propagation, and (4) providing cushioning effect. In foods, they (1) introduce zest and zip to beer, champagne and soft drinks, (2) improve aroma in coffee, (3) create texture in ice cream, (4) provide texture and volume to breads and cakes, and (5) impart crispness or crunchiness to puffed fruits and vegetables, popcorn and other expanded snacks and breakfast cereals. Foaming is induced through the following processes (Prins 1988): (1) agitation of a given amount of liquid in an unlimited amount of air, (2) allowing gas to be generated from the liquid, and (3) incorporating gas into the liquid. The last process (3) is accomplished by using steam or supercritical fluid, and extrusion process is one of the primary means of accomplishing this. In the extrusion process, nucleation of bubbles takes place inside the extruder barrel due to a drastic change in pressure, and results in expansion of the product.

Extrusion is a cooking, forming and puffing technique, whereby a grain-based material is forced, by compression, through a small opening (die) in a continuous fashion. Single or twin screw extrusion is widely used in converting raw biopolymeric materials, through a combination of mixing, shearing, shaping and foaming processes, into a finished or semi-finished product, with a particular shape and/or texture. The combined effect of shear, temperature and pressure inside the extruder barrel make the accompanying thermomechanical processes unique. Such a process is used with relatively dry materials to plasticize food mass, reduce microbial load, denature enzymes, gelatinize starch, polymerize proteins, and also expand and/or texturize the end product into a desirable form. Screw extrusion has proved to be a particularly very attractive

process in the food industry, with the advantages of versatility, high productivity, low cost, energy efficiency and no effluents causing waste problems.

Figure 1.1 shows a simplified schematic of numerous interactions going on during the formation of biopolymeric foams by extrusion. Material (i.e. raw components and component interactions) and process parameters (i.e. screw speed, thermal and mechanical energy input) greatly determine the final properties of an expanded extrudate. Both sets of parameters affect the final expansion, cell growth and cell structure (microstructure). In turn, the resultant microstructure greatly affects the mechanical or texture properties of the foam.

Cereal-based starchy materials are most commonly used to produce expanded biopolymer foams. Starch is the cheapest and most abundant food biopolymer worldwide. It occurs in a variety of botanical sources including potato, wheat and maize and has found diverse applications ranging from breakfast cereals, snacks and thickeners in the food industry to binders for drug delivery systems, and packaging, paper and adhesives in the non-food industry. For certain applications in the food and packaging industries, starch is extruded to achieve desired product mechanical properties. Expansion of starch by extrusion is a complex phenomenon which occurs during high-temperature, low-moisture cooking and is a consequence of several events including starch structural transformations and phase transitions, nucleation, extrudate swell, cell (or bubble) growth, and cell collapse, with cell dynamics dominantly contributing to the expansion phenomenon.

In some cases, foam formation is enhanced to a certain extent through the presence of another biopolymer, protein. Proteins have a significant effect on cell growth by creating discontinuities in the starch-based gas holding matrix or reducing shrinkage after extrusion and before the drying step (Alavi et al. 1999). In the latter effect, the cell walls set before reaching the critical cell size thus reducing cell rupture and preserving the cell structure. During extrusion, protein denaturation occurs causing partial gelation and therefore increased glass transition at the die.

Role of Glass Transition in Foam Formation

In order to understand further the mechanism behind expansion and cell growth in foams, one needs to look at the phase transition properties of the melt. In polymer science, glass transition temperature (T_g) is perhaps the single most significant parameter that helps us

understand the thermal and rheological processes associated with the melt. Physical properties such as specific heat, specific volume, expansion coefficients, and viscoelasticity, change as polymers transition from a "glassy" to "rubbery" state. Application of T_g in food science is critical as food components, such as starch and protein, are biopolymers. T_g is used to analyze the effects of recipes, process and storage conditions on textural attributes of foods. The processing of starch-based foods usually involves heating starch in the presence of water to a temperature above the gelatinization temperature causing a disruption of the starch granule structure. During gelatinization, the semicrystalline polymer structure in native granular starches is gradually transformed into an amorphous state, which is metastable and subject to time-dependent physical change such as recrystallization of amylopectin in starch gels. This phenomenon greatly affects the textural properties of starch based foods. Sufficient heating of a semi-crystalline polymer can induce a phase transformation, from a glassy, solid to a rubbery, amorphous matrix, known as the glass transition. At this state, a large decrease in viscosity and mobilization of the polymer chains occur. In the study of extruded starch-based materials, the phenomenon of T_g has been utilized to characterize the physical changes that occur during processing.

Phase transition analysis techniques are based on the ability to transfer heat to a material and monitor its effects. This class of techniques is known as thermal analysis. Several techniques can be used to measure T_g of biopolymeric materials, including differential scanning calorimetry (DSC), dynamic mechanical thermal analysis (DMTA), on-line viscometry and phase transition analysis (PTA).

The most widely used method to determine T_g is the DSC. Most studies have focused on systems of starch in excess water (Stevens and Elton 1971; Biliaderis et al. 1986; Yost and Hoseney 1986; Slade and Levine 1987, 1991; Marshall and Normand 1991; Liu and Lelievre 1991; Huang et al. 1994; Buera et al. 1998). A few studies have focused on starch/water systems at low moistures (Slade and Levine 1987, 1991; Zeleznak and Hoseney 1987; Liu and Lelievre 1991; Kalichevsky et al. 1992; Perdon et al. 2000).

Other measurements employed to characterize phase transition properties of materials involves examining the melt viscosity itself during extrusion. Viscosity of the melt is an important parameter that characterizes any food extrusion process. Melt viscosity affects the flow of material in the extruder, regulates extrudate properties and influences build-up of

pressure at the melting region (Li *et al.* 2004). Starch gelatinization, in turn, affects melt viscosity. Higher degree of gelatinization produces a more viscous melt. Both barrel temperature (Van Lengerich 1990) and moisture content (Riaz 2000) influence starch gelatinization during extrusion. Melt viscosity in an extruder can be measured on-line using a slit-die viscometer (Bindzus *et al.* 2002 and Li *et al.* 2004). Bindzus *et al.* (2002) used an in-line slit viscometer (rectangular flow channel 60 mm in length) installed between the barrel and die plate. Three measuring transducers were used to measure pressure and temperature of the material in the flow channel of the viscometer. Li *et al.* (2004) used an adapter between slit viscometer and extruder to allow diversion of flow. By adjusting two valves at the adapter, the flow rate at the slit die was varied to achieve different shear rates while maintaining die pressure and resulting SME at constant levels.

Viscosity can be related to phase transition properties of certain polymers (e.g. T_g) through the William-Landel-Ferry (WLF) equation:

$$\ln a_T = \ln \frac{\eta}{\eta_0} = \frac{-17.4(T - T_g)}{51.6 + (T - T_g)} \tag{1.1}$$

For most materials, C_1 and C_2 are given as 17.4 and 51.6, respectively.

In most cases, biopolymer foams are heterogeneous. Recent developments in instrumentation have the ability to overcome challenges in measuring raw material properties for these complex, heterogeneous biopolymers. One such innovation is the phase transition analyzer (PTA). The PTA greatly facilitates analysis of composite mixtures such as protein and starch-containing extrudates to give valuable information about the phase transition properties of the mixture (Strahm and Plattner, 2003). Moreover, the PTA has advantages over previous techniques, like differential scanning calorimetry, including the ability to handle relatively large sample size (~1.5 g). The PTA measures phase transition properties similar to glass transition and melt temperatures such as the softening temperature (T_s) of materials under elevated pressure. Moreover, the PTA determines the temperature required to lower viscosity sufficiently allowing a material to be forced through a small orifice (flow-point temperature, T_f) at pressures similar to those encountered during extrusion processing (~1-10 MPa). The PTA, therefore, has

the potential to help understand the role material properties play in extrusion processing (Strahm 1998; Strahm *et al.* 2000).

X-ray Microtomography and Microstructure

To understand the role of phase transition and rheological properties of biopolymers in controlling the final product quality, characterization of the microstructure is very important. Advances in imaging technology have led to powerful microscopes to probe into foods from atomic to micron range and in many cases, non-intrusively, in real time (video microscopy) and three dimensional (Flannery 1987; Sasov 1987). Studies done by Trater, Alavi and Rizvi (2005) has investigated the use of non-invasive, 3-D X-ray microtomography (XMT) for microstructure characterization, which eliminated the limitations of traditional 2-D and destructive imaging techniques like SEM and optical microscopy. In the study, XMT proved to be efficient in accurately characterizing several microstructural features such as average cell equivalent diameter, wall thickness, and void fraction. Moreover, XMT generated images were more conducive to digital image processing than SEM or light microscope images because of 'razor-thin' depth of focus and sharp contrast between solid and void areas.

Microstructure--Mechanical Relationships

Microstructure of extruded biopolymeric foams controls its texture or mechanical properties. Food foams such as expanded food products are characterized mainly by their crunchiness or crispiness. Shape, size, density of air cells, cell wall thickness, and uniformity of cells formed during extrusion contribute to the perception of extruded-puffed food texture (Barrett and Peleg 1992; Barrett *et al.* 1994a). Texture properties such as breaking or plateau stress have been correlated to mean cell size (Barrett and Peleg 1992), whereas failure strain and Young's modulus have been associated with cell size, cell wall thickness and cell size uniformity (Gao *et al.* 1996; Gao *et al.* 1999). Gibson and Ashby (1997) described the mechanics of linear-elastic deformation of closed-cell foams and the relationship between microstructure characteristics and mechanical properties.

Structure-mechanical studies have used Gibson and Ashby's models to define the compression behavior of puffed extrudates (Hutchinson and Siodlak 1987; Hayter and Smith 1988; Barrett and Peleg 1992; Warburton *et al.* 1992). The 'jaggedness' or 'ruggedness' of the brittle plateau, however, has not been studied extensively nor characterized in quantitative terms

(Barletta and Barbosa-Canovas 1993; Barrett *et al.* 1992; Gregson and Lee 2003). The 'jaggedness' could be associated with the perception of multiple successive rapid fractures, of one or a combination of cells, resulting from forces applied during mastication. The 'jaggedness' has been equated with crispness or crunchiness of brittle foods (Barrett *et al.* 1994b; Barrett and Peleg 1995; Bouvier *et al.* 1997; Luyten et al. 2004). Crispness is a useful descriptor of food texture indicating freshness (e.g., fresh vegetables, fruits, and snacks). Instrumental measurement of crispness involves a simple compression test (Seymour and Hamann 1988; Vickers 1988; Duizer and Campanella 1998; Gao *et al.* 1999; Meullenet and Gross 1999; Meullenet *et al.* 1999; Rovedo *et al.* 1999) or puncture (Bouvier *et al.* 1997; Zoulias *et al.* 2002) test producing a force-deformation curve from which, texture properties are quantified.

Van Hecke *et al.* (1995) quantified crispness into several parameters: (1) number of spatial ruptures (ratio of total number of peaks to distance of puncturing or compression), (2) average specific force of structural ruptures (ratio of work to distance of puncturing) and (3) crispness work (ratio of average specific force of structural ruptures to number of spatial ruptures).

Scope of the Study

The first part of this study (Chapter 2) investigated microstructure of biopolymer foams (extruded cornstarch) and its effect on its mechanical properties. Non-invasive X-ray Microtomography (XMT) and texture analysis (TA.TX2) were used to investigate the relationships between microstructure (cell size, cell wall thickness, and cell number) and extrudate texture properties (compression modulus, crushing stress, number of spatial ruptures, average specific force of structural ruptures, and crispness work). Foams of differing microstructures were producing by varying in-barrel moisture contents (22.7, 24.8, 26.8, and 28.8% wet basis) and extruded screw speeds (200, 300, and 400 RPM).

The second part of this study (Chapter 3) investigated the effects of formulation, using model systems comprising of cornstarch, whey protein isolate (WPI) and sucrose, on phase transition behavior, and physical, microstructure and mechanical properties of extruded cornstarch. Different levels of WPI (6,12 and 18%), sucrose (2, 4 and 6%) and in-barrel moisture (23 and 27%) were extruded with cornstarch. A third experiment with WPI (6 and 12%), sucrose (2 and 4%) at 23% in-barrel moisture was performed to see the combined effect.

The concluding part of this study (Chapter 4) focused on the phase transition and rheological properties of cornstarch. The glass transition temperature was measured by differential scanning calorimetry (DSC), viscosity was measured by on-line viscometry (slit-die apparatus), and softening and flow temperatures was measured by phase transition analysis (PTA). This study was useful in characterizing the phase transition properties of cornstarch and the role they play in expansion, cell growth and propagation of foams during extrusion.

REFERENCES

Alavi, S. H., Gogoi, B. K., Khan, M., Bowman, B. J. and Rizvi, S. S. H. 1999. Structural properties of protein-stabilized cornstarch-based supercritical fluid extrudates. Food Research International, 32, 107-118.

Barletta, B. J. and Barbosa-Canovas, G. V. (1993). Fractal analysis to characterize ruggedness changes in tapped agglomerated food powders. Journal of Food Science, 58(5), 1030-1035.

Barrett, A. M., Normand, M. D., Peleg, M. and Ross, E. (1992). Characterization of the jagged stress-strain relationships of puffed extrudates using the fast fourier transform and fractal analysis. Journal of Food Science, 57(1), 227-235.

Barrett A. H. and Peleg, M. (1992). Extrudate cell structure-texture relationships. Journal of Food Science, 57(5), 1253-1257.

Barrett, A. H., Cardello, A. V., Lesher, L. L. and Taub, I. A. (1994a). Cellularity, mechanical failure, and texture perception of corn meal extrudates. J. Texture Studies, 25, 77-95.

Barrett, A. H., Rosenberg, S. and Ross, E. W. (1994b). Fracture intensity distributions during compression of puffed corn meal extrudates: method of quantifying fracturability. Journal of Food Science, 59(3), 617-620.

Barrett, A. H. and Peleg, M. (1995). Applications of fractal analysis to food structure. Lebensm.-Wiss. u.-Technol., 28, 553-563.

Biliaderis, C. G., Page, C. M., Maurice, T. J. and Juliano, B. O. (1986). Thermal characterization of rice starches: A polymeric approach to phase transitions of granular starch. J. Agric. Food Chem., 34: 6-14.

Bindzus, W., Fayard, G., Van Lengerich, B. and Meuser, F. (2002). Application of an in-line viscometer to determine the shear stress of plasticised wheat starch. Starch/Stärke, 54, 243.

Bouvier, J. M., Bonneville, R. and Goullieux, A. (1997). Instrumental methods for the measurement of extrudate crispiness. Agro-food-Industry Hi-Tech, 16-17.

Buera, M. P., Jouppila, P. K., Roos, Y. H. and Chirife, J. (1998). Differential scanning calorimetry glass transition temperatures of white bread and mold growth in the putative glassy state. Cereal Chem., 75, 64-69.

Duizer, L. M. and Campanella, O. H. (1998). Sensory, instrumental and acoustic characteristics of extruded snack food products. J. Texture Studies, 29, 397-411.

Fennema, O. R. (1985). Food Chemistry. New York, NY: Marcel Dekker, Inc.

Flannery, B. P., Deckman, H. W., Roberge, W. G. and D'Amico, K. L. (1987). Three dimensional x-ray microtomography.Science, 237, 1439-1444.

Fligner, K. L. and Mangino, M. E. (1991). Interactions of Food Proteins. Washington, DC: American Chemical Society.

Gao, X. and Tan, J. (1996). Analysis of expanded-food texture by image processing. Part II. Mechanical properties. Journal of Food Process Engineering, 19, 445-456.

Gao, X., Tan, J., Shatadal, P. and Heymann, H. (1999). Evaluating expanded-food sensory properties by image analysis. J. Texture Studies, 30, 291-304.

Gibson, L. G., & Ashby, M. F. (1997). Cellular Solids: Structure and Properties, 2nd ed. Cambridge, UK : Cambridge University Press.

Gregson, C. M. and Lee, T. C. (2003). Evaluation of numerical algorithms for the instrumental measurement for bowl life and changes in texture over time for ready-to-eat breakfast cereal. J. Texture Studies, 33, 505-528.

Hayter, A. L. and Smith, A. C. (1988). The mechanical properties of extruded food foams. Journal of Materials Science, 23, 736-743.

Huang, R., Chang, W., Chang, Y. and Li, C. (1994). Phase transitions of rice starch and flour getls. Cereal Chem., 71, 202-207.

Hutchinson, R. J., Siodlak, G. D. E. (1987). Influence of processing variables on the mechanical properties of extruded maize. Journal of Materials Science, 22, 3956-3962.

Kalichevsky, M. T., Jaroszkiewicz, E. M., Ablett, S., Blanshard, J. M. V. and Lillford, P. J. (1992). The glass transition of amylopectin measured by DSC, DMTA and NMR. Carbohydrate Polym., 18, 77-88.

Kinsella, J. and Phillips, L. G. (1989). Food Proteins. Phoenix, AR: The American Oil Chemists' Society.

Li, P. X., Campanella, O. H. and Hardacre, A. K. (2004). Using an in-line slit-die viscometer to study the effects of extrusion parameters on corn melt rheology. Cereal Chem., 81(1), 70.

Liu, H. and Lelievre, J. (1991). A differential scanning calorimetry study of glass and melting transitions in starch suspensions and gels. Carbohydrate Res., 219, 23-32.

Luyten, H., Plijter, J. J. and Van Vliet, T. (2004). Crispy/crunchy crusts of cellular solid foods: a literature review with discussion. J. Texture Studies, 35, 445-492.

Marshall, W. E. and Normand. F. L. (1991). Exothermic transitions in whole grain milled rice flour studied by differential scanning calorimetry. Cereal Chem., 68, 606-609.

Meullenet, J.-F. C. and Gross, J. (1999). Instrumental single and double compression tests to predict sensory texture characteristics of foods. J. Texture Studies, 30, 167-180.

Meullenet, J.-F. C., Sitakalin, C. and Marks, B. P. (1999). Prediction of rice texture by spectral stress strain analysis: a novel technique for treating instrumental extrusion data used for predicting sensory texture profiles. J. Texture Studies, 30, 435-450.

Perdon, A. A., Siebenmorgen, T. J. and Mauromoustakos, A. (2000). Glass state transition and rice drying: Development of a brown rice state diagram. Cereal Chem., 77, 708-713.

Phillips, L. G., Whitehead, D. M., and Kinsella, J. (1994). Structure-Function Properties of Food Proteins. San Diego, CA.: Academic Press Inc.

Prins, A. (1988). Advances in Food Emulsion and Foams. New York, NY: Elsevier Applied Science Publishers Ltd.

Riaz, M. N. ed. (2000). Extruders in Food Applications. Boca Raton, FL: CRC Pres

Rovedo, C. O., Pedreno-Navarro, M. M. and Singh, R. P. (1999). Mechanical properties of a corn starch product during the post-frying period. J. Texture Studies, 30, 279-290.

Sasov, A. Y. (1987). Microtomography. II. Examples of applications. Journal of Microscopy, 147(2), 179-192.

Seymour, S. K. and Hamann, D. D. (1988). Crispness and crunchiness of selected low moisture foods. J. Texture Studies, 19, 79-95.

Siebenmorgen, T. J., Yang, W. and Sun, Z. (2004). Glass transition temperature of rice kernels determined by dynamic mechanical thermal analysis. Transactions of the ASAE, 47(3), 835-839.

Slade, L. and Levine, H. (1987). Industrial Polysaccharides: The Impact of Biotechnology and Advanced Methodologies. New York, NY: Gordon and Breach.

Slade, L. and Levine, H. (1991). Beyond water activity: Recent advances based on an alternative approach to the assessment of food quality and safety. Crit. Reveiws Food Sci. Nutr., 30, 115-360.

Stevens, D. J. and Elton, G. A. H. (1971). Thermal properties of the starch/water system: Part 1. Measurement of heat of gelatinization by differential scanning calorimetry. Starch/Stärke, 23: 8-11.

Strahm, B. (1998). Fundamentals of polymer science as an applied extrusion tool. Cereal Foods World, 43, 621-625.

Strahm, B., Plattner, B., Huber, G., and Rokey, G. (2000). Application of food polymer science and capillary rheometry in evaluating complex extruded products. Cereal Foods World, 45(7), 300-302.

Strahm, B., and Plattner, B. (2003). Phase Transition Analyzer. United States Patent: Patent No. US 6,534,005 B1.

Sun, Z., Yang, W., Siebenmorgen, T. J., Stelwagen, A. M. and Cnossen, A. G. (2002). Thermomechanical transitions of rice kernels. Cereal Chem., 79, 349-353.

Trater, A. M., Alavi, S. H., and Rizvi, S. S. H. (2005). Study of microstructure development in extruded biopolymeric foams: non-invasive image analysis using computer-aided X-ray microtomography. Food Research International, 38, 709-719.

Van Hecke, E., Allaf, K. and Bouvier, J. M. (1995). Texture and structure of crispy-puffed food products. I: Mechanical properties in bending. J. Texture Studies, 26, 11-25.

Van Lengerich, B. (1990). Dough Rheology and Baked Product Texture. New York, NY: Van Nostrand Reinhold.

Vickers, Z. M. (1988). Instrumental measures of crispness and their correlation with sensory assessment. J. Texture Studies, 19, 1-14.

Warburton, S. C., Donald, A. M. and Smith, A. C. (1992). Structure and mechanical properties of brittle starch foams. Journal of Materials Science, 27, 1469-1474.

Weaire, D. and Hutzler, S. (1999). The Physics of Foams. New York, NY: Oxford University Press.

Yost, D. A. and Hoseney, R. C. (1987). Annealing and glass transition of starch. Starch/Stärke, 38, 289-292.

Zeleznak, K. J. and Hoseney, R. C. (1987). The glass transition in starch. Cereal Chem., 64, 121-124.

Zoulias, E. I., Oreopoulou, V. and Tzia, C. (2002). Textural properties of low-fat cookies containing carbohydrate- or protein-based fat replacers. Journal of Food Engineering, 55, 337-342.

Figure 1.1 Interaction of material and process parameters to produce a foamed extrudate with specific microstructure and texture.

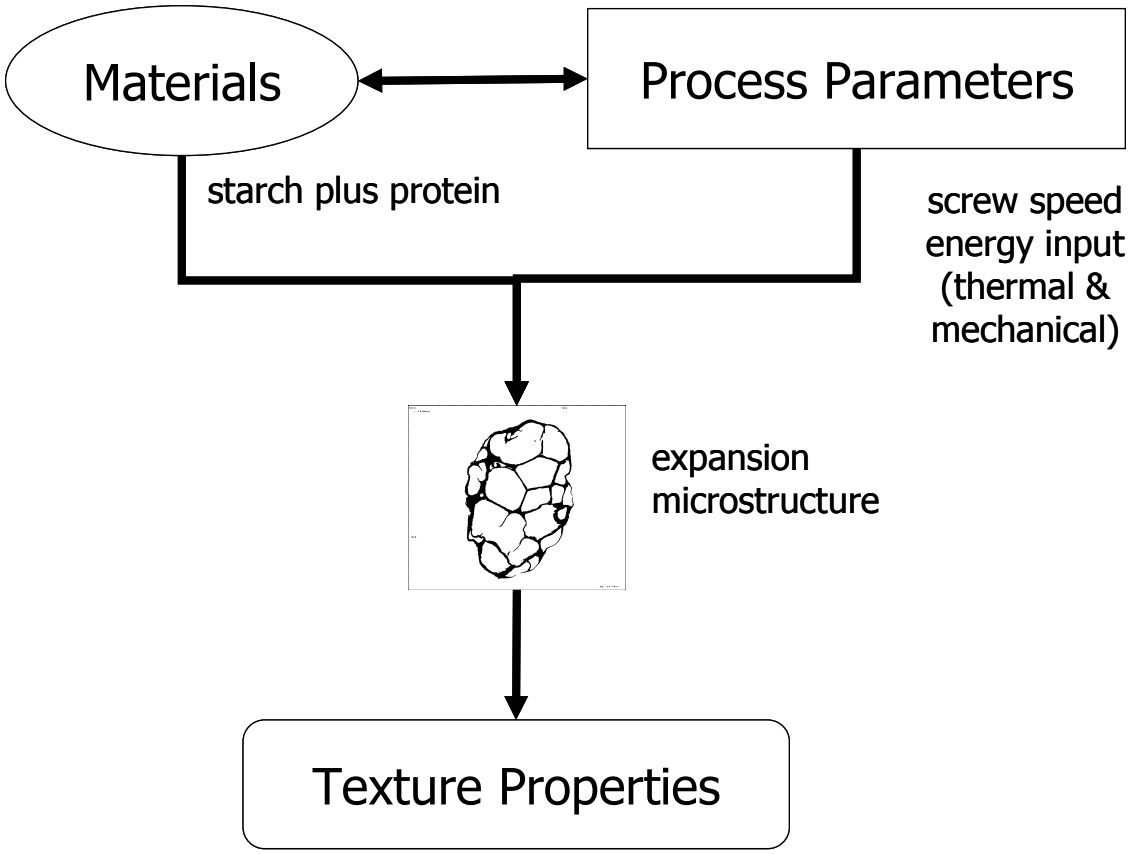

CHAPTER 2 - RELATIONSHIPS BETWEEN MICROSTRUCTURE AND MECHANICAL PROPERTIES OF CELLULAR CORNSTARCH EXTRUDATES

ABSTRACT

Relationships between mechanical properties and microstructure of brittle biopolymer foams were investigated using non-invasive imaging as a tool. Corn starch was processed in a twin-screw extruder to produce brittle foams with varying microstructure. X-ray microtomography was used to measure microstructure features of the foams, including average cell diameter (2.07-6.32 mm), cell wall thickness (0.13-0.25 mm) and cell number density (18-146 cm^{-3}). Mechanical properties, including compression modulus (2.2-7.8 MPa), crushing stress (42-240 kPa), number of spatial ruptures (2.6-3.6 mm^{-1}), average crushing force (22-67 N) and crispness work (6.4-22 N-mm), were determined instrumentally. Compression modulus had a reasonably good fit ($R^2 = 0.72$) with the Gibson-Ashby model for brittle foams, while crushing stress did not fit as well ($R^2 = 0.41$). Cellular characteristics had moderate to high correlation ($|r| = 0.48 - 0.81$) with mechanical properties, and provided significant insight into the deformation mechanism of the foams.

Mechanical properties of extruded biopolymeric foams are largely determined by their microstructure but the relationships involved have not been properly understood. This study used mechanical testing in combination with non-invasive x-ray microtomography to investigate these relationships. Results from this study furthered understanding of the deformation mechanism of brittle foams, and represent an important step towards the ability to better design crisp and crunchy food products with desired textures.

INTRODUCTION

In an effort to understand the physical and rheological behavior, as well as the mechanical and sensory attributes of foods, processing focus and emphasis have shifted to the microstructure level (less than 100 μm). Microstructure elements such as air bubbles or cells, starch granules, protein assemblies, and food biopolymer matrices contribute greatly to the identity and quality of foods (Aguilera 2005).

Extrusion processing is an important technology used for producing a variety of expanded snacks and breakfast cereals having a cellular structure. Microstructure parameters like size and number density of air cells, and their contribution to mechanical properties of extrusion-puffed foods have been studied before (Barrett and Peleg 1992; Barrett *et al.* 1994a; Van Hecke *et al.* 1995; Gao and Tan 1996). For example, breaking and plateau stress of cellular extrudates have been correlated to mean cell size (Barrett and Peleg 1992; Barrett *et al.* 1994a), whereas modulus of deformability, Young's modulus and failure strain have been associated with cell size, cell edge thickness and cell density (Van Hecke *et al.* 1995; Gao and Tan 1996).

However, the underlying mechanism relating cellular structure to the mechanics of extruded brittle foams is still not well understood. The limitations of traditional imaging techniques like scanning electron microscopy (SEM) and optical microscopy, that are two-dimensional and destructive in nature and also provide poor contrast, make it difficult to characterize cellular structure accurately. In fact, most studies on extrusion puffed foods either ignore their cellular structure or merely present a few cross-sectional images and discuss microstructure qualitatively without making measurements of important features such as cell size distribution or average cell wall thickness (Lai *et al.* 1985; Lee *et al.* 1999; Autio and Salmenkallio-Martilla 2001; Gropper *et al.* 2002).

X-ray microtomography or XMT is an important development in imaging technology that has eliminated some of the drawbacks of traditional imaging and enabled non-invasive characterization of foam microstructure in three dimensions (Flannery *et al.*1987; Sasov and Van Dyck 1998). XMT-generated images are more conducive to digital image processing than SEM or light microscope images because of 'razor-thin' depth of focus and sharp contrast between solid and void areas. XMT has only lately been applied to food foams and has led to some

important advances in the understanding of their cellular structure (Whitworth and Alava 1999; Maire *et al.* 2003; Lim and Barigou 2004; Falcone *et al.* 2004; Falcone *et al.* 2005; Trater *et al.*, 2005; Babin *et al.* 2006). Our laboratory was one of the first to use XMT for characterizing the cellular structure of extrusion puffed brittle foams (Trater *et al.*, 2005). In our study involving cornstarch-based extrudates, XMT proved to be successful in accurately characterizing several microstructural features that cannot be evaluated using traditional imaging techniques such as SEM or optical microscopy. These features included the true cell distribution (bi-modal), average diameter (0.58 to 2.27 mm), cell wall thickness (0.09 to 0.15 mm) and true void fraction (0.63 to 0.84). The open wall area fraction (ratio of broken or inter-connected wall area to total cell wall area) was measured to be 0.068 to 0.099, indicating that the extruded brittle foams were primarily closed cellular in nature.

Greater accuracy and objectivity in microstructure measurements has lead to the possibility of applying theoretical models to understand the mechanics of solid foams and eventually relate sensory properties of crisp or crunchy foods to their cellular structure. One such model was described by Gibson and Ashby (1997) for brittle foams using cubic cell geometry, and cellular parameters such as edge length (l) and wall thickness (t_{wall}). To simplify the application of this model, the ratio $t_{wall}/\,l$ was related to relative density ρ/ρ_s (the ratio of foam density ρ to solid density ρ_s), which is the most important but easy to measure 'macro' characteristic of solid foams. For true solid foams, $\rho/\rho_s < 0.3$, while values above 0.3 indicate solids containing isolated pores. For closed cell foams with $\rho/\rho_s < 0.2$, such as starch-based brittle extrudates, the Gibson-Ashby model demonstrated that ρ/ρ_s always scales as $t_{wall}/\,l$, with a constant of proportionality near unity. However, in many closed cell foams, solids are drawn preferentially from the walls to the edges because of a phenomenon called drainage, and a drainage factor ϕ (volume fraction of the solid material present in the cell edges) is used as a correction. This leads to the following more complex relationship that holds true for most closed cell foams.

$$\frac{t_{wall}}{l} = 1.4(1-\phi)\frac{\rho}{\rho_s} \tag{2.1}$$

The Gibson-Ashby model divided a typical stress-strain (or force-deformation) curve for brittle foams under compression into three distinct regions - linear elastic compression, jagged crushing plateau and densification. Each of these regions was described in terms of a

characteristic mechanical property, which was a function of mechanical strength of the solid material and cellular parameters.

The linear-elastic region during crushing was characterized by the compression modulus (E), which is given by the following equation applicable to closed-cell brittle foams.

$$\frac{E}{E_s} \approx \phi^2 \left(\frac{\rho}{\rho_s} \right)^2 + (1-\phi)\frac{\rho}{\rho_s} + \frac{p_0(1-2\nu)}{E_s\left(1-\frac{\rho}{\rho_s}\right)} \tag{2.2}$$

Where, E_s is the solid compression modulus, p_0 is the atmospheric pressure (0.1 MPa), and υ is the Poisson's ratio. The ratio E/E_s is also called the relative modulus of the foam. Poisson's ratio υ is mainly based on cell geometry and was estimated to be 0.33 based on data for foams with a wide range of densities.

The crushing plateau for closed-cell brittle foams was characterized by the crushing stress σ_{cr}, which is described by Equation 3.

$$\frac{\sigma_{cr}}{\sigma_{fs}} \approx 0.2\left(\phi \frac{\rho}{\rho_s} \right)^{\frac{3}{2}} + (1-\phi)\left(\frac{\rho}{\rho_s} \right) \tag{2.3}$$

Where, σ_{fs} is the modulus of rupture of solid material. The ratio σ/σ_{fs} is also called the relative crushing stress of the foam.

The first term in Equations 2 and 3 represents the contribution of cell edge bending when there is significant drainage of material from the cell walls to the edges (non-trivial ϕ). This term was derived from the standard theory for bending and failure of beams. The second term in equations 2 and 3 represents the contribution of stresses due to cell wall stretching. The third term in Equation 1 represents the contribution caused by the compression of air inside the cells and is relatively small. The Gibson-Ashby model was developed and validated primarily for non-food foams, but its various forms have also been applied to understand the compression behavior of extrusion puffed cellular foods (Hutchinson *et al.* 1987; Hayter and Smith 1988; Warburton *et al.* 1992) albeit with only limited success.

The Gibson-Ashby model, however, does not describe the 'jaggedness' of the crushing plateau of brittle foods, which has also been associated with the sensory properties of crispness and crunchiness (Barrett *et al.* 1994b; Barrett and Peleg 1995). Previous studies have used fractal analysis to quantify the jaggedness of the force-deformation curves during compression of

expanded extrudates (Barrett *et al.* 1992; Barrett *et al.* 1994b; Barrett and Peleg 1995). Fractal analysis involves complex mathematical treatments like Fast Fourier Transform (FFT) and is not easy to relate to microstructure parameters. Bouvier *et al.* (1997) extracted several parameters from the force-deformation curve during puncture testing of expanded extrudates. These parameters included the number of structural ruptures, average specific force of structural ruptures, average puncture force and crispness work. This was a simpler method to quantify the jagged mechanical response of brittle foams, but the study provided only limited understanding of how jaggedness is affected by cellular structure.

The primary objective of this study was to test the validity of the Gibson-Ashby model for describing mechanical properties of cellular extrudates, and to relate microstructure features of these brittle foams to their mechanical response including jaggedness of the force-deformation curve. Utilization of the non-invasive XMT technique for accurate characterization of cellular structure would provide greater meaning to this endeavor, as compared to previous studies. This study hopes to be an initial step towards developing models that would help in design of crisp and crunchy food products with targeted mechanical properties and sensory attributes.

MATERIALS AND METHODS

Extrusion Processing

Unmodified cornstarch (~25% amylose and 75% amylopectin; Cargill Gel 03457, Cargill, Inc., Minneapolis, MN) was used as the only ingredient for all extrusion runs. A Wenger TX-52 twin-screw extruder (Wenger Manufacturing, Sabetha, KS), with screw diameters of 52 mm, L/D ratio of 16:1, medium-shear screw profile (Figure 2.1) and circular die opening of 3.3 mm, was used to process all materials. Corn starch was extruded at four in-barrel moisture contents (23, 25, 27 and 29 %, wb) and three screw speeds (200, 300 and 400 RPM). The feed rate of raw material was 60 kg/hr. Water flow to the preconditioner was maintained at a constant 9.0 kg/hr. Water flow in the extruder was adjusted to 0.0, 2.0, 4.0, or 6.0 kg/hr, depending on treatment. Extruder conditions were allowed to stabilize for approximately 10 min before samples were collected. The product was cut, immediately after exiting the extruder die, with a face-mounted rotary cutter turning at 690 RPM, and was dried at 100°C with a double-pass dryer/cooler (4800 Series, Wenger Manufacturing, Inc., Sabetha, KS) adjusted for 15 min

retention time (7.5 min each for the top and bottom belts). Cooling was accomplished at 24°C, with a 5 min retention time on the cooling belt.

Image Acquisition and Processing for Determining Microstructure Parameters

Representative samples from two replicate extrusion runs were selected for image analysis. A desk-top X-ray microtomography imaging system (Model 1072, 20-100 kV/0-250 μA, SkyScan, Aartselaar, Belgium) set at 40 kV/100 μA (to obtain optimum contrast between solid and gaseous phases) was used to scan the samples. For each sample, a set of 15 two-dimensional virtual "slices" were obtained after reconstruction. Calculations of 3-D microstructural parameters were based on measurement of 2-D features from each slice using image analysis software (Scion Image for Windows®, Scion Corp., Frederick, MD), and their subsequent integration over all the slices. These 2-D features included individual cell perimeters and void areas, and overall solid and void areas for each slice. The computed 3-D parameters included volume weighted average cell diameter ($\overline{D}$), cell wall thickness (t_{wall}) and cell number density (N). Details of XMT scanning, image reconstruction, thresholding, measurement of 2-D features and computation of 3-D microstructural parameters have been described previously (Trater *et al.* 2005).

Analysis of Mechanical Properties

Thirty samples with approximately the same dimensions (diameter and height) were chosen from each treatment. Force-deformation data for each extrudate were obtained using a texture analyzer (TA-XT2, Stable Micro Systems, Surrey, United Kingdom) in the compression mode. A test probe of 38 mm diameter was used at a speed of 10 mm/s to compress samples to 90% of their original height. A stress-strain curve was determined from the force deformation data and sample dimensions. Compression modulus was calculated as the slope of the linear viscoelastic region before first rupture (or fracture). Crushing stress was calculated as the mean stress from the point of first rupture (or fracture) to first point of densification.

For determining jaggedness parameters, a Kramer shear press consisting of five 1.5-mm thick plates was used in conjunction with the texture analyzer. Five samples were used at a time for each test, and three replicates per treatment were conducted. The test speed was 8 mm/s in the compression mode. A force-deformation curve was obtained, and the number of peaks, n,

integral of the curve, *S* (or area below the curve from 0 to 100% strain), and distance of compression, *d*, were computed. From *n*, *S* and *d* values, the following parameters were calculated (Bouvier *et al.* 1997).

$$N_{sr} = \frac{n}{d} \quad (\text{mm}^{-1}) \tag{2.4}$$

$$F_{cr} = \frac{S}{d} \quad (\text{N}) \tag{2.5}$$

$$W_c = \frac{F_c}{N_{sr}} = \frac{S/d}{n/d} \quad (\text{N-mm}) \tag{2.6}$$

Where N_{sr} is the number of spatial ruptures, F_{cr} is average crushing force and W_c is crispness work.

Physical Properties (Piece and Solid Densities)

Piece densities, ρ, were obtained by the rapeseed displacement method. Solid densities, ρ_s, were obtained for the ground extrudate by using a helium pycnometer (Model NVP-1, Quantachrome, Boynton Beach, FL). All density measurements were adjusted to 0% moisture basis to eliminate the contribution of water to material density. Relative density, ρ/ρ_s, was computed from piece and solid densities.

Experimental Design and Statistical Analysis

A 3x 4 factorial design, with four levels of in-barrel moisture and three levels of screw speed, was used to produce extrudates with different microstructures. Each extrusion treatment was replicated twice. For measurement of mechanical properties of extrudates, thirty replicates were conducted for the compression test, and three for the Kramer shear test. Microstructure parameters were measured using one representative sample from each replicate treatment. Non-linear regression using the least squares method was used for fitting data to model equations and corresponding R^2 values were generated to test the goodness of fit. The 'PEARSON' function of EXCEL™ software (2002 edition, Microsoft Corporation, Seattle, WA) was used for finding the Pearson's coefficient of correlation (r) between any two data sets. To provide descriptive terms to the degree of correlation, criteria outlined by Franzblau (1958) were used ($|r| < 0.20$, negligible; $|r| = 0.20$ to 0.40, low; $|r| = 0.40$ to 0.60, moderate; $|r| = 0.60$ - 0.80, marked; and $|r| > 0.80$, high).

RESULTS AND DISCUSSION

Microstructure of Cornstarch Extrudates

Representative 2-D XMT slices of samples from each treatment are shown in Figure 2.2. Extrudates exhibited different cell structures depending on the in-barrel moisture and screw speed, but were mostly closed-cell in nature as has been observed by our research group previously (Trater *et al.* 2005). Cell diameter ($\overline{D}$), cell wall thickness (t_{wall}) and cell number density (N) ranged from 2.07 to 6.32 mm, 0.13 to 0.25 mm, and 18 to 146 cells/cm^3, respectively. Cell diameter increased and cell number density decreased with decreasing in-barrel moisture or increasing screw speed. No specific trend was observed for cell wall thickness at different in-barrel moistures and screw speeds. Average solid density for all samples was 1350 kg/m^3. Piece density (ρ) ranged from 128 to 302 kg/m^3. Piece density decreased, indicating greater expansion, with decreasing in-barrel moisture or increasing screw speed. The main driving force for expansion of extrudates is the mechanical energy input. Reduced in-barrel moisture would lead to an increase in melt viscosity, which in turn would increase the mechanical energy input and therefore increase expansion. Increase in extruder screw speed would also lead to higher mechanical energy input, and therefore increased expansion. Detailed analyses on effect of process parameters on micro-structural characteristics of these extrudates will be presented in a separate paper. However, increase in cell diameter and decrease in cell number density with higher overall expansion of extrudates is consistent with previously observed results (Trater *et al.* 2005), and has been attributed to the phenomena of cell expansion and coalescence occurring simultaneously.

Relationship between Macro and Micro-Structural Parameters

Figure 2.3-A shows a plot of relative density (ρ/ρ_s) versus cell wall thickness to cell diameter ratio ($t_{wall}/\overline{D}$). For the most part, $\rho/\rho_s < 0.2$, an important condition for applicability of the Gibson-Ashby model equations described earlier. There was also a marked degree of correlation (r = 0.72) between ρ/ρ_s and $t_{wall}/\overline{D}$, indicating the validity of Equation 2.1. The ρ/ρ_s and $t_{wall}/\overline{D}$ data were fitted to Equation 2.1 to obtain the drainage factor ϕ for each treatment.

The average cell diameter ($\overline{D}$) is different from the edge length (l), so a scaling factor, $l = 0.36\,\overline{D}$, was used based on relationships for typical closed cell foams (Gibson and Ashby, 1997). No particular trend was observed for ϕ versus ρ/ρ_s (r = -0.13, Figure 2.3-B). In fact, ϕ was within a narrow band ranging from 0.31 to 0.56, except for a few outliers (a couple of ϕ values were negative, which did not make sense physically so these were taken as 0). The average value of ϕ within this band was calculated to be 0.42.

Mechanical Profile of Extruded Cornstarch

Typical stress-strain curves of extrudates under compression are shown in Figure 2.4. Stress levels rose linearly with strain until the first fracture, followed by a crushing region with multiple peaks. Densification occurred at approximately 85 to 90% strain. For cornstarch extruded at the lowest in-barrel moisture (23%), as compression of the sample continued, a fracture point was reached and the sample broke into two pieces. Compression of the remaining pieces resumed shortly thereafter, creating a brittle crushing plateau with numerous peaks. For extrudates processed at 25, 27, and 29% in-barrel moisture, after fracturing the sample collapsed and broke into numerous pieces. For these treatments, peaks in the crushing region were relatively higher and so was the drop-off force after each fracture, as compared to treatments with 23% in-barrel moisture. As detailed previously in this paper, compression modulus and crushing stress were calculated from the stress-strain curves, while the jaggedness parameters were extracted from the force-deformation curves obtained from the Kramer shear test.

Microstructure-Mechanical Property Relationships

Figure 2.5 shows plots of extrudate compression modulus (E) and crushing stress (σ_{cr}) versus $\overline{D}$. Compression modulus ranged between 2.2-7.8 MPa, and crushing stress between 42-240 kPa. High correlations were observed (r = -0.81) between both mechanical properties and $\overline{D}$. It was clear that both E and σ_c decreased with an increase in cell diameter, which indicated a general weakening of the foam structure with greater expansion of the cells. Some previous studies have observed similar relationships between mechanical properties of expanded extrudates and their average cell diameter (Barrett and Peleg 1992; Barrett *et al.* 1994a; Van Hecke *et al.* 1995). Compression modulus (E) and crushing stress (σ_{cr}) were also plotted versus $t_{wall}/\overline{D}$ (Figure 2.6). Moderate to marked correlations were observed for E and σ_{cr} with $t_{wall}/\overline{D}$ (r

= 0.64 and 0.54, respectively). This demonstrated the combined effect of cell diameter and cell wall thickness on mechanical properties of the starch-based brittle foams. According to standard beam theory, from which the Gibson-Ashby model is partially derived, increasing thickness and decreasing length of beams leads to higher stiffness and failure strength. It is clear from our data that foams with higher $t_{wall}/\overline{D}$, which meant thicker cell walls and smaller cell diameters, had higher compression modulus and crushing stress as compared to foams with a lower $t_{wall}/\overline{D}$ (thinner walls and larger cell diameters). Lower correlation coefficients with respect to the ratio $t_{wall}/\overline{D}$, as compared to $\overline{D}$, does not necessarily imply that the compression modulus and crushing stress are more closely related to the latter and that the Gibson-Ashby model is inadequate. Instead it might indicate that the relationship between the mechanical properties and $t_{wall}/\overline{D}$ is more non-linear. The latter is definitely true, as can be seen from the Gibson-Ashby model equations (Equations 2.2 and 2.3).

It was difficult to measure the mechanical properties of the solid matrix with precision as has been observed in previous studies as well (Hutchinson *et al.* 1987; Gibson and Ashby 1997). Moreover, it would be inappropriate to measure these properties for unfoamed material involving very different processing conditions, therefore E_s (52.64 MPa) and σ_{fs} (1.74 MPa) were obtained by fitting experimental data to Equations 2.2 and 2.3, respectively. The solid lines in Figure 2.7 represent the best fit curves obtained using non-linear regression (least squares method). The average value of ϕ (=0.42) was used for the fitting. The dotted curves represent the predicted mechanical properties of extruded foams using the upper and lower bounds of ϕ (0.56 and 0.31, respectively). The compression modulus data had a much better fit (R^2 = 0.72) with the Gibson-Ashby model than the crushing stress data (R^2 = 0.41), although about two-thirds of the data points for both E and σ_{cr} lay within the upper and lower bounds. Gibson and Ashby (1997) also observed a relatively poorer fit of σ_{cr} data for brittle glass and metal foams to their model. They attributed this to inaccuracies in estimation of the cell wall modulus of rupture (σ_{fs}).

Figure 2.8 shows the plot of the jaggedness parameters (F_{cr} and W_c), obtained from the Kramer shear test, versus microstructure features of the extrudates. Average crushing force ranged between 22-67 N and crispness work between 6.4-22 N-mm. Both average crushing force and crispness work had marked to high correlations with cell diameter (r = -0.79 and -0.81, respectively). As expected, both F_{cr} and W_c increased with a decrease in cell diameter,

indicating that more force and work were needed to deform/fracture smaller size cells. This was similar to the observation for compression modulus and crushing stress, which showed a high negative correlation with $\overline{D}$. The number of spatial ruptures (N_{sr}) of extrudates ranged between 2.6-3.6 mm^{-1} (data not shown). It was expected that the number of spatial ruptures during deformation would increase with higher cell number density. On the contrary, a moderate negative correlation (r = -0.48) was observed between N_{sr} and N. This gave a unique insight, not provided by the Gibson-Ashby model, into the mechanics of brittle foam deformation. As foams deform under compression, the resultant stress is transmitted uniformly through the microstructure. Larger cells with walls that are relatively thin and/ or weakened due to cracks represent 'weak-spots' in the structure. These weaker cells reach their fracture point earlier. Often more than one cell fracture at the same time, with each peak in the force-deformation curve representing the combined effect. It is likely that foams with higher N had numerous smaller cells fracturing at the same time, thus resulting in lower N_{sr}. This also explained the higher magnitude of the peaks as compared to foams with lower cell number density.

Shortcomings of the Gibson-Ashby Model

As described earlier, compressive modulus data for brittle foams had a reasonably good fit (R^2 = 0.72) with the Gibson-Ashby model, however crushing stress data did not fit as well (R^2 = 0.41). The Gibson-Ashby equations were derived using some simplifying assumptions including cubic cell geometry and a uniform microstructure. In reality, cell shapes are more complex and microstructure features, such as cell diameter and wall thickness, are non-uniform and distributed over a range (Figure 2.2). Moreover, the constants associated with various terms in the model equations were either estimations or fitted using available data. The Gibson-Ashby equations are also inadequate for modeling the jaggedness of the force-deformation curve. Other models that can overcome some of the above mentioned shortcomings should be explored. One such model was described by Cuitino and Zheng (2003) based on a thin-walled spherical unit cell. This micromechanical model takes into account cell size distribution of the foam (average radius, variance and skewness), and the mechanics of cell wall bending and stretching. It uses a strain energy density function and averages the response of unit cells of different sizes using Taylor averaging. Cuitino and Zheng have successfully used this approach to model the deformation behavior of yellow cake. Further details of this model is beyond the scope of the

current study, however there is potential of applying it to estimate the jagged response curve associated with deformation of brittle foams.

CONCLUSIONS

X-ray microtomography was used to characterize the three-dimensional microstructure features of extruded starch-based brittle foams. Compressive modulus and crushing stress of the foams were measured, and jaggedness parameters (number of spatial ruptures, average crushing force and crispness work) also extracted from force-deformation curves. Microstructure data, such as average cell diameter, cell wall thickness and drainage factor, were utilized to assess the applicability of the Gibson-Ashby model towards prediction of mechanical properties of brittle foams. Compression modulus data showed a good fit to the Gibon-Ashby model, whereas crushing stress data had a relatively poor fit. Moderate to high correlations were observed between all mechanical properties and microstructure features. This study furthered understanding of the deformation mechanism of brittle foams, and is an important step towards the ability to better design crisp and crunchy food products with desired textures. However, assumptions such as cubic cell geometry and uniform microstructure limit the applicability of the Gibson-Ashby model. Other models, which can overcome these shortcomings as well as predict the jagged deformation response of brittle foams, should also be evaluated in the future. Non-invasive imaging techniques such as XMT will be crucial in this endeavor as it enables a degree of cellular characterization that is much higher than possible by SEM or optical microscopy.

ACKNOWLEDGEMENTS

This study was funded by the USDA, CSREES, National Research Initiative (NRI) Competitive Grants Program (Award Number 2003-35503-13999). The authors would like to thank Mr. Eric Maichel for his technical assistance, and Wenger Manufacturing, Inc. (Sabetha, KS) and Micro Photonics, Inc. (Allentown, PA) for their continued support to the extrusion laboratory at Kansas State University. This is Contribution Number 06-257-5 from the Kansas Agricultural Experiment Station, Manhattan, Kansas.

REFERENCES

AUTIO, K. and SALMENKALLIO-MARTILLA, M. 2001. Light microscopic investigations of cereal grains, doughs and breads. Lebensm.-Wiss. Technol. *34*, 18-22.

AGUILERA, J. M. 2005. Why food microstructure? J. Food Eng. 67, 3-11.

BABIN, P., DELLA VALLE, G., CHIRON, H., CLOETENS, P., HOSZOWSKA, J., PERNOT, P., REGUERRE, A. L., SALVO, L. and DENDIEVEL, R. 2006. Fast X-ray tomography analysis of bubble growth and foam setting during breadmaking. J. Cereal Sci. *43*, 393-397.

BARRETT, A. H., CARDELLO, A. V., LESHER, L. L. and TAUB, I. A. 1994a. Cellularity, mechanical failure, and texture perception of corn meal extrudates. J. Texture Studies *25*, 77-95.

BARRETT, A. M., NORMAND, M. D., PELEG, M. and ROSS, E. 1992. Characterization of the jagged stress-strain relationships of puffed extrudates using the fast fourier transform and fractal analysis. J. Food Sci. *57*(1), 227-235.

BARRETT A. H. and PELEG, M. 1992. Extrudate cell structure-texture relationships. J. Food Sci. *57*(5), 1253-1257.

BARRETT, A. H. and PELEG, M. 1995. Applications of fractal analysis to food structure. Lebensm.-Wiss. Technol. *28*, 553-563.

BARRETT, A. H., ROSENBERG, S. and ROSS, E. W. 1994b. Fracture intensity distributions during compression of puffed corn meal extrudates: method of quantifying fracturability. J. Food Sci. *59*(3), 617-620.

BOUVIER, J. M., BONNEVILLE, R. and GOULLIEUX, A. 1997. Instrumental methods for the measurement of extrudate crispiness. Agro-Food-Industry Hi-Tech *Jan/Feb 1997*, 16-17.

CUITINO, A. M., and ZHENG, S. 2003. Taylor averaging on heterogeneous foams. J. Compos. Mater. *37*(8), 701-713.

FALCONE, P. M., BAIANO, A., ZANINI, F., MANCINI, L., TROMBA, G., MONTANARI, F. and DEL NOBILE, M. A. 2004. A novel approach to the study of bread porous structure: phase-contrast X-ray microtomography. J. Food Sci. *69*(1), 38-43.

FALCONE, P. M., BAIANO, A., ZANINI, F., MANCINI, L., TROMBA, G., DREOSSI, D., MONTANARI, F., SCUOR, N. and DEL NOBILE, M. A. 2005. Three-dimensional quantitative analysis of bread crumbs by X-ray microtomography. J. Food Sci. *70*(4), 265-272.

FLANNERY, B. P., DECKMAN, H. W., ROBERGE, W. G. and D'AMICO, K. L. 1987. Three dimensional x-ray microtomography. Science *237,* 1439-1444.

FRANZBLAU, A. 1958. *A Primer of Statistics for Non-Statistician,* Harcourt Brace and World, New York, NY.

GAO, X. AND TAN, J. 1996. Analysis of expanded-food texture by image processing. Part II. Mechanical properties. J. Food Process Eng. 19, 445-456.

GIBSON, L. G., and ASHBY, M. F. 1997. *Cellular Solids: Structure and Properties*, Cambridge University Press, Cambridge, UK.

GROPPER, M., MORARU, C. and KOKINI, J.L. 2002. Effect of specific mechanical energy on properties of extruded protein-starch mixtures. Cereal Chem. *79*, 429-433.

HAYTER, A. L. and SMITH, A. C. 1988. The mechanical properties of extruded food foams. J. Mater. Sci. *23*, 736-743.

HUTCHINSON, R. J., SIODLAK, G. D. E. and SMITH, A.C. 1987. Influence of processing variables on the mechanical properties of extruded maize. J. Mater. Sci. *22,* 3956-3962.

LAI, C. S., DAVIS, A. B. and HOSENEY, R. C. 1985. The effect of a yeast protein concentrate and some of its components on starch extrusion. Cereal Chem. *62*(4), 293-300.

LEE, E. Y., RYU, G. H. and LIM, S.-T. 1999. Effects of processing parameters on physical properties of corn starch extrudates expanded using supercritical CO_2 injection. Cereal Chem. *76*(1), 63-69.

LIM, K. S. and BARIGOU, M. 2004. X-ray micro-computed tomography of cellular food products. Food Res. Int. *37,* 1001-1012.

MAIRE, E., FAZEKAS, A., SALVO, L., DENDIEVEL, R., YOUSSEF, S., CLOENTENS, P. and LETANG, J. M. 2003. X-ray tomography applied to the characterization of cellular materials. Related finite element modeling problems. Compos. Sci. Technol. *63*, 2431-2443.

SASOV, A. and VAN DYCK, D. 1987. Desktop X-ray microscopy and microtomography. J. Microsc. *191(*2), 151-158.

TRATER, A. M., ALAVI, S., and RIZVI, S. S. H. 2005. Use of non-invasive X-ray microtomography for characterizing microstructure of extruded biopolymer foams. Food Res. Int. *38*, 709-719.

VAN HECKE, E., ALLAF, K. and BOUVIER, J. M. 1995. Texture and structure of crispy-puffed food products. I: Mechanical properties in bending. J. Texture Studies *26,* 11-25.

WARBURTON, S. C., DONALD, A. M. and SMITH, A. C. 1992. Structure and mechanical properties of brittle starch foams. J. Mater. Sci. *27*, 1469-1474.

WHITWORTH, M.B. and ALAVA, J.M. 1999. The imaging and measurement of bubbles in bread doughs. In *Bubbles in Food* (G. M. Campbell, C. Webb, S. S. Pandiella and K. Niranjan eds.) pp. 221-231, Eagan Press, St. Paul, MN.

FIGURES

Figure 2.1 Diagram of the extruder screw configuration, water injection sites and barrel temperatures used for all treatments. Lengths of screw elements are not to scale.

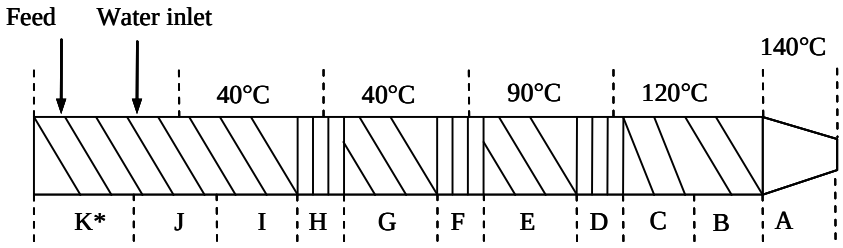

Section	Number of elements	Element length, mm	Element description
A	1	78	¾ pitch, double flighted, conical
B	1	78	¾ pitch, double flighted
C	1	52	½ pitch, double flighted
D	1	26	kneading block, forward
E	1	78	¾ pitch, double flighted
F	1	26	kneading block, forward
G	1	78	¾ pitch, double flighted
H	1	26	kneading block, forward
I	1	78	¾ pitch, double flighted
J	2	78	full pitch, double flighted
K	2	78	¾ pitch, double flighted

*The first two elements of the right shaft at the inlet (K) are ¾ pitch, single flighted.

Figure 2.2 X-ray microtomography images of representative 2-D slices (perpendicular to the direction of extrusion) of foams from each treatment. All images correspond to the scale indicated on the bottom right.

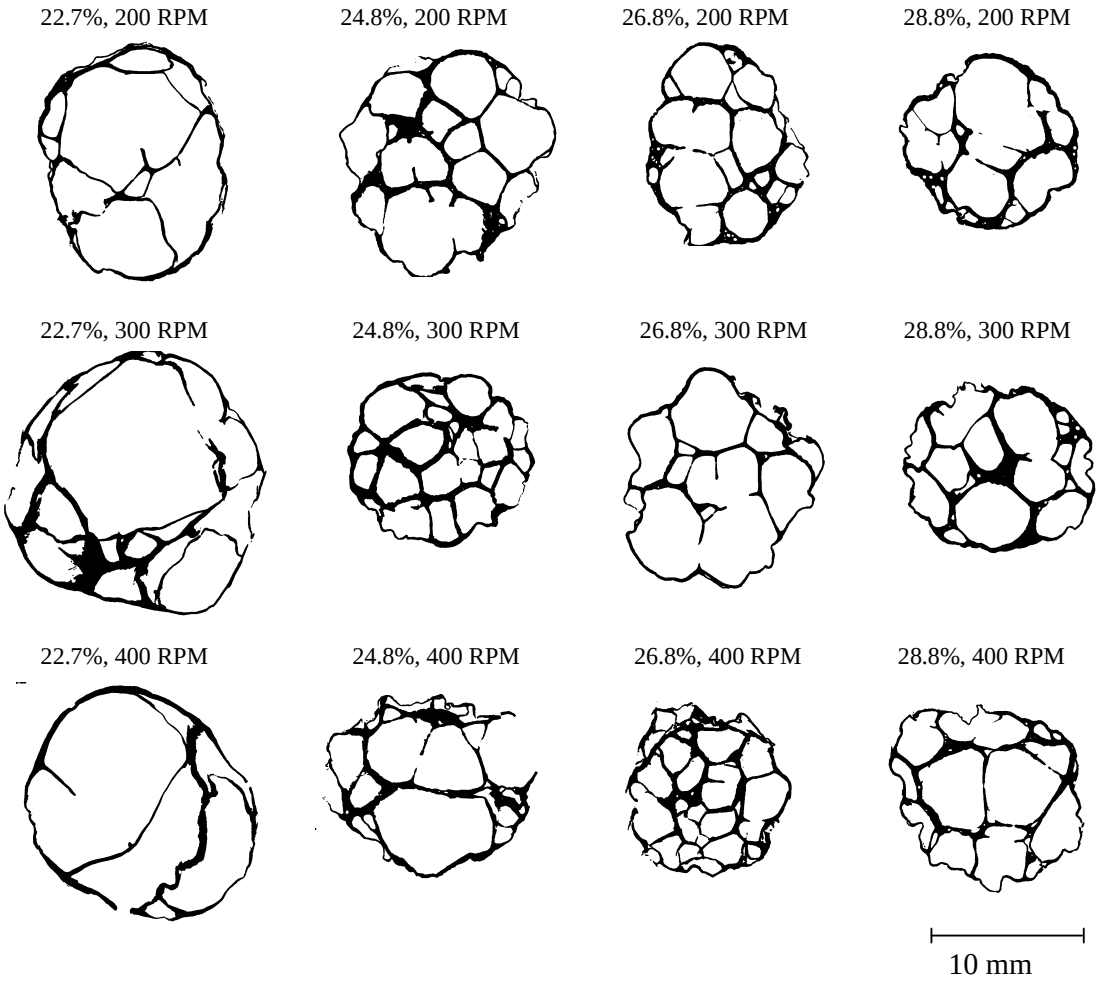

Figure 2.3 (A) Relative density (ρ/ρ_s) versus cell wall thickness to cell diameter ratio ($t_{wall}/\overline{D}$). Solid line represents the linear trendline for the data set; (B) drainage factor (ϕ) versus relative density. Horizontal solid line represents average value of ϕ (0.42) after excluding some outliers.

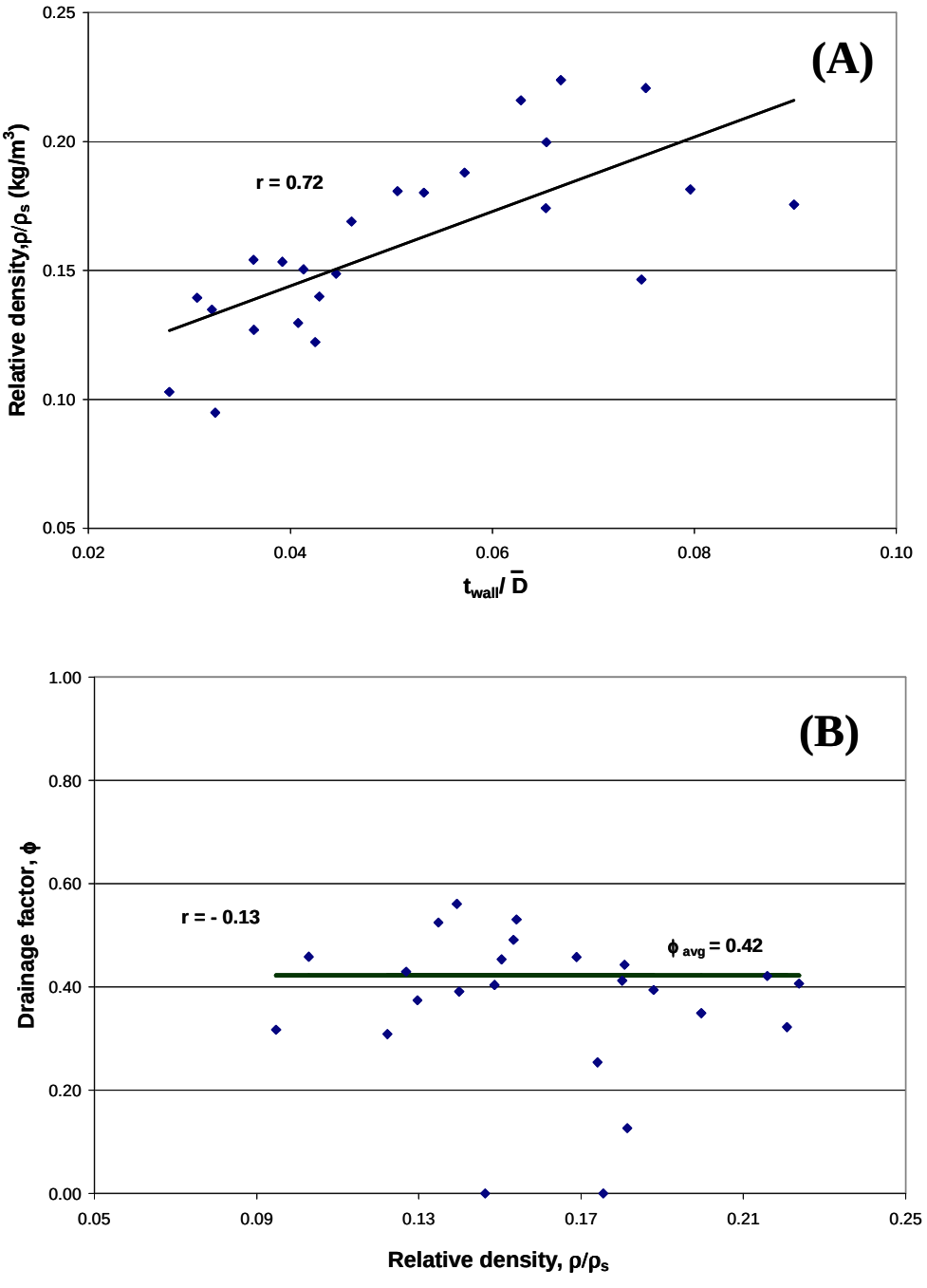

Figure 2.4 Representative stress-strain curves for corn starch based brittle foams extruded at 23, 25, 27 and 29% in-barrel moistures at 200 rpm screw speed.

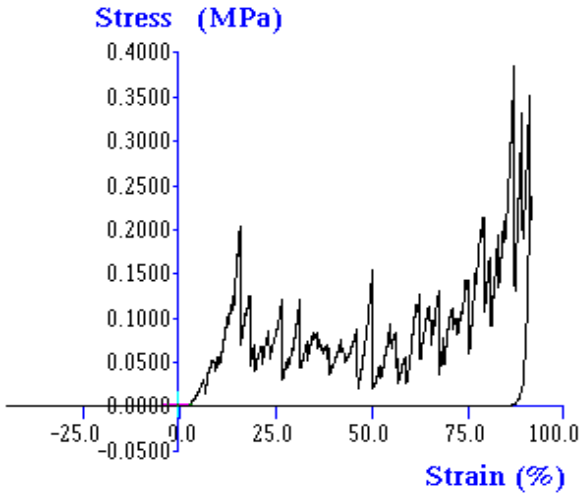

23% In-barrel MC

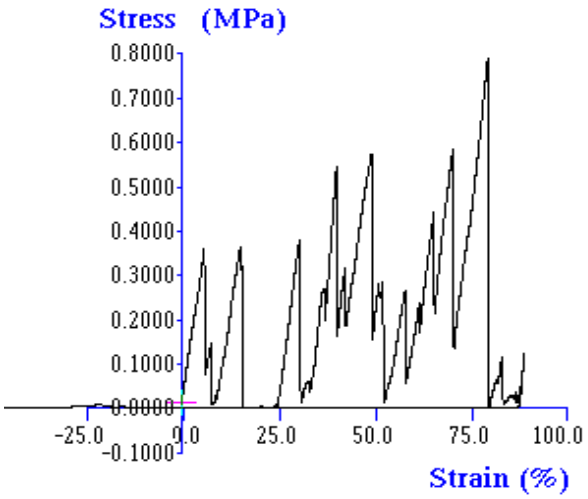

25 % In-Barrel MC

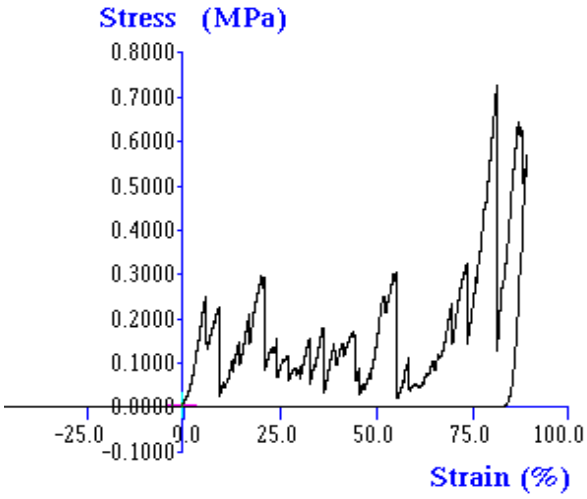

27 % In-Barrel MC

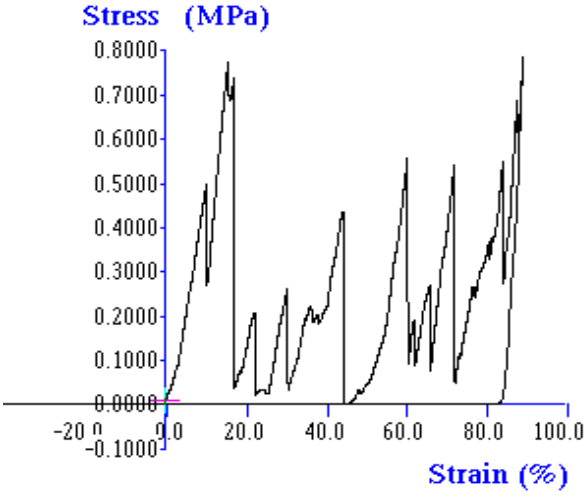

29 % In-Barrel MC

Figure 2.5 (A and B) Compressive modulus (*E*) and crushing stress (σ_{cr}) versus average cell diameter ($\overline{D}$) of extruded corn starch based brittle foams. Solid lines represent linear trendlines for the data sets.

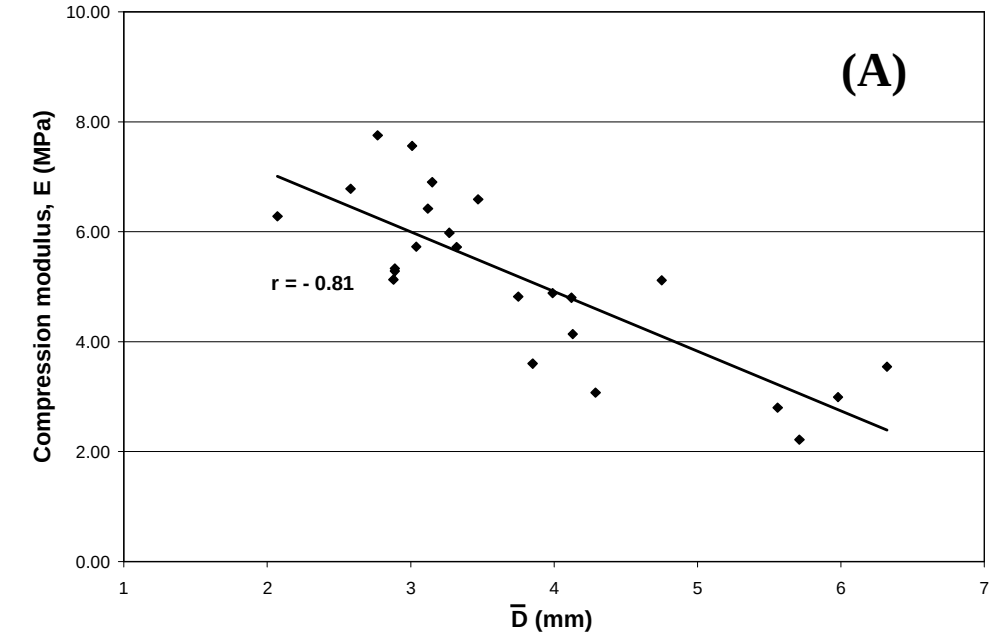

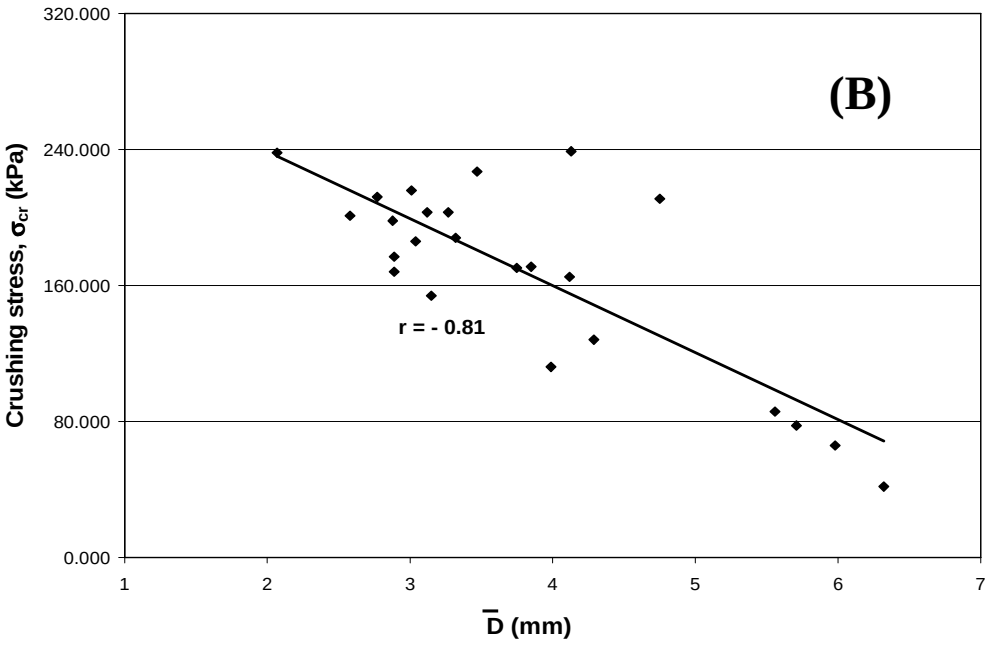

Figure 2.6 (A and B) Compression modulus (E) and crushing stress (σ_{cr}) versus cell wall thickness to cell diameter ratio ($t_{wall}/\overline{D}$) of extruded corn starch based brittle foams. Solid lines represent linear trendlines for the data sets.

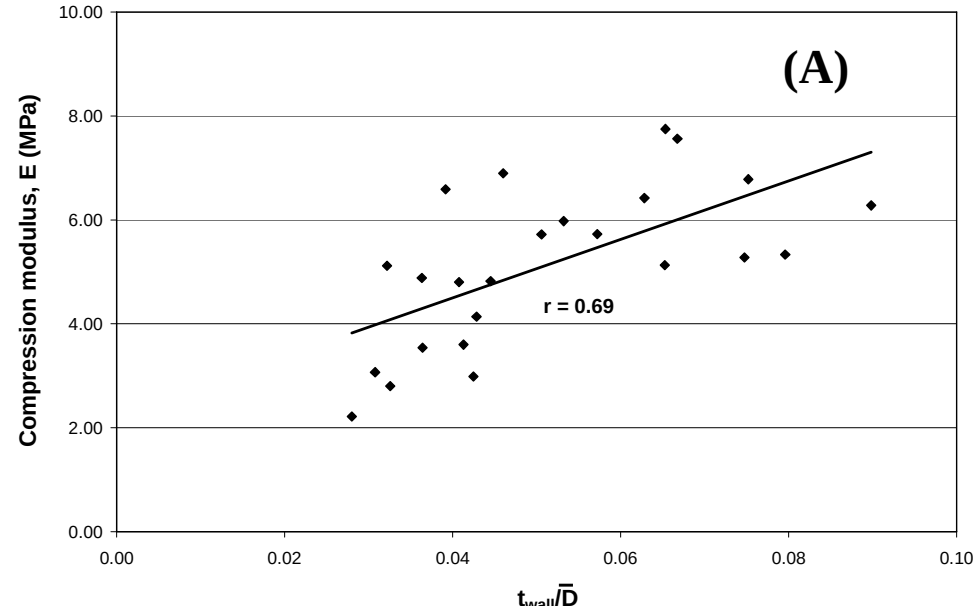

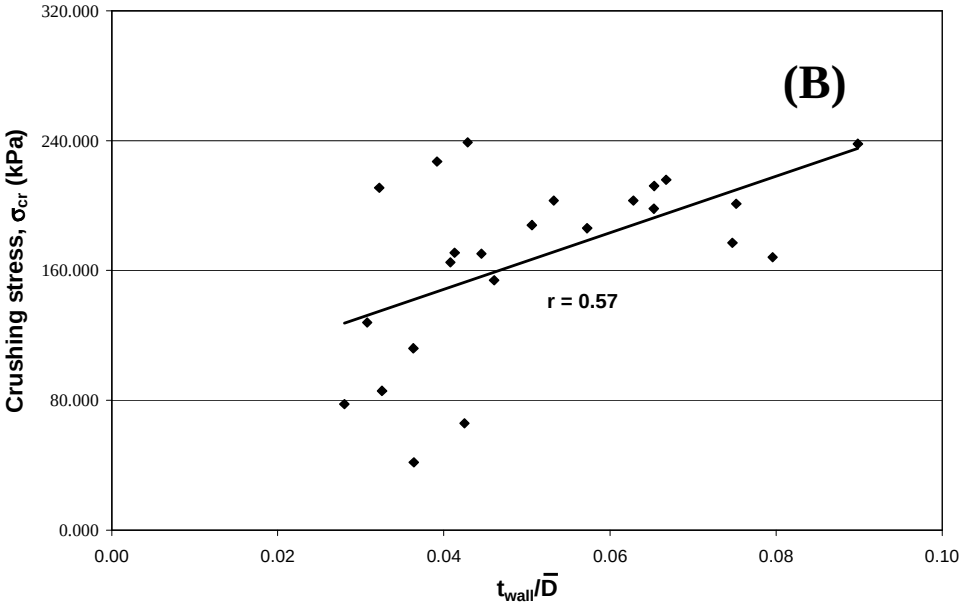

Figure 2.7 (A and B) Compression modulus (*E*) and crushing stress (σ_{cr}) data fitted to the Gibson-Ashby model (solid lines) using the average value of drainage factor (ϕ = 0.42). The dotted lines represent predicted mechanical properties using the upper and lower bounds of ϕ (0.56 and 0.31, respectively).

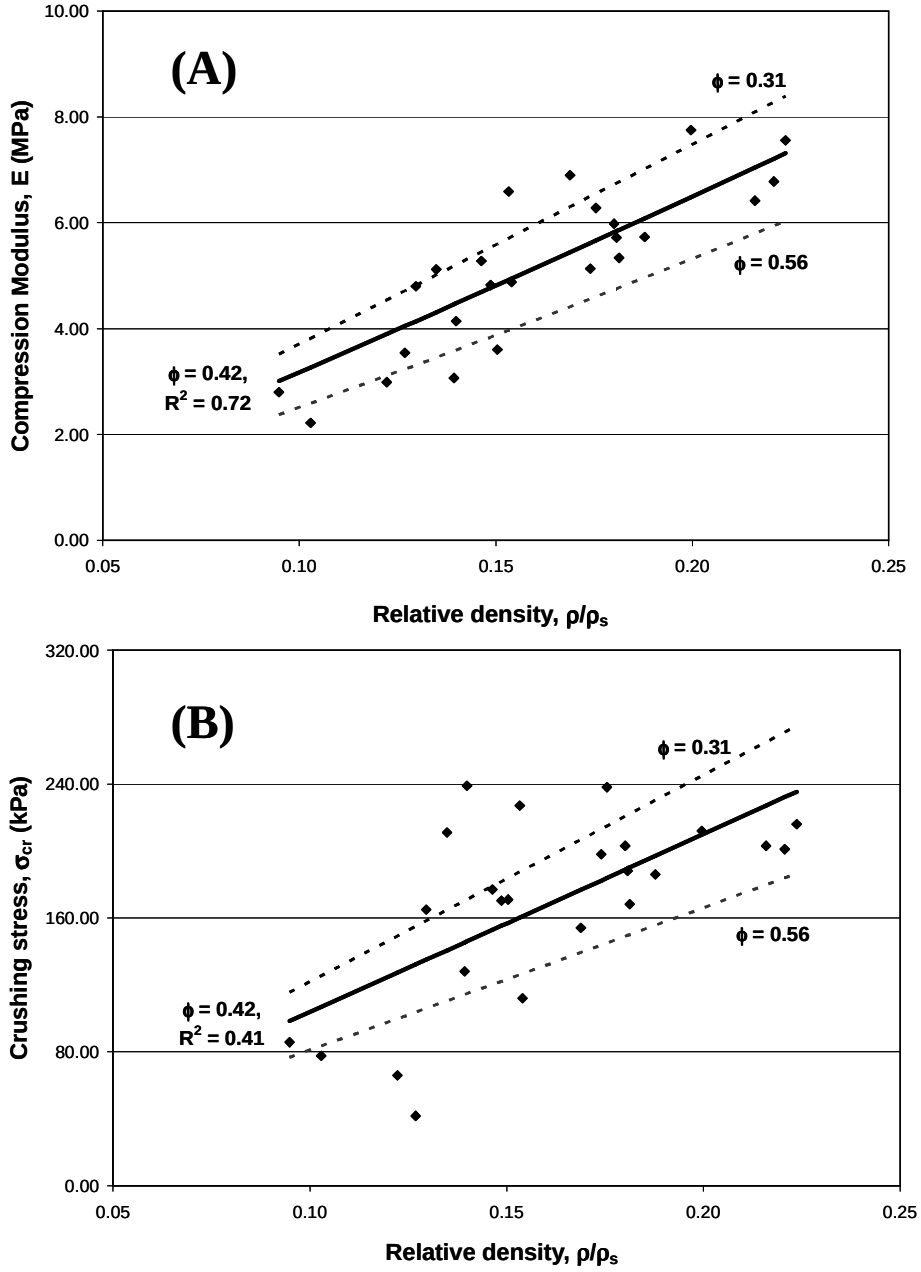

Figure 2.8 (A and B) Jaggedness parameters, average crushing force (F_{cr}) and crispness work (W_c), versus average cell diameter ($\overline{D}$) of extruded corn starch based brittle foams. Solid lines represent linear trendlines for the data sets.

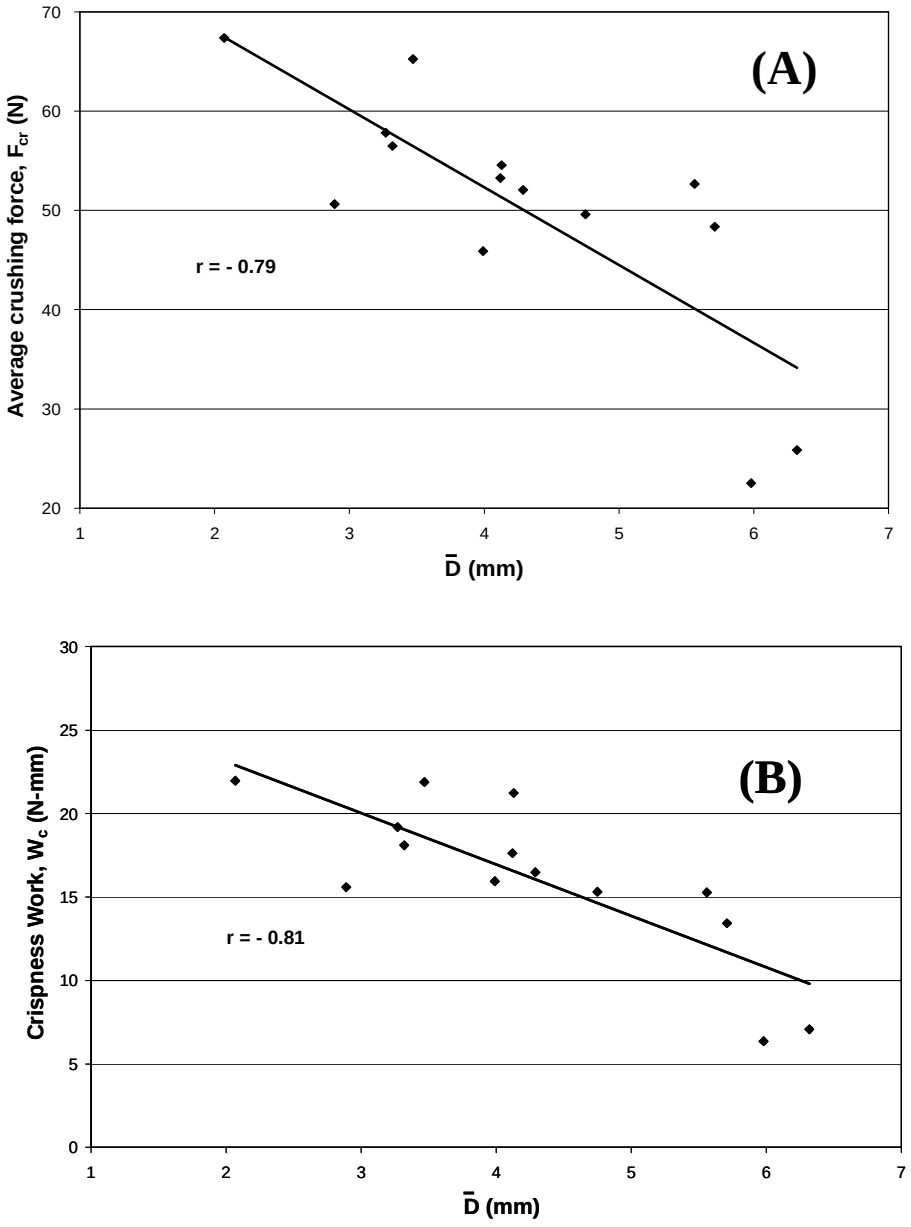

CHAPTER 3 - RELATIONSHIPS BETWEEN MATERIAL PROPERTIES AND MICROSTRUCTURE-MECHANICAL ATTRIBUTES OF EXPANDED CORNSTARCH EXTRUDATES: MODEL SYSTEM STUDIES

To be submitted to Food Research International, May, 2007

ABSTRACT

Material formulation and extrusion process parameters affect cell nucleation and growth, and the resultant foam microstructure, which greatly controls the mechanical properties of extrudates. To understand the dynamics of the foaming process, it is important to study the material properties critical for expansion/collapse, and characterize the foam microstructure in an objective and accurate manner. This study aims to understand foam formation during extrusion by investigating relationships between material properties, processing parameters and microstructure of biopolymeric extrudates. Model formulation systems, based on cornstarch, whey protein isolate (WPI) and sucrose, were utilized for this purpose. Mechanical properties of extrudates were also studied in relation to their expansion and microstructure characteristics. Softening temperature (T_s) decreased from 83.1 to 41.2°C with increase in WPI (6 to 18%). T_s increased from 57.0 to 91.4°C with increase in sucrose (2 to 6%). There was an inverse correlation between T_s and specific mechanical energy (SME) for cornstarch-WPI model system (r range of -0.88 to -0.94). None to inverse correlations were observed between T_s and SME for cornstarch-sucrose model systems (r range of 0 to 0.83). Difference between melt temperature behind the die and softening temperature (T_{ds}), which is a measure of the net driving force of expansion, was positively correlated with SME (r range of 0.79 to 0.80). Expansion characteristics of extrudates, such as piece density (116 to 302 g/L) and bulk density (67 to 201 g/L), were in most cases well correlated with both SME and T_{ds} (r of -0.61 to -0.90). Cell diameter ($\overline{D}$) decreased from 2.94 to 1.00 mm, while cell number density (N_{cell}) increased from 7 to 193 cells/ cm^3 with increase in WPI. WPI had a foaming effect as seen by the increase in N_{cell} accompanied by a decrease in $\overline{D}$. With increase in sucrose, $\overline{D}$ decreased from 2.70 to 1.29 mm, while N_{cell} did not change substantially. Sucrose did not contribute to the expansion and

foaming during extrusion. Number of spatial ruptures (7.7 to 11 mm^{-1}) during mechanical testing increased with N_{cell} which showed strong influence of microstructure on mechanical property. Lower in-barrel moisture (23%) exhibited higher T_s and SME, accompanied by higher expansion (lower piece and bulk densities).

INTRODUCTION

Material formulation and extrusion process parameters affect the foaming process during extrusion of biopolymers in terms of cell nucleation, expansion, collapse, and resultant foam microstructure. Foam microstructure, in turn, controls mechanical properties and texture. In order to understand the aforementioned relationships, this study investigated the material properties of biopolymeric model systems comprising of cornstarch, whey protein isolate and sucrose. The same model systems were extruded to produce brittle foams. A novel, more accurate and objective method for microstructure measurement was utilized to establish a link between material formulation, extrusion process parameters and cell structure. Moreover, the mechanical properties of the resultant foam were related to their microstructure.

Extrusion processing of biopolymeric materials involves a complex interaction of various physical, chemical and thermodynamic phenomena, making it very difficult to understand. In the case of expanded biopolymeric extrudates, various interactions between ingredients and process parameters result in vastly different foam characteristics. Besides starch which is usually the base biopolymer, other components such proteins and sucrose contribute to modify the physiochemical interactions and rheological behavior of the melt. They determine not only the overall expansion but also the internal microstructure of the extrudate. Certain proteins, such as whey proteins, are extremely important as a foaming agent in the food industry. The behavior of proteins at air-water interfaces can influence can influence foaming properties of biopolymers. Proteins are surface active agents capable of reducing surface tension, and enhancing foam stabilization (Kinsella and Soucie 1989, Phillips *et al.*1994). Rapid diffusion of protein molecules to the interface followed by unfolding and increased concentration allows them to entrap air. At the interface, proteins decrease surface energy and interfacial tension by interacting with both air and water molecules (Fennema 1985). In the presence of starch,

interaction between the two biopolymers is expected. Under extrusion conditions, starch fragmentation and protein denaturation cause stronger interaction between both polymers and formation of inter- and intramolecular bonds (Fernandez-Gutierrez *et al.* 2004). This causes changes in water absorption, water solubility indices and viscosity at the melt. Proteins also are able to aggregate, form larger structures and higher viscosity complexes allowing the retention of more water vapor during expansion. Upon cooling, the viscosity is enough to reduce shrinkage in the expanded extrudate. Gropper *et al.* (2002) studied the effect of specific mechanical energy (SME) on glass transition temperature (T_g) of protein-starch extrudates. Results from their study indicated that SME did not affect T_g. Fernandez-Gutierrez *et al.* (2004) studied the effect of protein (casein) on expansion index, bulk density and compression. Higher casein concentrations (at lower in-barrel moisture) had higher expansion index with lower bulk density and compression force. Wen *et al.* (1990) studied the same interaction under extrusion conditions. They observed that starch component of corn meal (composed of starch, lipid and protein) degraded more compared to starch in pure cornstarch and, therefore, led to lower viscosities for corn meal during extrusion. Other studies looked at protein and their effect on flour dough viscoelasticity as well as interaction with starch matrix (Shim and Mulvaney 2002, Apichartsrangkoon 2002).

Sucrose is another common additive in commercially extruded foods such as breakfast cereals and snack foods. It contributes to binding, flavor and browning characteristics. It is critical in controlling texture and mouthfeel, and acts as a humectant and carrier of flavor (Barrett *et al.* 1995). Together with high moisture, sucrose tends to act as a plasticizer and thus reducing the viscosity of the overall product. In the presence of starch, sucrose leads to competition for moisture (Sterling 1978) and delays starch gelatinization. Hsieh *et al.*(1990) reported radial and longitudinal expansion of extrudates, and lower bulk density with increased sucrose concentration (6 to 8%). At lower concentrations (0-4%), sucrose led to lower viscosities indicating more starch degradation. Other studies have also shown the effects of sucrose on specific mechanical energy, die pressure, melt temperature and collapse (Sopade and Le Grys 1991); on microstructure, mechanical strength and thermal properties (Barrett *et al.* 1995, Farhat *et al.* 2003); on glass transition (Sopade *et al.* 1991, Fan *et al.* 1996, Truong *et al.* 2004); and on expansion (Carvalho and Mitchell 2000).

In order to understand the dynamics of foaming, it is imperative to investigate the critical material properties responsible for cell nucleation, expansion, collapse, and formation of final microstructure of the extruded foam. The concept of glass transition is relevant to food processing. For example during extrusion of cereal-based food products, starch matrix lose their semi-crystalline structure and result in amorphous viscoelastic matrices. Food biopolymers unlike synthetic polymers, however, exhibit chemical heterogeneity due to their complex nature. This makes the measurement of glass transition by traditional methods, such as differential scanning calorimetry (DSC), more difficult (Roudaut *et al.* 2003). The phase transition analyzer (PTA) based on capillary rheometry, has the potential for measuring material properties of complex, heterogeneous biopolymers. The PTA greatly facilitates analysis of composite mixtures such as protein, sucrose and starch-containing matrices and provides valuable information on the phase transition properties (Strahm and Plattner, 2003). The PTA also utilizes relatively large sample size (~1.5 g) which helps in characterizing "bulk" material properties as opposed to micro-level properties in the case of DSC. The PTA measures the softening temperature (T_s), which is a phase transition property similar to glass transition temperature, of materials at elevated temperatures similar to those encountered during extrusion processing (~1-10 MPa). Moreover, the PTA determines the temperature required to lower viscosity sufficiently, (flow point temperature, T_f), allowing a material to be forced through a small orifice at similar pressures. The PTA, therefore, has the potential to help understand the role material properties play in extrusion processing (Strahm 1998, Strahm *et al.* 2000).

In order to understand the foaming process, it is also important to characterize the microstructure of extrudates. Processing focus and emphasis have shifted to the microstructure level (less than 100 μm) in an effort to understand the textural and sensory attributes of foods. Structural elements such as gas bubbles contribute greatly to food identity and quality (Aguilera 2005). Advances in imaging technology have led to powerful microscopes that can probe into foods from the atomic to the micron range, and in many instances, can do so non-intrusively, in real time (video microscopy) and in three dimensions (Flannery *et al.*1987; Sasov 1987). X-ray microtomography (XMT) successfully visualizes structure of various foams, non-intrusively, and in three dimensions. Studies done by Trater, Alavi and Rizvi (2005) has investigated the use of non-invasive, 3-D X-ray microtomography (XMT) for microstructure characterization, which eliminated the limitations of traditional 2-D and destructive imaging techniques like SEM and

optical microscopy. In their study, XMT proved to be efficient in accurately characterizing several microstructural features such as average cell equivalent diameter, wall thickness, and void fraction. Moreover, XMT generated images were more conducive to digital image processing than SEM or light microscope images because of 'razor-thin' depth of focus and sharp contrast between solid and void areas.

This study aims to understand foam formation by extrusion by investigating the relationships between material properties, processing parameters, and microstructure. The mechanical properties of the extrudates were also related to their expansion and microstructure. Model formulation systems based on cornstarch, whey protein isolate (WPI) and sucrose were utilized to investigate these relationships.

MATERIALS AND METHODS

Formulation

Unmodified cornstarch (~25% amylose and 75% amylopectin; Cargill Gel 03457, Cargill, Inc., Minneapolis, MN), whey protein isolate (~89% protein, <3% lactose, INPRO 90, Vitalus Nutrition Inc., Bellingham, W.A., UK) and sucrose (Great Value, Walmart Inc., Benington, AR) were used for the model formulation systems. Cornstarch was the base ingredient in each model system. WPI (0, 6, 12 and 18%) and sucrose (0, 2, 4 and 6%) were varied for the different treatments. Each formulation was pre-blended using a ribbon mixer.

Extrusion Processing

A Wenger TX-52 twin-screw extruder (Wenger Manufacturing, Sabetha, KS) with screw diameters of 52 mm and L/D ratio of 16:1, and a circular die diameter of 3.3 mm was used to extrude all materials. The feed rate of raw material was 60 kg/hr. The barrel temperature settings, screw profile and water injection points are presented in Figure 3.1. Water flow to the preconditioner was maintained at a constant 9.0 kg/hr. In-barrel moistures were adjusted to 23% or 27% by controlling the water flow into the extruder and taking into account the initial moisture (~10%) of the pre-mix going into the pre-conditioner. Extruder conditions were allowed to stabilize for approximately 10 min before samples were collected. The product was cut immediately after exiting the extruder die with a face-mounted rotary cutter turning at 690 RPM, and dried at 100°C with a double-pass dryer/cooler (4800 Series, Wenger Manufacturing,

Inc., Sabetha, KS) adjusted for 15 min. retention time (7.5 min. each for the top and bottom belts). Cooling was accomplished at 24°C with a 5 min. retention time on the cooling belt. Final moistures of the extrudate after drying ranged from 10 to 14%. The extrudates were allowed to further dry at room temperature to ~4%. All moisture contents are expressed on wet basis (wb).

Phase Transition Temperatures

Phase transition temperatures - softening temperature (T_s) and flow temperature (T_f), were determined for the raw materials. Moisture contents of the different treatments were elevated to in-barrel moisture levels (22.7% and 26.8%) by mixing approximately 5 g of cornstarch (~10% moisture) with the appropriate amounts of water (using an air displacement micropipette) in a small resealable plastic bag. The bag was sealed and the mixture thoroughly mixed. The different treatments were allowed to equilibrate for 12 hours at 5°C. T_s and T_f were determined using a Phase Transition Analyzer (PTA; Wenger Manufacturing, Inc., Sabetha, KS). The PTA cooling system was allowed to circulate for approximately 30 minutes. Chamber temperature was allowed to reach -5°C before each run. Approximately 1.85 g of sample was loaded unto the chamber. After installing the plunger and locking the system, a pressure of 10.0 MPa was applied initially to compact the sample. An operating pressure of 8.0 MPa was applied subsequently throughout the remainder of the testing. Temperature was increased at a rate of 8°C/min until the sample T_s (point of maximum sample compaction) was reached. Subsequently, pressure was temporarily released to allow the insertion of a 2 mm orifice beneath the sample. Once in place, the pressure was resumed and heating was continued from approximately 10°C below the T_s to 5°C above T_f at the same rate until the material flowed through the orifice. The flow temperature (T_f) was the initiation temperature for flow.

Process Parameters

Die pressure was measured using a pressure gauge located at the die. Die temperature (T_d) was measured using a thermocouple located at the die. This value estimates the product temperature at the extruder exit. Specific mechanical energy (*SME*) was computed as

$$SME = \frac{(L_r - L_e)\left(N_a / N_b\right)(P)(36)}{\dot{m}} \tag{3.1}$$

where L_r, motor load while running with product (%), L_e, motor load while running empty (~4%), N_a, actual screw speed, RPM (if <336, if screw speed ≥ 336 then N_a = 336), N_b, base screw speed, 336 RPM, P, rated power of extruder, 22.4 kW, $\dot{m}$, mass flow rate, kg/h

Extrudate Physical Properties

Bulk densities (δ) were determined by completely filling a 1 liter cup with extrudate pieces and measuring the mass of the filled pieces. Piece densities (ρ) were obtained by rapeseed displacement method (Penfield and Griswold 1979). Maximum expansion ratio (ER_{max}) and final expansion ratio (ER_{final}) were computed as shown in equations 3.2 and 3.3. Collapse ratio, ε, was computed as shown in equation 3.4:

$$ER_{\max} = \left(\frac{\pi \times r_m^{\,2}}{\pi \times r^2} \right) \tag{3.2}$$

$$ER_{final} = \left(\frac{\pi \times r_f^{\,2}}{\pi \times r^2} \right) \tag{3.3}$$

$$\varepsilon = 1 - \frac{ER_{final}}{ER_{\max}} \tag{3.4}$$

where r_m, maximum radius of the extrudate coming off the die, r, radius of the extruder die, r_f, final extrudate radius after drying.

Microstructure

One extrudate sample from each replicate extrusion run (2 replications) was selected for image analysis. A desk-top X-ray microtomography imaging system (Model 1072, 20-100 kV/0-250 μA, SkyScan, Aartselaar, Belgium) set at 40 kV/100 μA (to obtain optimum contrast between solid and gaseous phases) was used to scan the samples. A CCD camera was used to collect the X-ray data. Image reconstruction software was provided by Skyscan. For each treatment, a set of 2-D images, or "slices", for the entire sample was obtained after reconstruction. This set was partitioned into a volume of interest (VOI), which consisted of 15 consecutive 2-D slices separated by a constant distance t, from the central portion of the cylindrical sample. This VOI was used for all further analyses. Calculations of microstructure

parameters measured were based on measurements of cell perimeter, void (white) area and solid (black) area obtained for each slice using image analysis software developed by Das and Alavi (unpublished). The computed 3-D parameters included volume weighted average cell diameter ($\overline{D}$), cell wall thickness (t_{wall}) and cell number density (N_{cell}). Details of XMT scanning, image reconstruction and measurement of 2-D features and computation of 3-D microstructure have been described previously (Trater et al. 2005). Measurement and analysis of the microstructure required a significant amount of time so only one representative sample from each extrusion treatment and its duplicate was analyzed.

Mechanical Properties

Thirty samples for each treatment were analyzed using a Model TA.XT2 Texture Analyzer (Stable Micro Systems, Surrey, United Kingdom) for compression. Samples with approximately the same dimensions (diameter and height) were chosen. Settings were 'measure force in compression' (test mode), 10 mm/s (test speed) and 90% (distance of compression). A 38 mm diameter probe was used for compression. Stress-strain curve was determined from the force deformation data and sample dimensions. Compression modulus (E_c) was calculated as the slope of the linear viscoelastic region before first rupture (or fracture). Crushing stress (σ_{cr}) was calculated as the mean stress from the point to first rupture (or fracture) to first point of densification. Number of peaks (n) integral of the curve (S or area below the curve from 0 to maximum strain), and distance of compression (d) were computed. From n, S and d values, the following parameters were calculated (Bouvier *et al.* 1997).

$$N_{sr} = \frac{n}{d} \quad (\text{mm}^{-1}) \tag{3.5}$$

$$F_{cr} = \frac{S}{d} \quad (\text{N}) \tag{3.6}$$

$$W_c = \frac{F_c}{N_{sr}} = \frac{S/d}{n/d} \quad (\text{N-mm}) \tag{3.7}$$

Where N_{sr} is the number of spatial ruptures, F_{cr} is average crushing force and W_c is crispness work.

Experimental Design and Statistical Analysis

A 2x 4 factorial experimental design, with two levels of MC (23 and 27%) and four levels of WPI (0, 6, 12, and 18%) was used for the cornstarch-WPI model formulation system. Similarly, 2x4 factorial experimental design, with two levels of MC (23 and 27%) and four levels of sucrose (0, 2, 4, and 6%) was used for the cornstarch-sucrose model formulation system. A 2x2 factorial design, with two levels of WPI (6 and 12%) and two levels of sucrose (2 and 4%) was used for another set of model systems to study interaction between WPI and sucrose. Each extrusion treatment was duplicated on a different day. Phase transition and extrudate physical properties were measured in triplicates for each model system and extrusion treatment, respectively. Mechanical test was performed on thirty samples per treatment. Microstructure parameters were measured for one sample from each replicate of an extrusion treatment. Standard deviation for replicated parameters was computed. Pairwise comparison using least significant difference (LSD) was used to determine statistical difference among treatments. LSD computations were done using SAS (SAS System for Windows, Release 8.2, SAS Institute, Inc., Cary, NC). The 'PEARSON' function of EXCEL™ software (2002 edition, Microsoft Corporation, Seattle, WA) was used for finding the Pearson's coefficient of correlation (r) between any two data sets. To provide descriptive terms to the degree of correlation, criteria outlined by Franzblau (1958) were used ($|r| < 0.20$, negligible; $|r| = 0.20$ to 0.40, low; $|r| = 0.40$ to 0.60, moderate; $|r| = 0.60$ - 0.80, marked; and $|r| > 0.80$, high).

RESULTS AND DISCUSSION

Figures 3.2, 3.3 and 3.4 show representative two dimensional slices and cell size distributions from different experimental treatments. Figures 3.5, 3.6, 3.7, 3.8 and 3.9 are plots of material, process and extrudate properties at different WPI levels. Figures 3.10, 3.11, 3.12 and 3.13 are plots of material, process and extrudate properties at different sucrose levels. Tables 3.1 and 3.2 show Pearson's correlation coefficients (r) for different parameters measured in this study.

Phase Transition Properties (T_s and T_f)

For the cornstarch-WPI model system (Figure 3.5), depending on the WPI level, softening temperature (T_s) ranged from 41.2 to 83.1°C, while flow temperature (T_f) ranged from

93.6 to 130°C. Due to high variability, there were no significant differences (α=0.05) between measurements of these phase transition temperatures at different WPI levels. However, T_s and T_f both had decreasing trends with increase in WPI level at 23% in-barrel moisture. Both T_s and T_f exhibited high negative correlation with WPI level (r=-0.94 and -0.86, respectively; Table 3.1). At 27% in-barrel moisture, T_s exhibited a similar trend with increase in WPI level, with a high negative correlation of -0.88 (Table 3.2). However, T_f had negligible correlation with WPI level. Madeka and Kokini (1992) studied interaction between starch and whey proteins. They reported an increase in viscosity with greater interaction between starch and protein. On the contrary, in our experiments, T_s and T_f had a general decreasing trend with increasing WPI level indicating a decrease in viscosity. One drawback of the PTA technique is the absence of any mixing or shear during the testing. This possibly led to very little interaction between the starch and WPI biopolymers, and thus, a negligible viscosity increasing effect. In fact, the lower starch fraction with increasing WPI level probably led to reduction in overall viscosity and the phase transition temperatures (T_s and T_f) in the absence of significant interactions between starch and WPI.

For the cornstarch-sucrose model system (Figure 3.10), depending on the sucrose level, T_s ranged from 57.0 to 91.4°C, while T_f ranged from 72.9 to 130°C. There were no significant differences (α=0.05) between phase transition temperatures at different sucrose levels. No particular trends were observed for either T_s and T_f with increase in sucrose level, and the correlation between these parameters were inconsistent (Tables 3.1 and 3.2). Sucrose is known to have plasticizing effects on starch-based melts, and it also competes with starch for moisture thus affecting the degree of gelatinization and the resultant viscosity (Jin *et al.* 1994). However, this was not evident with the phase transition data.

Lower T_s and T_f were evident for higher moisture (27%). It is a well known fact that water acts as a plasticizer in starch based materials, and high in-barrel moisture has been shown to result in lower melt viscosities during extrusion (Li *et al.* 2004).

Specific Mechanical Energy (SME), T_{ds} and T_{df}

For the cornstarch-WPI model system, SME ranged from 275 to 359 kJ/kg. Figure 3.5 clearly shows increasing SME with increasing WPI levels. SME was highly correlated with WPI with r values of 0.95 and 0.91 for 23 and 27% in-barrel moisture, respectively (Tables 3.1 and 3.2). Temperature behind the die, T_s and T_f were used to compute the net driving force of

expansion T_{ds} and T_{df}. T_{ds} was the difference between T_d and T_s while T_{df} , the difference between T_d and T_f. T_{ds} ranged from 51.9 to 98.8°C while T_{df} ranged from 5.00 to 46.4°C. Similar to SME, T_{ds} increased with increase in WPI levels (r=093 and 0.96 for 23% and 27% in-barrel moisture, respectively).

For the cornstarch-sucrose model system, SME (235 to 290 kJ/kg) decreased with increase in sucrose levels. SME had moderate to high correlation with sucrose level (r=-0.89 and -0.54 for 23% and 27%, respectively; Tables 3.1 and 3.2). Other studies (Barrett *et al.* 1995, Fan *et al.* 1996, Carvalho and Mitchell 2000) showed a similar trend wherein addition of sucrose decreased expansion, SME and starch conversion. T_{ds} ranged from 58.0 to 77.3°C, and T_{df} ranged from 12.3 to 61.9°C. It is clear from Figure 3.10 that T_{ds} had a decreasing trend with increasing sucrose level although the differences were not significant (α=0.05). T_{ds} and SME were in agreement indicating reduced driving force for expansion due to the plasticizing effect of sucrose and resultant less viscous dissipation.

Both SME and T_{ds} are process dependent parameters that represent the driving force for expansion, which was greater with increasing WPI level possibly due to the viscosity enhancing effect and greater viscous dissipation with WPI (Madeka and Kokini 1992).

Extrudate Physical Properties

Figure 3.6 shows bulk density (δ) and piece density (ρ) trend along with SME at varying WPI levels. ρ ranged from 116 to 257 g/L, while δ ranged from 67.0 to 184 g/L. Both δ and ρ decreased with increase in WPI indicating greater expansion, and had a marked to high correlation (r =-0.72 to -0.98 for 23% and 27%, respectively; Tables 3.1 and 3.2). Higher driving force (SME and T_{ds}) accompanied by reduced collapse due to gelation of whey proteins (Alavi *et al.* 1999) were probably the primary factors responsible for higher expansion with increase in WPI level. Figure 3.11 shows δ and ρ trend along with SME at varying sucrose levels. ρ ranged from 157 to 302 g/L while δ ranged 92.5 to 201 g/L. Both δ and ρ, increased with increase in sucrose indicating reduced expansion. SME had marked to high correlations (r ranging from 0.61 to -0.90) with δ and ρ, with the exception of ρ at 27% (Tables 3.1 and 3.2). Jin et al. (1994) also observed decreased in δ with addition of sucrose. Lower driving force (SME and T_{ds}) accompanied by greater collapse due to the plasticizing effect of sucrose (Sopade and Le Grys 1991) were probably the primary factors responsible for decrease in expansion with

increase in sucrose level. This has been commonly observed in extrusion of biopolymeric foams and several studies have reported increase in extrudate expansion with higher SME (Garber *et al.* 1997, Desrumaux *et al.* 1998 and Carvalho *et al*. 2000).

In general, higher in-barrel moisture led to reduced expansion (Figures 3.6 and 3.11), because of lower SME.

Extrudate Microstructure

Figure 3.7 shows average cell diameter ($\overline{D}$) and cell number density (N_{cell}) along with ρ of extrudates at varying WPI levels. $\overline{D}$ ranged 1.00 to 2.94 mm, t_{wall} ranged from 0.04 to 0.27 mm and N_{cell} ranged from 7 to 193 cells/cm^3. $\overline{D}$ decreased with increase in WPI. However, N_{cell} increased with WPI, indicating enhanced nucleation in the extrusion melt because of the foaming characteristics of WPI. It was clear that the increase in expansion with WPI levels as indicated by decrease in ρ was mainly due to greater nucleation rather than higher growth of cells. N_{cell} had marked to high correlation with WPI (r =0.82 and 0.69 for 23% and 27%, respectively; Tables 3.1 and 3.2). Figure 3.12 shows $\overline{D}$ and N_{cell} along with ρ at varying sucrose levels. $\overline{D}$ ranged 1.29 to 2.70 mm, t_{wall} ranged from 0.07 to 0.27 mm and N_{cell} ranged from 1 to 55 cells/cm^3. $\overline{D}$ decreased with increase in sucrose indicating less expansion. Barrett *et al.* (1995) also observed the same results (reduced cell size with addition of sucrose). N_{cell} did not show any increasing or decreasing trend indicating no change in nucleation with increase in sucrose level. $\overline{D}$ exhibited a high correlation with sucrose level with r=-0.86 and -0.90 for 23% and 27% in-barrel moistures, respectively (Table 3.1 and 3.2). It is clear that the lower expansion with increase in sucrose level as indicated by higher densities was due to lower cell size, which in turn was probably caused by less cell growth and/or collapse of cells.

Extrudate Mechanical Properties

For cornstarch-WPI model system, compression modulus (E_c) ranged from 0.31 to 1.3 MPa, crushing stress (σ_{cr}) ranged from 42 to 120 kPa, number of spatial ruptures (N_{sr}) ranged from 7.7 to 11 mm^{-1}, average crushing force (F_{cr}) ranged from 12 to 26 N and crispness work (W_c) ranged from 1.3 to 4.1 N-mm. Figure 3.8 shows E_c along with ρ at varying WPI levels. Both parameters decreased with increasing WPI. For cornstarch-sucrose model systems, E_c ranged from 0.45 to 2.1 MPa, σ_{cr} ranged from 56 to 150 kPa, N_{sr} ranged from 8.3 to 11 mm^{-1}, F_{cr}

ranged from 14 to 30 N and W_c ranged from 1.3 to 3.6 N-mm. Figure 3.13 shows E_c along with ρ at varying sucrose levels. Both parameters were increasing with increasing sucrose. High correlations were between observed between δ and ρ and E_c (r=0.81 to 0.94) with the exception of ρ at 27% in-barrel moisture (Tables 3.1 and 3.2). Foam density is known to be proportional to its modulus based on several existing mechanical models. Agbisit *et al*. (2007) also observed high correlation between ρ and E_c for cornstarch based extrudates. Figure 3.9 shows N_{cell} and N_{sr} at varying WPI levels. Both N_{cell} and N_{sr} increased with increase in WPI. This was as expected since more cells meant more individual ruptures during compression, therefore, higher N_{sr}.

Whey Protein-Sucrose Interactions

Table 3.3, 3.4 and 3.5 show the material properties, process related parameters, physical, microstructure and mechanical properties of extrudates from model systems based on cornstarch and varying levels of WPI and sucrose. T_s values ranged from 65.4 to 83.1°C while T_f ranged from 79.8 to 130°C. WPI-sucrose combinations exhibited lower T_s and T_f compared to the control (0% WPI, 0% sucrose). T_s values were not significantly different among treatments while T_f were significantly different only between WPI levels. No significant differences in SME and ρ could be seen among treatments although δ values were significantly different between WPI levels. (Table 3.3). Similarly, microstructure parameters did not differ significantly among treatments (Table 3.4). Mechanical properties σ_{cr}, F_{cr} and W_c were significantly different between treatments only between WPI levels (Table 3.5). WPI apparently had greater effect compared to sucrose on different extrudate properties. Inconsistencies and lack of trend can be attributed to interactions among cornstarch, WPI and sucrose. Their interactions together with moisture led to the formation of complex structural matrices during the extrusion process.

CONCLUSION

WPI was a key ingredient in enhancing foam formation by increased nucleation. Sucrose, on the other hand, inhibited expansion and did not promote nucleation. Marked to high correlations were observed between WPI and sucrose levels, key process related (T_{ds} and SME) and extrudate expansion, and enabled greater understanding of the foaming and expansion process during extrusion. In general, material formulation and extrusion process parameters

clearly affected the foaming process in terms of expansion, cell nucleation, and resultant foam microstructure.

The use of the PTA is a valuable tool in evaluating material properties of complex formulations. However, the lack of mixing and shear during testing results in limitations of this technique for characterizing key material properties that can "predict" behavior of biopolymers in extrusion conditions. Non-invasive XMT technique enabled objective quantification of key microstructure parameters, and aided in understanding of the complex interrelationships between material formulation, process parameters, microstructure and mechanical properties of extruded foams from cornstarch-based model formulation systems.

ACKNOWLEDGEMENTS

This study was funded by the USDA, CSREES, National Research Initiative (NRI) Competitive Grants Program (Award Number 2003-35503-13999). The authors would like to thank Mr. Eric Maichel for his technical assistance, Dr. X. Susan Sun for the conceptualization of this project, Wenger Manufacturing, Inc. (Sabetha, KS) and Micro Photonics, Inc. (Allentown, PA) for their continued support to the extrusion laboratory at Kansas State University.

REFERENCES

Agbisit, R., Alavi, S., Cheng, E., Herald, T., and Trater, A. (2007). Relationships between microstructure and mechanical properties of cellular cornstarch extrudates. *J. Texture Studies* 38, 199-219.

Aguilera, J. M. (2005). Why food microstructure? *Journal of Food Engineering*, 67, 3-11.

Apichartsrangkoon, A. (2002). Dynamic viscoelastic properties of heated gluten/soy protein gels. *Journal of Food Science*, 67(2), 653-657.

Barrett, A., Kaletunc, G., Rosenburg, S. and Breslauer, K. (1995). Effect of sucrose on the structure, mechanical strength and thermal properties of corn extrudates. *Carbohydrate Polymers*, 26, 261-269.

Carvalho, C. W. P. and Mitchell, J. R. (2000). Effect of sugar on the extrusion of maize grits and wheat flour. *International Journal of Food Science and Technology,* 35, 569-576.

Desrumaux, A., Bouvier, J. M. and Burri, J. (1998). Corn grits particle size and distribution effects on the characteristics of expanded extrudates. *Journal of Food Science*, 63(5), 858-863.

Fan, J., Mitchell, J. R. and Blanshard, J. M. V. (1996). The effect of sugars on the extrusion of maize grits: I. the role of the glass transition in determining product density and shape. *International Journal of Food Science and Technology,* 31, 55-65.

Farhat, I. A., Mousia, Z. and Mitchell, J. R. (2003). Structure and thermomechanical properties of extruded amylopectin-sucrose system. *Carbohydrate Polymers*, 52, 29-37.

Fennema, O. R. ed. (1985). *Food Chemistry*. New York:Marcel Dekker, Inc.

Fernández-Gutiérrez, J. A., San Martín-Martínez, E., Martínez-Bustos, F. and Cruz-Orea, A. (2004). Physicochemical properties of casein-starch interaction obtained by extrusion process. *Starch/Stärke*, 56, 190-198.

Flannery, B. P., Deckman, H. W., Roberge, W. G. and D'Amico, K. L. (1987). Three dimensional x-ray microtomography. *Science*, 237, 1439-1444.

Garber, B. W., Hsieh, F., and Huff, H. E. (1997). Influence of particle size on the twin-screw extrusion of corn meal. *Cereal Chem*. 74, 656-661.

Gropper, M., Moraru, C. I. and Kokini, J. L. (2002). Effects of specific mechanical energy on properties of extruded protein-starch mixtures. *Cereal Chem.*, 79(3), 429-433.

Hsieh, F., Peng, I. C. and Huff, H. E. (1990). Effects of salt, sugar and screw speed on processing and product variables of corn meal extruded with a twin screw extruder. *Journal of Food Science*.

Jin, Z., Hsieh, F., and Huff, H. E. (1994). Extrusion cooking of corn meal with soy, fiber, salt and sugar. *Cereal Chem.* 71(3), 227-234.

Kaletunc, G., and Breslauer, K. J. (1993). Glass transitions of extrudates: relationship with processing-induced fragmentation and end-product attributes. *Cereal Chem*, 70(5), 548-552.

Kinsella, J. E. ed. (1995). *Advances in Food and Nutrition Research*. London: Academic Press, Inc.

Kinsella, J. E. and Soucie, W. G. eds. (1989). *Food Proteins*. Phoenix, AR: American Oil Chemists' Society.

Li, P. X., Campanella, O. H. and Hardacre, A. K. (2004). Using an in-line slit-die viscometer to study effects of extrusion parameters on corn melt rheology. *Cereal Chemistry*, 81(1), 70-76.

Madeka, H. and Kokini, J. L. (1992). Effect of addition of zein and gliadin on the rheological properties of amylopectin starch with low-to-intermediate moisture. *Cereal Chem.* 69(5), 489-494.

Penfield, M.P. and Griswold, R.H. (1979). *The Experimental Study of Food*. Boston, MA:Houghton Mifflin Company.

Phillips, L. G., and Kinsella, J. E. eds. (1994). *Structure-Function Properties of Food Proteins*. San Diego, CA:Academic Press Inc.

Roudaut, G., Dacremont, C., Valles Pamies, B., Colas, B. and Le Meste, M. (2002). Crispness: a critical review on sensory and material science approaches. *Trends in Food Science & Technology*, 13, 217-227.

Sasov, A. Y. (1987). Microtomography. II. examples of applications. *Journal of Microscopy*, 147(2), 179-192.

Shim, J. and Mulvaney, S. J. (2002). Effects of pregelatinization conditions and added whey protein isolate on corn starch dough properties. *Cereal Foods World*, 47(9), 440-446.

Sterling, C. (1978). Textural qualities and molecular structure of starch products. *J. Texture Studies*, 9, 225.

Strahm, B. (1998). Fundamentals of polymer science as an applied extrusion tool. *Cereal Foods World*, 43, 621-625.

Strahm, B., Plattner, B., Huber, G., and Rokey, G. (2000). Application of food polymer science and capillary rheometry in evaluating complex extruded products. *Cereal Foods World*, 45(7), 300-302.

Strahm, B., and Plattner, B. (2003). Phase Transition Analyzer. *United States Patent*: Patent No. US 6,534,005 B1.

Sopade, P. A. and Le Grys, G. A. (1991). Effect of added sucrose on extrusion cooking of maize starch. *Food Control*, 103-109.

Sopade, P. A., Kearsley, M. W. and Le Grys, G. A. (1991). Significance of starch-sucrose interaction in extrusion cooking. *Food Control*, 181-184.

Trater, A. M., Alavi, S. H., and Rizvi, S. S. H. (2005). Study of microstructure development in extruded biopolymeric foams: non-invasive image analysis using computer-aided X-ray microtomography. *Food Research International*, 38, 709-719.

Truong, V., Bhandari, B. R., Howes, T. and Adhikari, B. (2004). Glass transition behaviour of fructose. *International Journal of Food Science and Technology*, 39, 569-578.

Wen, L-F, Rodis, P., and Wasserman, B. P. (1990). Starch fragmentation and protein insolubilization during twin-screw extrusion of corn meal. *Cereal Chem.*, 67(3), 268-275.

FIGURES AND TABLES

Figure 3.1 Diagram of screw configuration, injection sites, and barrel temperatures for all treatments.

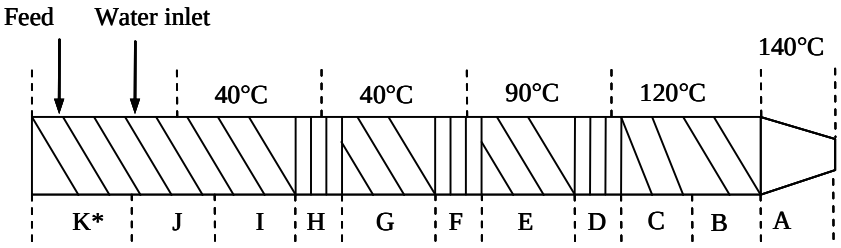

Section	Number of elements	Element length, mm	Element description
A	1	78	¾ pitch, double flighted, conical
B	1	78	¾ pitch, double flighted
C	1	52	½ pitch, double flighted
D	1	26	kneading block, forward
E	1	78	¾ pitch, double flighted
F	1	26	kneading block, forward
G	1	78	¾ pitch, double flighted
H	1	26	kneading block, forward
I	1	78	¾ pitch, double flighted
J	2	78	full pitch, double flighted
K	2	78	¾ pitch, double flighted

*The first two elements of the right shaft at the inlet (K) are ¾ pitch, single flighted.

Figure 3.2 Representative sample slices of cornstarch-WPI extrudates and their cell size distribution.

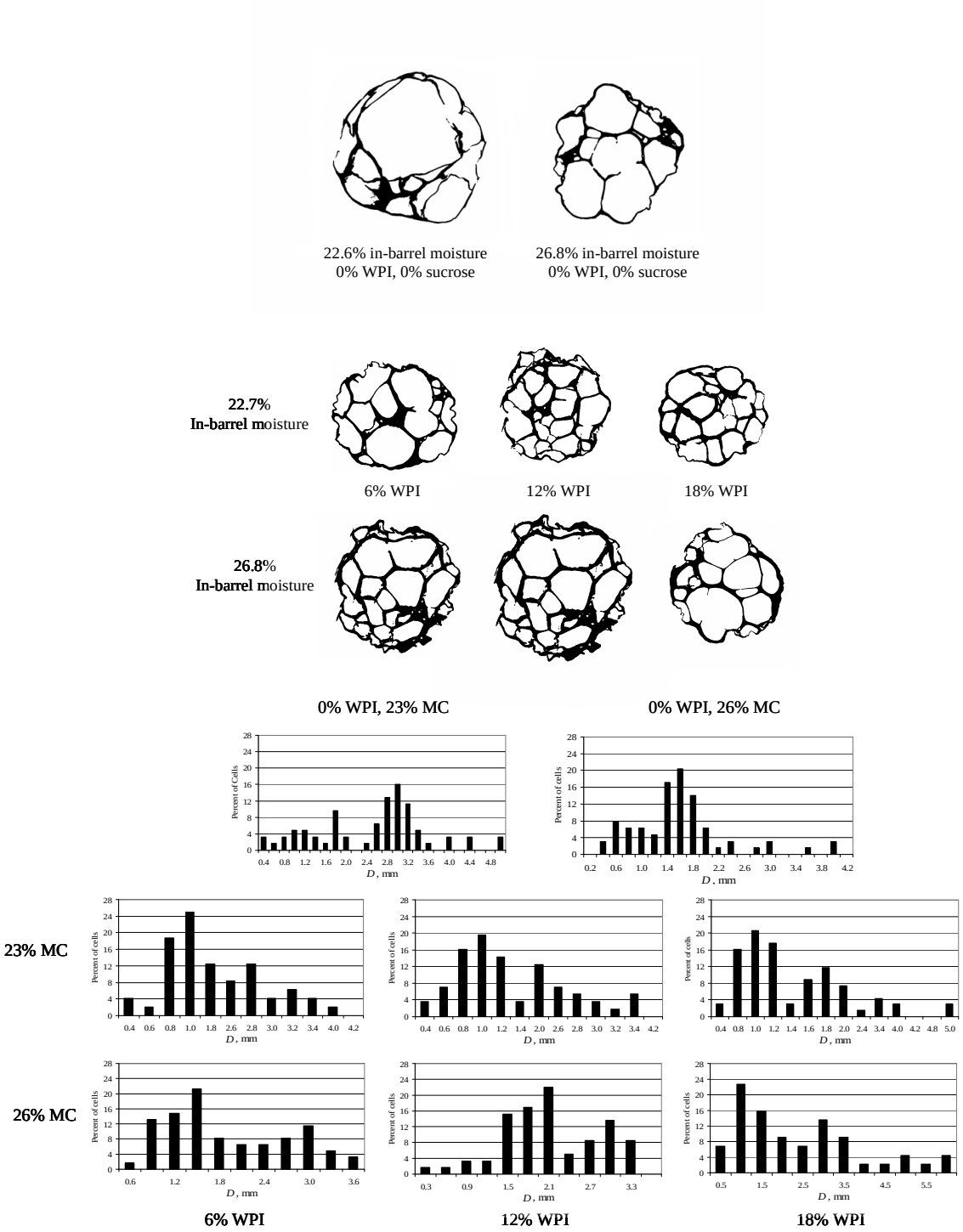

Figure 3.3 Representative sample slices of cornstarch-sucrose extrudates and their cell size distribution.

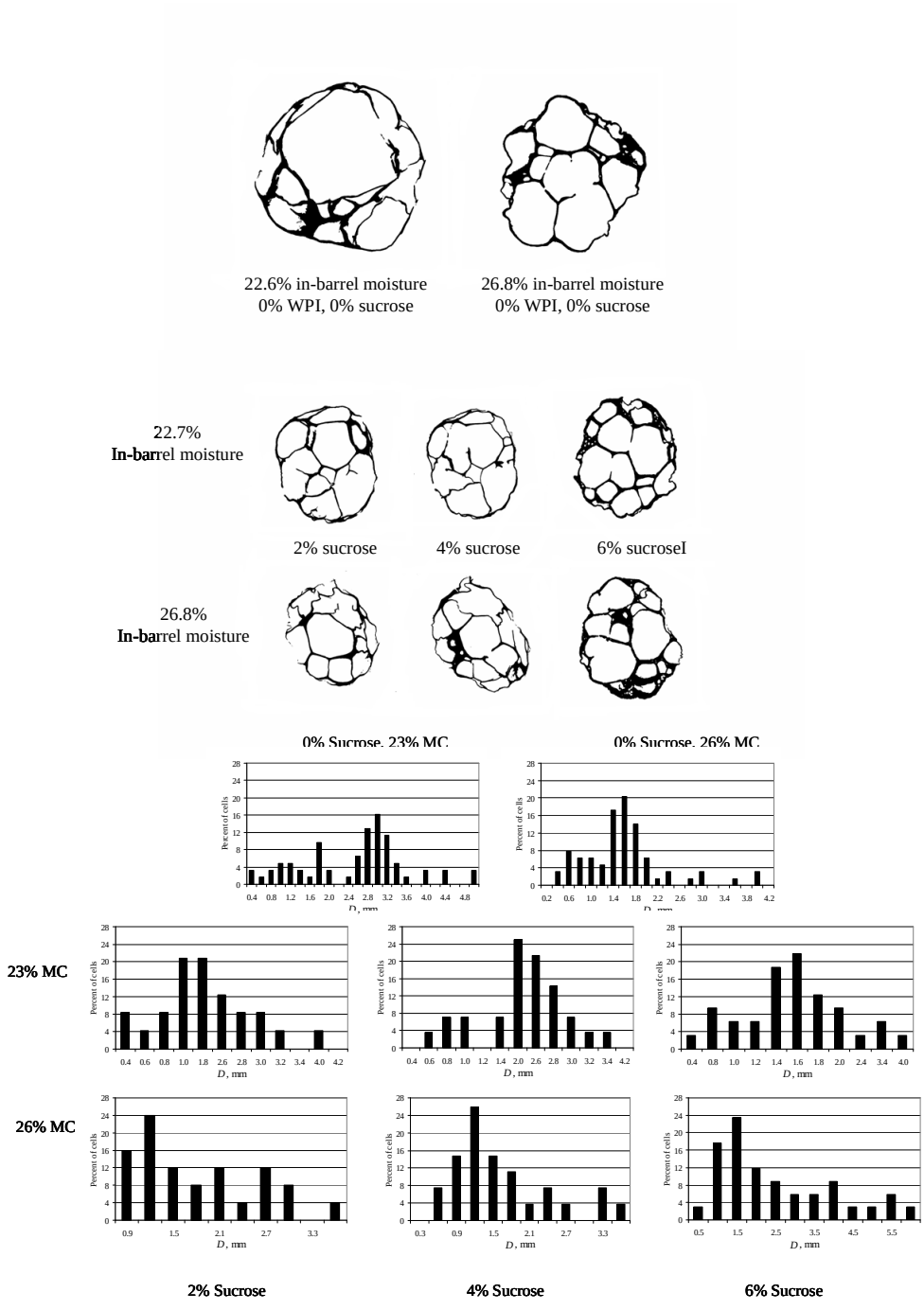

Figure 3.4 Representative sample slices of cornstarch-WPI-sucrose extrudates and their cell size distribution.

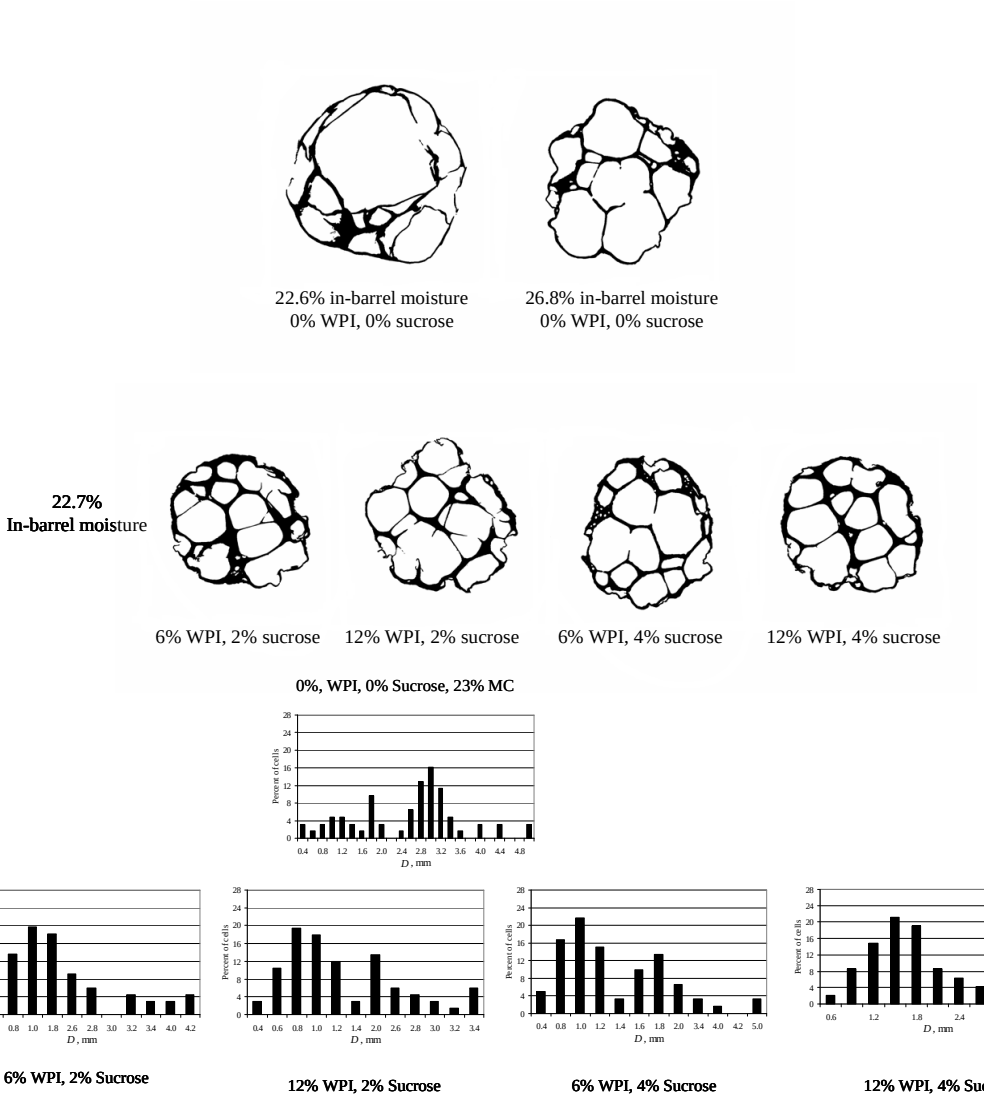

Figure 3.5 Softening temperature (T_s), difference between melt and softening temperature (T_{ds}) and specific mechanical energy (SME) at different whey protein isolate (WPI) levels and moisture contents. Error bars represent least significant differences (LSD).

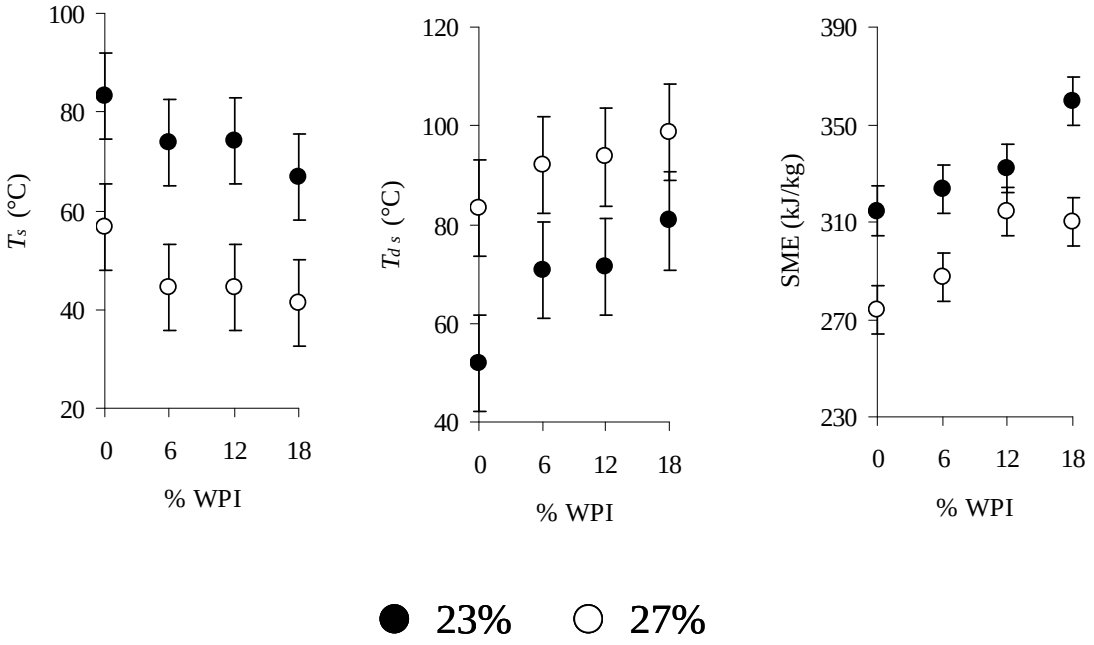

Figure 3.6 Specific mechanical energy (SME), bulk density (δ) and piece density (ρ) at different whey protein isolate (WPI) levels and moisture contents. Error bars represent least significant differences (LSD).

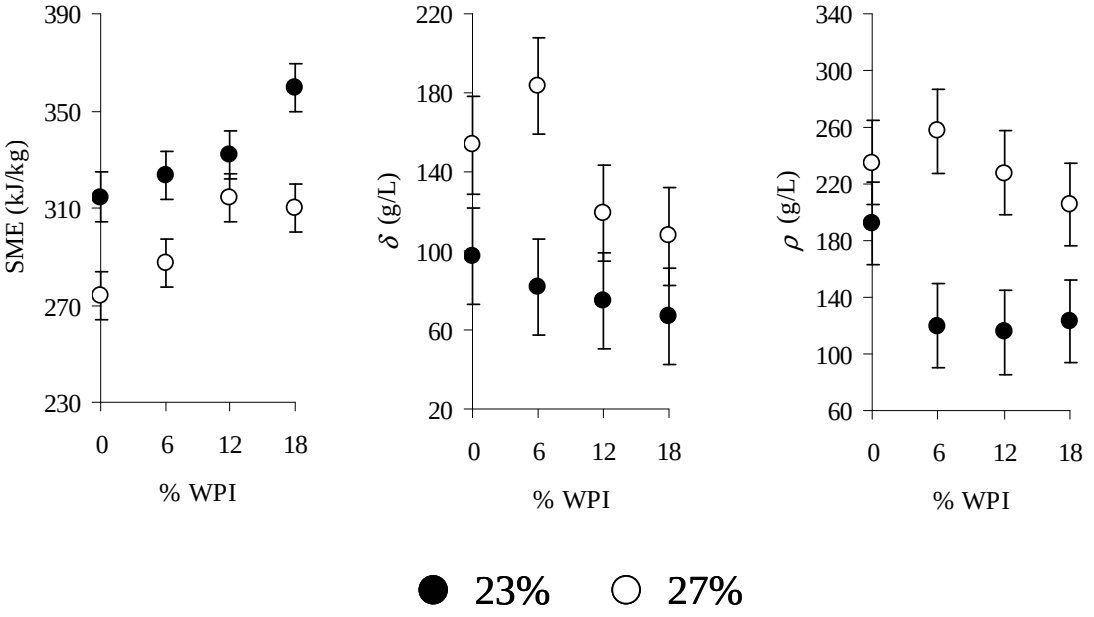

Figure 3.7 Piece density (ρ), cell diameter ($\overline{D}$) and cell number density (N_{cell}) at different whey protein isolate (WPI) levels and moisture contents. Error bars represent least significant differences (LSD).

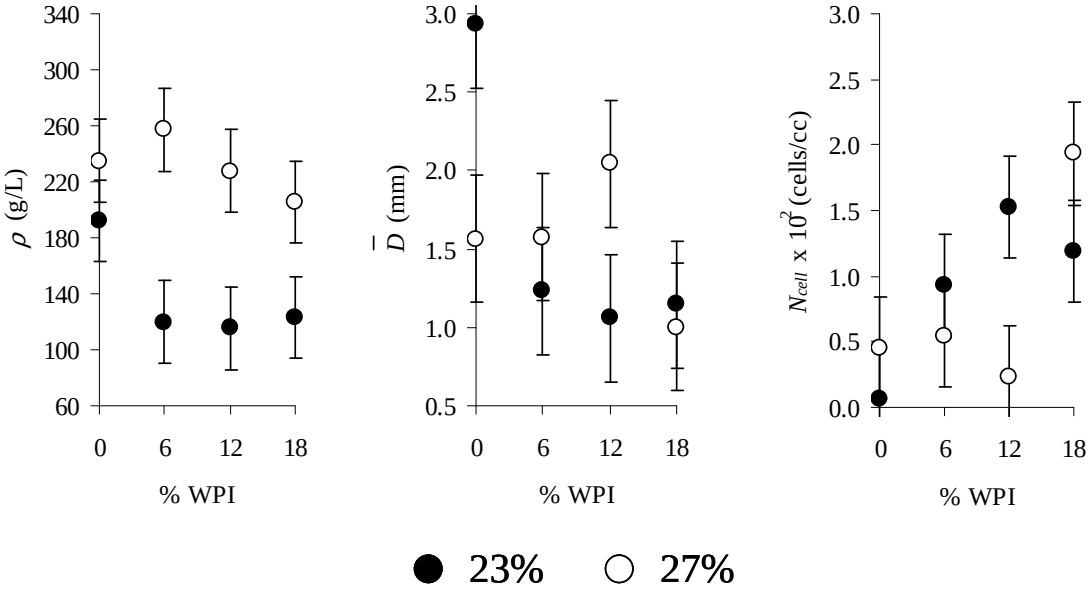

Figure 3.8 Piece density (ρ) and compression modulus (E_c) at different whey protein isolate (WPI) levels and moisture contents. Error bars represent least significant differences (LSD).

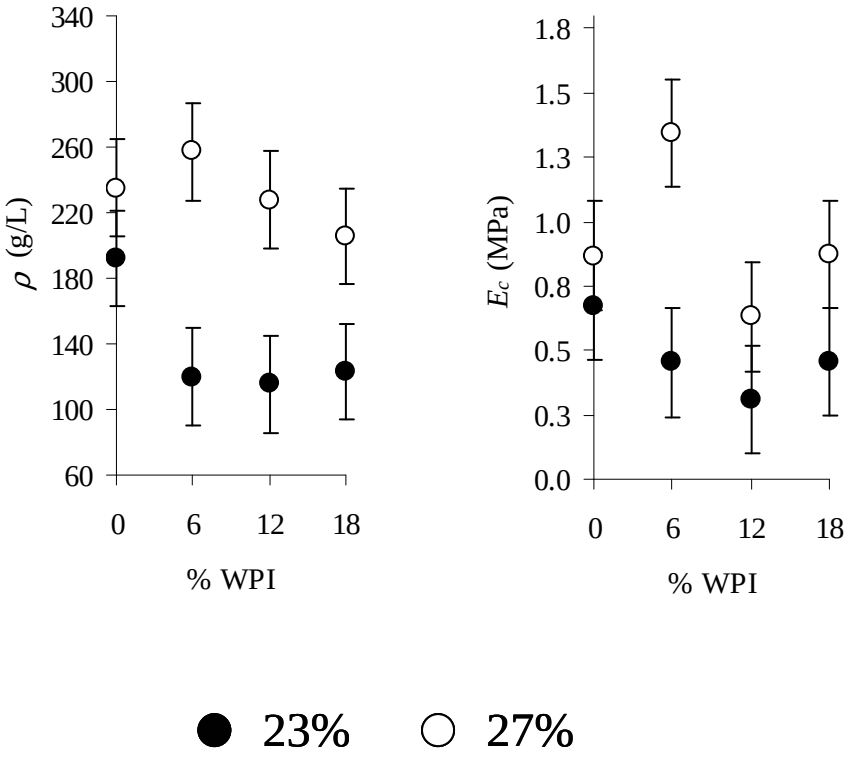

Figure 3.9 Cell number density (N_{cell}) and number of spatial ruptures (N_{sr}) at different whey protein isolate (WPI) levels and moisture contents. Error bars represent least significant differences (LSD).

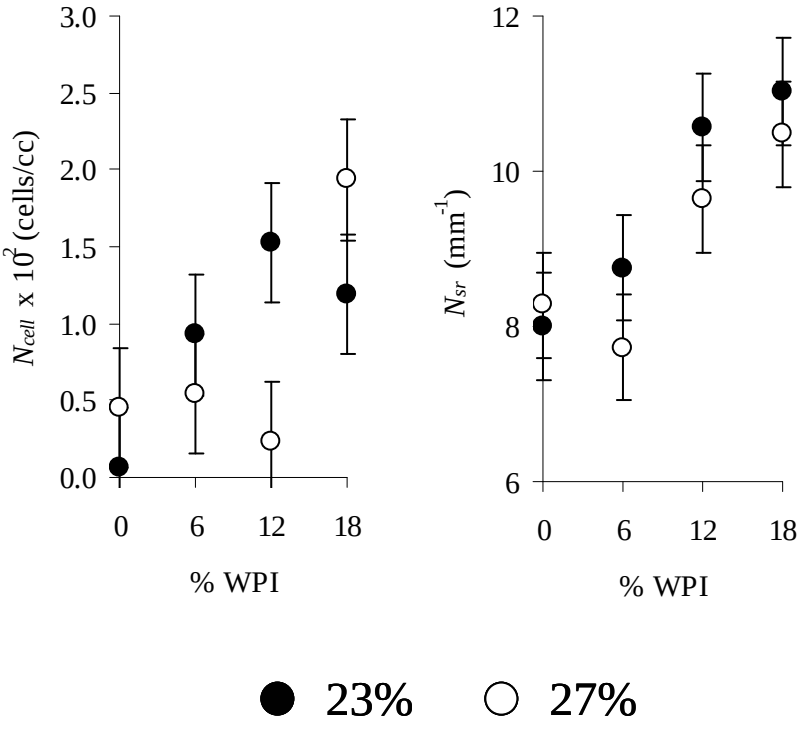

Figure 3.10 Softening temperature (T_s), difference between melt and softening temperature (T_{ds}) and specific mechanical energy (SME) at different sucrose levels and moisture contents. Error bars represent least significant differences (LSD).

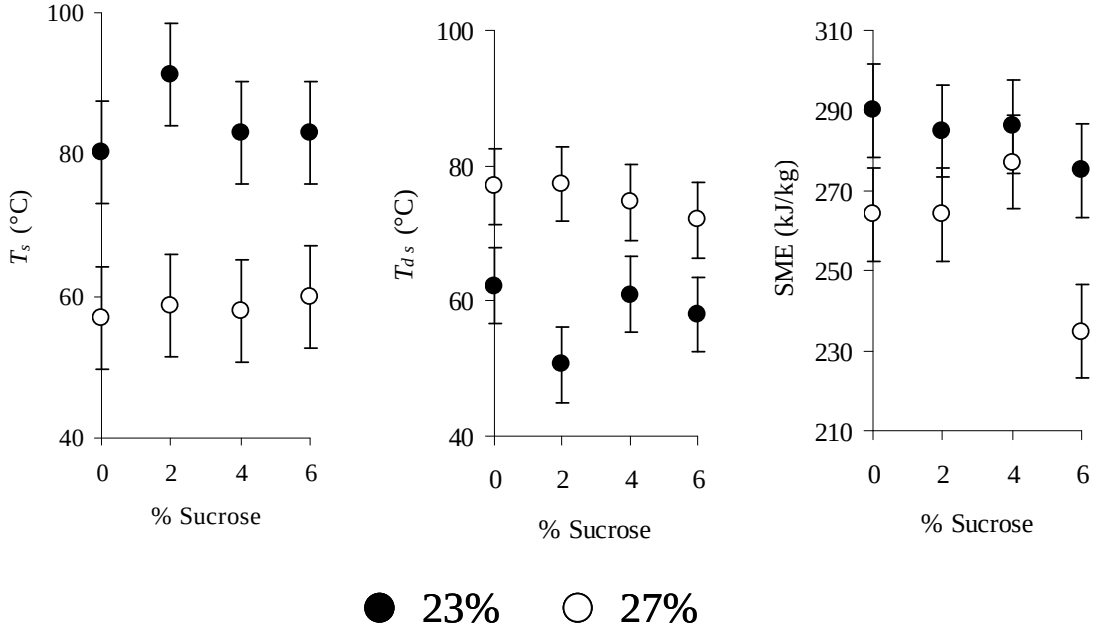

Figure 3.11 Specific mechanical energy (SME), bulk density (δ) and piece density (ρ) at different sucrose levels and moisture contents. Error bars represent least significant differences (LSD).

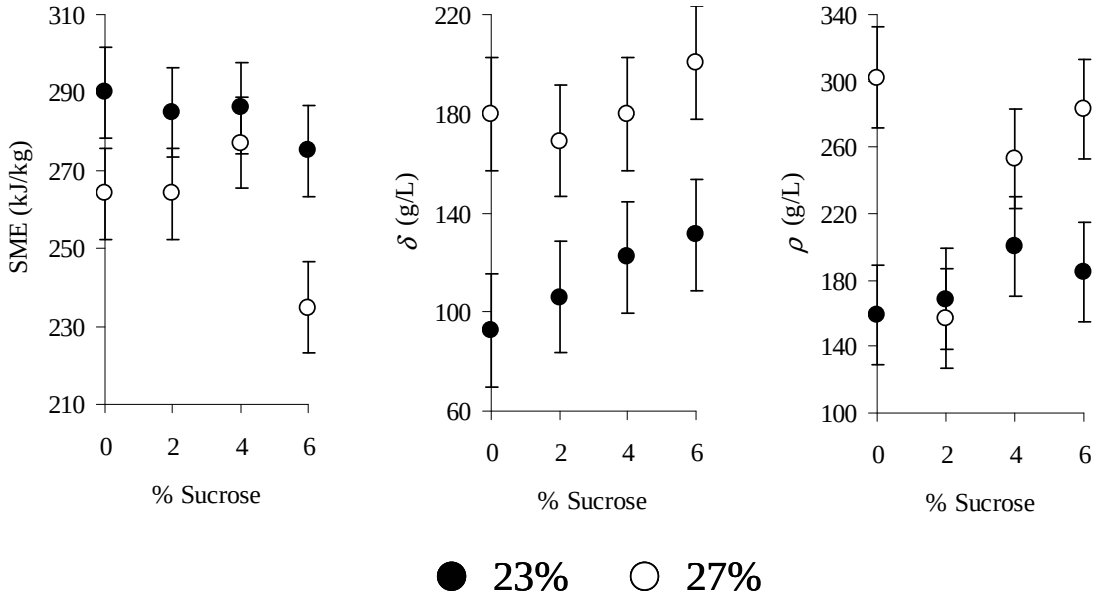

Figure 3.12 Piece density (ρ), cell diameter ($\overline{D}$) and cell number density (N_{cell}) at different sucrose levels and moisture contents. Error bars represent least significant differences (LSD).

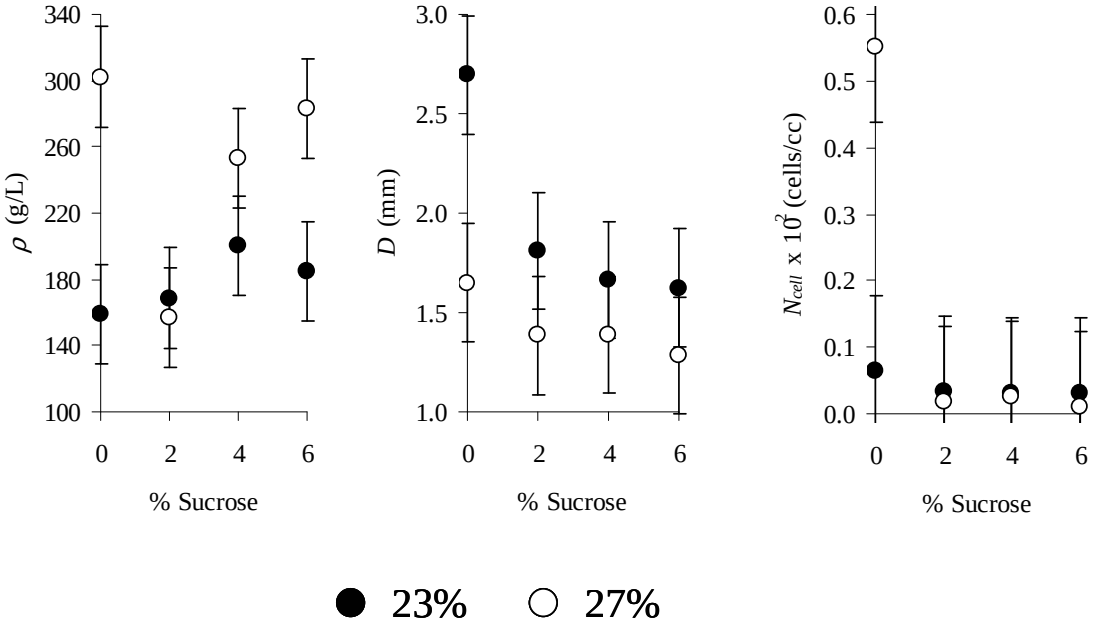

Figure 3.13 Piece density (ρ) and compression modulus (E_c) at different whey protein isolate (WPI) levels and moisture contents. Error bars represent least significant differences (LSD).

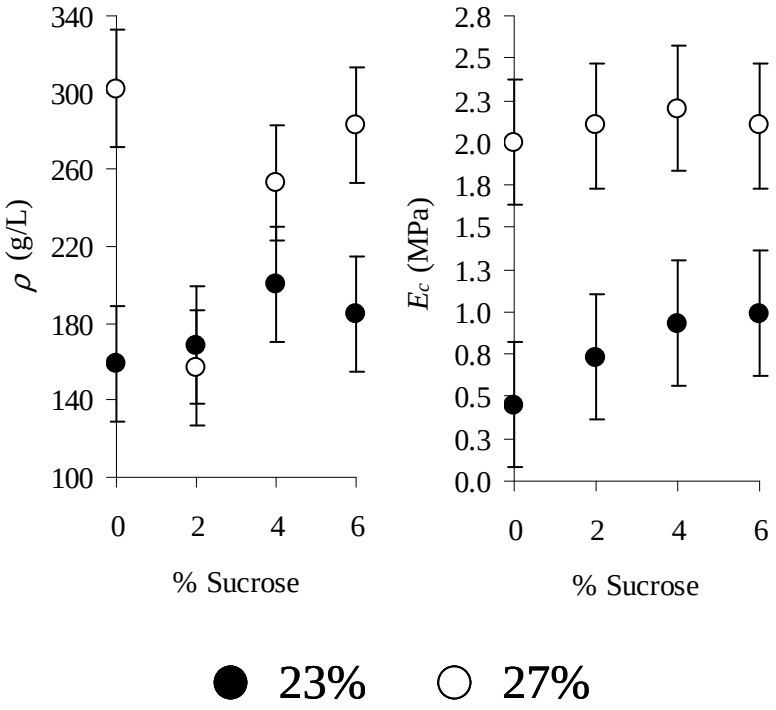

Table 3.1 Correlations between WPI levels, sucrose levels, material properties, extrusion parameters, expansion, collapse, microstructure and mechanical properties at 23% moisture.

	WPI	Sucrose	T_s	T_f	T_{ds}	T_{df}	δ	ρ	SME	Die Pressure	ER_{max}	ER_{final}	ε	D	t_{wall}	N_{cell}	E_c	σ_{cr}	N_{sr}	F_{cr}	W_c
W_c	-0.72	0.30	-0.25	-0.07	0.05	-0.13	-0.37	-0.10	0.53	0.71	0.62	0.46	0.50	0.15	-0.43	0.18	-0.19	0.86	-0.78	0.94	1
F_{cr}	-0.28	0.63	-0.43	-0.37	0.27	0.19	-0.45	-0.22	0.67	0.80	0.58	0.32	0.58	-0.07	-0.60	0.31	-0.19	0.94	-0.56	1	
N_{sr}	0.97	0.41	-0.24	-0.55	0.39	0.66	0.06	-0.19	-0.05	-0.32	-0.36	-0.49	-0.03	-0.43	-0.08	0.18	0.04	-0.49	1		
σ_{cr}	-0.14	0.57	-0.34	-0.34	0.23	0.20	-0.30	-0.08	0.60	0.59	0.35	0.01	0.53	-0.17	-0.54	0.26	-0.01	1			
E_c	-0.69	0.96	0.65	0.19	-0.62	-0.33	0.94	0.86	-0.73	-0.53	-0.68	-0.67	-0.43	0.20	0.59	-0.76	1				
N_{cell}	0.82	-0.81	-0.83	-0.49	0.85	0.65	-0.82	-0.91	0.85	0.37	0.35	0.18	0.42	-0.72	-0.81	1					
t_{wall}	-0.89	-0.18	0.98	0.66	-0.91	-0.70	0.76	0.70	-0.91	-0.64	-0.51	-0.22	-0.62	0.50	1						
D	-0.80	-0.86	0.52	0.47	-0.68	-0.71	0.29	0.62	-0.42	0.04	0.35	0.40	0.11	1							
ε	0.29	-0.62	-0.55	-0.55	0.39	0.35	-0.60	-0.25	0.75	0.60	0.78	0.26	1								
ER_{final}	-0.89	-0.81	-0.23	0.13	0.08	-0.21	-0.57	-0.41	0.32	0.66	0.80	1									
ER_{max}	-0.37	-0.81	-0.47	-0.25	0.26	0.06	-0.72	-0.39	0.66	0.80	1										
Die Pressure	0.06	-0.71	-0.58	-0.51	0.43	0.35	-0.70	-0.49	0.72	1											
SME	0.95	-0.89	-0.86	-0.60	0.79	0.62	-0.90	-0.75	1												
ρ	-0.75	0.78	0.76	0.45	-0.80	-0.63	0.87	1													
δ	-0.98	0.99	0.76	0.40	-0.72	-0.49	1														
T_{df}	0.97	0.72	-0.75	-0.90	0.84	1															
T_{ds}	0.93	-0.06	-0.96	-0.67	1																
T_f	-0.86	-0.60	0.67	1																	
T_s	-0.94	0.00	1																		
Sucrose	---	1																			
WPI	1																				

WPI, whey protein isolate

δ, bulk density

ε, collapse ratio

σ_{cr}, crushing stress

T_s, softening temperature

ρ, piece density

$\overline{D}$, cell diameter

N_{sr}, number of spatial ruptures

$T_{f,}$ flow temperature

SME, specific mechanical energy

t_{wall}, cell wall thickness

F_{cr}, average crushing force

T_{ds}, difference between T_d and T_s

ER_{max}, maximum expansion ratio

N_{cell}, cell number density

W_c, crispness work

T_{df}, difference between T_d and T_f

ER_{final}, final expansion ratio

E, Young's modulus

Table 3.2 Correlations between WPI levels, sucrose levels, material properties, extrusion parameters, expansion, collapse, microstructure and mechanical properties at 27% moisture.

	WPI	Sucrose	T_s	T_f	T_{ds}	T_{df}	δ	ρ	SME	Die Pressure	ER_{max}	ER_{final}	ε	D	t_{wall}	N_{cell}	E_c	σ_{cr}	N_{sr}	F_{cr}	W_c
W_c	-0.34	-0.19	0.43	-0.44	-0.53	0.34	0.86	0.32	-0.55	-0.30	-0.71	-0.59	-0.61	-0.25	0.63	-0.30	0.75	0.68	-0.74	0.85	1
F_{cr}	0.01	-0.21	0.64	-0.72	-0.74	0.61	0.77	0.21	-0.78	-0.39	-0.89	-0.79	-0.60	-0.40	0.47	-0.33	0.95	0.92	-0.43	1	
N_{sr}	0.88	0.14	-0.52	0.17	0.53	-0.08	-0.84	-0.44	0.36	0.61	0.15	-0.05	0.62	-0.25	-0.48	0.59	-0.43	-0.17	1		
σ_{cr}	0.33	0.38	0.57	-0.79	-0.64	0.74	0.57	0.07	-0.71	-0.18	-0.95	-0.93	-0.41	-0.69	0.40	-0.08	0.85	1			
E_c	-0.30	0.63	0.76	-0.81	-0.86	0.69	0.81	0.23	-0.85	-0.48	-0.83	-0.68	-0.74	-0.29	0.55	-0.52	1				
N_{cell}	0.69	-0.78	-0.68	0.45	0.72	-0.35	-0.65	-0.15	0.58	0.68	0.06	-0.21	0.86	-0.48	-0.43	1					
t_{wall}	-0.38	0.91	0.29	-0.60	-0.41	0.54	0.70	0.15	-0.38	0.08	-0.60	-0.41	-0.79	-0.31	1						
D	-0.37	-0.90	-0.08	0.55	0.08	-0.62	-0.05	0.20	0.22	-0.45	0.73	0.83	-0.06	1							
ε	0.70	-0.77	-0.66	0.71	0.74	-0.61	-0.81	-0.07	0.72	0.41	0.48	0.20	1								
ER_{final}	-0.53	-0.88	-0.26	0.65	0.36	-0.61	-0.38	-0.08	0.45	-0.14	0.96	1									
ER_{max}	-0.38	-0.96	-0.43	0.79	0.54	-0.72	-0.59	-0.09	0.62	-0.01	1										
Die Pressure	0.83	0.58	-0.78	0.21	0.76	-0.10	-0.59	-0.48	0.47	1											
SME	0.91	-0.54	-0.80	0.82	0.80	-0.78	-0.61	0.22	1												
ρ	-0.72	0.08	0.20	0.12	-0.32	-0.28	0.50	1													
δ	-0.76	0.71	0.71	-0.58	-0.80	0.44	1														
T_{df}	-0.13	0.70	0.69	-0.98	-0.68	1															
T_{ds}	0.96	-0.93	-0.97	0.78	1																
T_f	0.20	-0.80	-0.75	1																	
T_s	-0.88	0.83	1																		
Sucrose	---	1																			
WPI	1																				

WPI, whey protein isolate

δ, bulk density

ε, collapse ratio

σ_{cr}, crushing stress

T_s, softening temperature

ρ, piece density

$\overline{D}$, cell diameter

N_{sr}, number of spatial ruptures

T_f, flow temperature

SME, specific mechanical energy

t_{wall}, cell wall thickness

F_{cr}, average crushing force

T_{ds}, difference between T_d and T_s

ER_{max}, maximum expansion ratio

N_{cell}, cell number density

W_c, crispness work

T_{df}, difference between T_d and T_f

ER_{final}, final expansion ratio

E, Young's modulus

Table 3.3 Phase transition properties, SME, die pressure, bulk and piece densities at different WPI and sucrose levels (Mean ± standard deviation of duplicates).

WPI %	Sucrose %	T_s °C	T_f °C	T_{ds} °C	T_{df} °C	SME kJ/kg	Die Pressure MPa	δ, g/L	ρ, g/L
0	0	83.1 ± 2.69^{a}	130 ± 2.82^{a}	65.9 ± 1.27^{c}	19.0 ± 1.41^{b}	274 ± 30.6^{c}	9.2 ± 0.73^{a}	129 ± 29.6^{a}	162 ± 13.3^{c}
6	2	65.4 ± 1.56^{b}	120 ± 0.212^{a}	84.6 ± 2.97^{a}	30.1 ± 1.63^{b}	292 ± 14.9^{b}	9.2 ± 0.73^{a}	133 ± 23.0^{a}	192 ± 27.7^{b}
6	4	72.2 ± 0.919^{b}	119 ± 3.75^{a}	78.7 ± 1.63^{b}	31.4 ± 3.04^{b}	293 ± 1.02^{b}	9.2 ± 0.24^{a}	134 ± 19.2^{a}	216 ± 73.3^{a}
12	2	67.9 ± 2.40^{b}	79.8 ± 2.12^{b}	84.5 ± 0.778^{a}	72.6 ± 5.30^{a}	331 ± 26.5^{a}	8.7 ± 0.98^{b}	97.0 ± 4.70^{b}	145 ± 3.96^{c}
12	4	68.1 ± 0.849^{b}	83.5 ± 2.26^{b}	87.0 ± 0.141^{a}	71.6 ± 1.56^{a}	289 ± 4.30^{b}	7.9 ± 0.73^{c}	97.8 ± 5.28^{b}	139 ± 4.16^{c}
LSD		4.17	11.9	4.98	12.7	13.5	0.31	8.73	18.2

WPI, whey protein isolate
T_s, softening temperature
T_f, flow temperature
T_{ds}, difference between T_d and T_s
T_{df}, difference between T_d and T_f
SME, specific mechanical energy
δ, bulk density
ρ, piece density
LSD, least significant difference (values with the same letter superscript indicate no significant differences)

Table 3.4 Expansion ratios, collapse ratios, microstructure parameters at different WPI and sucrose levels (Mean ± standard deviation of duplicates).

WPI %	Sucrose %	ER_{max}	ER_{final}	ε	$\overline{D}$ mm	t_{wall} mm	N_{cell} cells/cm^3 ($\times 10^2$)
0	0	22.3 ± 1.65^{b}	20.6 ± 2.21^{c}	0.0748 ± 0.0303^{a}	2.84 ± 1.23^{a}	0.0570 ± 0.0238^{b}	0.0665 ± 0.0393^{c}
6	2	20.2 ± 2.21^{c}	19.6 ± 2.09^{d}	0.0288 ± 0.0027^{b}	1.21 ± 0.109^{b}	0.0412 ± 0.0177^{b}	0.799 ± 0.0216^{b}
6	4	21.6 ± 1.46^{b}	20.9 ± 1.55^{c}	0.0333 ± 0.0063^{b}	1.02 ± 0.0620^{b}	0.0243 ± 0.00788^{b}	1.11 ± 0.210^{a}
12	2	22.5 ± 1.68^{b}	21.7 ± 1.33^{b}	0.0373 ± 0.0124^{b}	0.97 ± 0.0428^{b}	0.0354 ± 0.00499^{b}	1.25 ± 0.565^{a}
12	4	23.3 ± 1.68^{a}	22.7 ± 1.43^{a}	0.0247 ± 0.0088^{c}	1.62 ± 0.351^{b}	0.459 ± 0.538^{a}	0.653 ± 0.127^{b}
LSD		0.73	0.73	0.012	0.44	0.103	0.279

WPI, whey protein isolate
ER_{max}, maximum expansion ratio
ER_{final}, final expansion ratio
ε, collapse ratio
$\overline{D}$, cell diameter
t_{wall}, cell wall thickness
N_{cell}, cell number density
LSD, least significant difference (values with the same letter superscript indicate no significant differences)

Table 3.5 Mechanical properties at different WPI and sucrose levels (Mean ± standard deviations of duplicates).

WPI %	Sucrose %	E_c MPa	σ_{cr} kPa	N_{sr} mm^{-1}	F_{cr} N	W_c N-mm
0	0	0.66 ± 0.11^{a}	100 ± 5.0^{b}	9.2 ± 0.86^{b}	15 ± 3.8^{d}	1.7 ± 0.30^{c}
6	2	0.51 ± 0.025^{b}	74 ± 40^{c}	10 ± 0.11^{b}	19 ± 2.9^{c}	1.9 ± 0.23^{c}
6	4	0.26 ± 0.19^{c}	78 ± 59^{c}	12 ± 1.1^{a}	19 ± 2.5^{c}	1.6 ± 0.014^{c}
12	2	0.51 ± 0.15^{b}	89 ± 2.1^{b}	10 ± 2.4^{b}	24 ± 8.7^{b}	2.6 ± 1.5^{b}
12	4	0.79 ± 0.082^{a}	120 ± 26^{a}	8.3 ± 0.57^{c}	31 ± 0.92^{a}	3.9 ± 0.13^{a}
LSD		0.13	10.9	0.87	3.8	0.54

WPI, whey protein isolate
E, Young's modulus
σ_{cr}, crushing stress
N_{sr}, number of spatial ruptures
F_{cr}, average crushing force
W_c, crispness work
LSD, least significant difference (values with the same letter superscript indicate no significant differences)

APPENDICES

Appendix 3.1 Phase transition temperatures of experimental treatments with different WPI and in-barrel moisture contents (Mean ± standard deviation of duplicates).

WPI %	X_w %	T_s °C	T_f °C
0	23	83.1 ± 2.69^{a}	130 ± 2.83^{a}
6	23	73.8 ± 2.19^{b}	129 ± 2.12^{a}
12	23	74.1 ± 2.83^{b}	128 ± 3.54^{a}
18	23	66.8 ± 4.81^{b}	116 ± 6.36^{b}
0	27	56.7 ± 0.919^{c}	93.6 ± 1.27^{c}
6	27	44.5 ± 4.53^{d}	98.8 ± 5.94^{c}
12	27	44.4 ± 5.30^{d}	106 ± 6.36^{c}
18	27	41.2 ± 11.0^{d}	94.2 ± 6.79^{c}
LSD		8.77	7.62

WPI, whey protein isolate
X_w, moisture content
T_s, softening temperature
T_f, flow temperature
LSD, least significant difference (values with the same letter superscript indicate no significant differences)

Appendix 3.2 Specific mechanical energy, die pressure, differences between melt temperature behind die and phase transition temperatures of experimental treatments with different WPI and in-barrel moisture contents (Mean ± standard deviation of duplicates).

WPI %	X_w %	SME kJ/kg	Die Pressure MPa	T_{ds} °C	T_{df} °C
0	23	315 ± 7.75^{b}	9.8 ± 0.49^{a}	51.9 ± 4.10^{b}	5.00 ± 4.24^{c}
6	23	324 ± 20.2^{b}	9.9 ± 0.70^{a}	70.8 ± 7.14^{a}	16.0 ± 7.07^{b}
12	23	332 ± 34.0^{b}	8.7 ± 0.014^{b}	71.4 ± 7.78^{a}	18.0 ± 8.49^{b}
18	23	359 ± 6.42^{a}	10 ± 0.21^{a}	80.7 ± 1.27^{a}	32.0 ± 9.90^{a}
0	27	274 ± 38.3^{d}	7.0 ± 0.0027^{c}	83.4 ± 4.74^{a}	46.4 ± 4.38^{a}
6	27	287 ± 32.3^{d}	7.7 ± 0.97^{b}	92.0 ± 8.06^{a}	37.7 ± 2.40^{a}
12	27	314 ± 30.5^{c}	7.3 ± 0.49^{b}	93.7 ± 0.354^{a}	32.5 ± 0.707^{a}
18	27	310 ± 1.38^{c}	8.3 ± 1.8^{b}	98.8 ± 16.7^{a}	45.8 ± 1.13^{a}
LSD		17.8	0.61	9.81	8.66

WPI, whey protein isolate
X_w, moisture content
SME, specific mechanical energy
T_{ds}, difference between T_d and T_s
T_{df}, difference between T_d and T_f
LSD, least significant difference (values with the same letter superscript indicate no significant differences)

Appendix 3.3 Bulk densities, piece densities, expansion and collapse ratios of experimental treatments with different WPI and in-barrel moisture contents (Mean ± standard deviation of duplicates).

WPI %	X_w %	δ g/L	ρ g/L	ER_{max}	ER_{final}	ε
0	23	97.5 ± 4.95^{c}	192 ± 127^{b}	30.4 ± 2.15^{a}	25.6 ± 0.0424^{a}	0.157 ± 0.061^{a}
6	23	81.5 ± 14.8^{c}	120 ± 22.6^{c}	26.2 ± 0.113^{b}	26.0 ± 4.24^{a}	0.007 ± 0.00^{d}
12	23	75.0 ± 14.1^{c}	116 ± 44.5^{c}	26.2 ± 1.03^{b}	23.7 ± 0.537^{a}	0.097 ± 0.056^{b}
18	23	67.0 ± 0.00^{c}	123 ± 17.0^{c}	28.4 ± 1.73^{a}	23.2 ± 0.141^{a}	0.186 ± 0.054^{a}
0	27	154 ± 6.36^{b}	235 ± 63.6^{a}	26.9 ± 3.01^{b}	24.7 ± 0.976^{a}	0.078 ± 0.000^{b}
6	27	184 ± 33.2^{a}	257 ± 52.3^{a}	21.9 ± 0.0849^{c}	21.2 ± 0.0283^{b}	0.031 ± 0.002^{c}
12	27	119 ± 7.07^{c}	228 ± 68.6^{a}	28.8 ± 0.0707^{a}	26.4 ± 0.750^{a}	0.083 ± 0.028^{b}
18	27	108 ± 0.707^{c}	206 ± 96.9^{b}	20.9 ± 1.56^{d}	17.7 ± 2.12^{c}	0.151 ± 0.039^{a}
LSD		24.5	29.5	1.78	1.82	0.037

WPI, whey protein isolate
X_w, moisture content
δ, bulk density
ρ, piece density
ER_{max}, maximum expansion ratio
ER_{final}, final expansion ratio
ε, collapse
LSD, least significant difference (values with the same letter superscript indicate no significant differences)

Appendix 3.4 Microstructure parameters of experimental treatments with different WPI and in-barrel moisture contents (Mean ± standard deviation of duplicates).

WPI %	X_w %	$\overline{D}$ mm	t_{wall} mm	N_{cell} cells/cm^3 ($\times 10^2$)
0	23	2.94 ± 0.262^a	0.0720 ± 0.0127^c	0.0699 ± 0.0342^c
6	23	1.24 ± 0.304^c	0.0575 ± 0.0191^c	0.925 ± 0.0325^b
12	23	1.06 ± 0.0849^c	0.0615 ± 0.0064^c	1.52 ± 0.162^b
18	23	1.15 ± 0.163^c	0.0430 ± 0.0071^c	1.19 ± 1.34^b
0	27	1.57 ± 0.261^c	0.161 ± 0.0566^b	0.455 ± 0.301^c
6	27	1.58 ± 0.177^c	0.272 ± 0.196^a	0.542 ± 0.136^c
12	27	2.05 ± 0.318^b	0.126 ± 0.0071^b	0.235 ± 0.205^c
18	27	1.00 ± 0.0283^c	0.145 ± 0.0141^b	1.93 ± 1.20^a

WPI, whey protein isolate
X_w, moisture content
$\overline{D}$, cell diameter
t_{wall}, cell wall thickness
N_{cell}, cell number density
LSD, least significant difference (values with the same letter superscript indicate no significant differences)

Appendix 3.5 Mechanical properties of experimental treatments with different WPI and in-barrel moisture contents (Mean ± standard deviation of duplicates).

WPI %	X_w %	E_c MPa	σ_{cr} kPa	N_{sr} mm^{-1}	F_{cr} N	W_c N-mm
0	23	0.67 ± 0.30^{b}	110 ± 44^{b}	8.0 ± 0.16^{c}	26 ± 8.8^{a}	3.4 ± 1.3^{b}
6	23	0.45 ± 0.13^{b}	98 ± 17^{b}	8.8 ± 0.69^{c}	24 ± 6.2^{a}	2.9 ± 0.93^{b}
12	23	0.31 ± 0.022^{b}	77 ± 47^{b}	11 ± 1.6^{a}	17 ± 10^{b}	1.7 ± 1.2^{c}
18	23	0.45 ± 0.038^{b}	110 ± 38^{b}	11 ± 1.5^{a}	26 ± 10^{a}	2.5 ± 1.3^{b}
0	27	0.87 ± 0.30^{b}	73 ± 19^{b}	8.3 ± 0.27^{c}	15 ± 1.8^{b}	2.2 ± 0.18^{b}
6	27	1.3 ± 0.47^{a}	91 ± 54^{b}	7.7 ± 1.5^{c}	23 ± 12^{a}	4.1 ± 2.0^{a}
12	27	0.63 ± 0.28^{b}	42 ± 3.2^{c}	9.6 ± 0.21^{b}	12 ± 1.1^{c}	1.3 ± 0.13^{c}
18	27	0.88 ± 0.039^{b}	120 ± 84^{a}	10 ± 2.0^{b}	19 ± 12^{b}	2.1 ± 1.6^{b}
LSD		0.21	16.3	0.69	2.9	0.59

WPI, whey protein isolate
X_w, moisture content
E_c, compression modulus
σ_{cr}, crushing stress
N_{sr}, number of spatial ruptures
F_{cr}, average crushing force
W_c, crispness work
LSD, least significant difference (values with the same letter superscript indicate no significant differences)

Appendix 3.6 Phase transition temperatures of experimental treatments with different sucrose and in-barrel moisture contents (Mean ± standard deviation of duplicates).

Sucrose %	X_w %	T_s °C	T_f °C
0	23	80.3 ± 1.34^{b}	130 ± 2.12^{a}
6	23	91.4 ± 8.84^{a}	130 ± 1.06^{a}
12	23	83.0 ± 0.849^{b}	131 ± 2.05^{a}
18	23	83.0 ± 0.141^{b}	124 ± 4.60^{a}
0	27	57.0 ± 0.424^{c}	95.0 ± 0.707^{b}
6	27	58.7 ± 0.566^{c}	74.2 ± 0.636^{c}
12	27	57.9 ± 0.283^{c}	73.8 ± 2.19^{c}
18	27	60.0 ± 0.566^{c}	72.9 ± 1.13^{c}
LSD		7.20	12.2

X_w, moisture content
T_s, softening temperature
T_f, flow temperature
LSD, least significant difference (values with the same letter superscript indicate no significant differences)

Appendix 3.7 Specific mechanical energy, die pressure, differences between melt temperatures behind die and phase transition temperatures of experimental treatments with different sucrose and in-barrel moisture contents (Mean ± standard deviation of duplicates).

Sucrose %	X_w %	SME kJ/kg	Die Pressure MPa	T_{ds} °C	T_{df} °C
0	23	290 ± 2.82^a	9.2 ± 0.57^a	62.3 ± 1.34^b	13.0 ± 2.12^c
6	23	285 ± 1.41^a	8.9 ± 0.42^a	50.7 ± 8.84^c	12.3 ± 1.06^c
12	23	286 ± 7.07^a	8.2 ± 0.14^a	61.0 ± 0.849^b	12.6 ± 2.05^c
18	23	275 ± 15.6^a	8.7 ± 0.014^a	58.0 ± 0.141^b	17.3 ± 4.60^c
0	27	264 ± 0.529^a	6.5 ± 0.71^b	77.0 ± 0.424^a	39.0 ± 0.707^b
6	27	264 ± 8.49^a	7.2 ± 0.28^b	77.3 ± 0.566^a	61.9 ± 0.636^a
12	27	277 ± 4.24^a	7.3 ± 0.028^b	74.6 ± 0.283^a	58.8 ± 2.19^a
18	27	235 ± 0.540^b	7.0 ± 0.71^b	72.0 ± 0.566^a	59.1 ± 1.13^a
LSD		11.5	0.56	5.57	10.4

X_w, moisture content
SME, specific mechanical energy
T_{ds}, difference between T_d and T_s
T_{df}, difference between T_d and T_f
LSD, least significant difference (values with the same letter superscript indicate no significant differences)

Appendix 3.8 Bulk densities, piece densities, expansion and collapse ratios of experimental treatments with different sucrose and in-barrel moisture contents (Mean ± standard deviation of duplicates).

Sucrose %	X_w %	δ g/L	ρ g/L	ER_{max}	ER_{final}	ε
0	23	92.5 ± 14.1^{b}	159 ± 4.24^{b}	27.5 ± 0.707^{a}	26.0 ± 1.41^{a}	0.0564 ± 0.0386^{b}
6	23	106 ± 35.8^{b}	169 ± 13.4^{b}	23.0 ± 0.283^{b}	22.9 ± 0.990^{b}	0.0057 ± 0.0000^{c}
12	23	122 ± 6.66^{b}	201 ± 21.9^{b}	20.6 ± 1.41^{b}	20.2 ± 0.566^{b}	0.0165 ± 0.0000^{c}
18	23	131 ± 2.83^{b}	185 ± 7.07^{b}	22.1 ± 1.27^{b}	21.7 ± 0.0424^{b}	0.0167 ± 0.0000^{c}
0	27	180 ± 1.41^{a}	302 ± 5.66^{a}	21.2 ± 1.13^{b}	19.5 ± 0.0990^{b}	0.0815 ± 0.0537^{a}
6	27	169 ± 28.3^{a}	157 ± 2.83^{b}	19.3 ± 1.03^{b}	19.2 ± 0.156^{b}	0.0029 ± 0.0000^{c}
12	27	180 ± 3.54^{a}	253 ± 15.6^{a}	19.1 ± 0.0424^{b}	19.1 ± 0.0141^{b}	0.0016 ± 0.0015^{c}
18	27	201 ± 7.07^{a}	283 ± 1.41^{a}	17.7 ± 0.0566^{b}	17.6 ± 0.424^{b}	0.0028 ± 0.0000^{c}
LSD		22.7	30.3	2.05	1.77	0.0165

X_w, moisture content
δ, bulk density
ρ, piece density
ER_{max}, maximum expansion ratio
ER_{final}, final expansion ratio
ε, collapse
LSD, least significant difference (values with the same letter superscript indicate no significant differences)

Appendix 3.9 Microstructure parameters of experimental treatments with different sucrose and in-barrel moisture contents (Mean ± standard deviation of duplicates).

Sucrose %	X_w %	$\overline{D}$ mm	t_{wall} mm	N_{cell} cells/cm^3 ($\times 10^2$)
0	23	2.70 ± 0.0778^a	0.0775 ± 0.00636^c	0.0646 ± 0.0267^b
2	23	1.81 ± 0.0990^b	0.0933 ± 0.0109^c	0.0338 ± 0.0191^b
4	23	1.67 ± 0.0636^b	0.0755 ± 0.0183^c	0.0308 ± 0.00141^b
6	23	1.63 ± 0.0212^b	0.0798 ± 0.00205^c	0.0312 ± 0.0163^b
0	27	1.65 ± 0.170^b	0.129 ± 0.0368^c	0.551 ± 0.341^a
2	27	1.39 ± 0.191^c	0.203 ± 0.00849^b	0.0191 ± 0.00233^b
4	27	1.39 ± 0.0283^c	0.269 ± 0.0495^a	0.0261 ± 0.0121^b
6	27	1.29 ± 0.0495^c	0.257 ± 0.0566^a	0.00931 ± 0.00235^b
LSD		0.295	0.0405	0.1133

X_w, moisture content
$\overline{D}$, cell diameter
t_{wall}, cell wall thickness
N_{cell}, cell number density
LSD, least significant difference (values with the same letter superscript indicate no significant differences)

Appendix 3.10 Mechanical properties of experimental treatments with different sucrose and in-barrel moisture contents (Mean ± standard deviation of duplicates).

Sucrose %	X_w %	E_c MPa	σ_{cr} kPa	N_{sr} mm^{-1}	F_{cr} N	W_c N-mm
0	23	0.45 ± 0.14^{c}	56 ± 18^{b}	11 ± 3.0^{a}	14 ± 0.70^{c}	1.3 ± 0.21^{d}
6	23	0.73 ± 0.59^{b}	82 ± 32^{b}	10 ± 0.44^{b}	18 ± 2.8^{c}	1.8 ± 0.14^{d}
12	23	0.93 ± 0.35^{b}	89 ± 7.4^{b}	10 ± 2.1^{b}	17 ± 3.0^{c}	1.7 ± 0.32^{d}
18	23	0.99 ± 0.014^{b}	75 ± 3.1^{b}	11 ± 0.28^{a}	17 ± 4.8^{c}	1.5 ± 0.19^{d}
0	27	2.0 ± 0.47^{a}	130 ± 16^{a}	8.3 ± 0.11^{c}	30 ± 0.14^{a}	3.6 ± 0.093^{a}
6	27	2.1 ± 0.31^{a}	140 ± 4.2^{a}	8.7 ± 0.57^{c}	30 ± 0.28^{a}	3.5 ± 0.14^{b}
12	27	2.2 ± 0.72^{a}	120 ± 1.4^{a}	9.0 ± 0.52^{c}	26 ± 7.1^{b}	2.9 ± 0.32^{c}
18	27	2.1 ± 0.057^{a}	150 ± 8.5^{a}	8.3 ± 1.3^{c}	30 ± 3.3^{a}	3.6 ± 0.38^{a}
LSD		0.37	19.7	0.56	3.3	0.48

X_w, moisture content
E_c, compression modulus
σ_{cr}, crushing stress
N_{sr}, number of spatial ruptures
F_{cr}, average crushing force
W_c, crispness work
LSD, least significant difference (values with the same letter superscript indicate no significant differences)

CHAPTER 4 - PHASE TRANSITION AND RHEOLOGICAL BEHAVIOR OF RAW AND EXTRUDED CORNSTARCH

To be submitted to Journal of Food Science, May, 2007

ABSTRACT

A new method of characterizing phase transition behavior of biopolymeric materials was evaluated and compared with traditional methods for evaluating phase transition and rheology. Glass transition and rheological properties of cornstarch at different moisture contents (18-30% wet basis) were characterized using differential scanning calorimetry (DSC), phase transition analyzer (PTA) and on-line slit-die extrusion. Glass transition temperatures of extruded cornstarch decreased from 57.55 to 31.20°C as moisture contents increased from 18 to 30%. Rate of decrease in glass transition temperature was slower at this moisture regime compared to studies reported in literature at 4 to 14% moisture. This implied that molecular degradation of the starch granules was slower at higher moistures. PTA parameters, softening temperature (T_s) and flow temperature (T_f) ranged from 42.5 to 85.6 °C and 109 to 136 °C, respectively, for the moisture range investigated in this study. Both parameters exhibited a high correlation (r = 0.89 and 0.86 for softening and flow temperature, respectively) with glass transition temperatures, indicating that these parameters were good estimates of phase transition properties of the complex and heterogeneous formulations. As expected, on-line rheological parameters, including flow behavior index, *n* (0.0438 - 0.304) and consistency coefficient, *K* (10,500 - 45,700 Pa-s^{n-1}), were functions of in-barrel moisture, and were related to phase transition properties using WLF kinetics.

INTRODUCTION

In order to provide more insight into the concept of glass transition and how it affects cell expansion, nucleation and collapse, this study looked into the use of different techniques to measure and/or estimate glass transition temperatures of extruded cornstarch. Different techniques have their own degree of accuracy and applicability. Some techniques are more

practical than others based on their ease of measurement and ability to handle more complex and heterogeneous materials. Such techniques are deemed more valuable in industrial applications.

Glass transition temperature (T_g) is probably the most significant single parameter that determines many polymer applications. Physical properties such as specific heat, specific volume, expansion coefficients, and viscoelasticity, change as polymers transition from a "glassy" to "rubbery" state. Application of the T_g concept in food science is critical as food components, such as starch and protein, are biopolymers. T_g is used to analyze the effects of recipes, process and storage conditions on textural attributes of foods. The processing of starch-based foods usually involves heating starch in the presence of water to a temperature above the gelatinization temperature causing a disruption of the starch granule structure. During gelatinization, the semicrystalline polymer structure in native granular starches is gradually transformed into an amorphous state, which is metastable and subject to time-dependent physical change such as recrystallization of amylopectin in starch gels. This phenomenon greatly affects the textural properties of starch based foods. Sufficient cooling of an amorphous polymer can induce a phase transformation of the rubbery amorphous matrix to a glassy, solid matrix known as the glass transition. At this state, a large increase in viscosity and immobilization of the polymer chains occur. In the study of extruded starch-based materials, the phenomenon of glass transitions (T_g) has been utilized to characterize the physical changes that occur during extrusion processing.

Phase transition analysis techniques are based on the ability to transfer heat to a material and monitor its effects. This class of techniques is known as thermal analysis. Several techniques can be used to measure T_g of biopolymeric materials, including differential scanning calorimetry (DSC), dynamic mechanical thermal analysis (DMTA) and on-line viscometry.

The most widely used method to determine T_g is the DSC. Most studies have focused on systems of starch in excess water (Stevens and Elton 1971; Slade 1984; Yost and Hoseney 1986; Slade and Levine 1987, 1991; Liu and Lelievre 1991). A few studies have focused on starch/water systems at low moistures (Slade 1984; Slade and Levine 1987, 1991; Zeleznak and Hoseney 1987; Liu and Lelievre 1991; Kalichevsky and others 1992).

Other measurements employed to characterize rheological properties of materials involves examining the melt viscosity during extrusion. Viscosity of the melt is an important parameter that characterizes any food extrusion process. Melt viscosity affects the flow of

material in the extruder, influences build-up of pressure in the barrel, and regulates extrudate properties (Li and others 2004). Starch gelatinization has a great effect on the viscosity of cereal-based melts. Higher degree of gelatinization produces a more viscous melt. Both barrel temperature (Van Lengerich 1990) and moisture content (Riaz 2000) influences starch gelatinization during extrusion. Melt viscosity in an extruder can be measured on-line using slit-die viscometry (Bindzus and others 2002 and Li and others 2004). Bindzus and others (2002) used an in-line slit viscometer (rectangular flow channel 60 mm in length) installed between the barrel and die plate. Three measuring transducers were used to measure pressure and temperature of the material in the flow channel of the viscometer. Li and others (2004) used an adapter between slit viscometer and extruder to allow diversion of flow. By adjusting two valves at the adapter, the flow rate at the slit die was varied to achieve different shear rates while maintaining die pressure and resulting SME at constant levels.

Viscosity has been extensively studied especially for shear dependent fluids. In extrusion, the melt viscosity is governed by the power law model given as:

$$\eta = K\dot{\gamma}^{n-1} \tag{4.1}$$

Where η = apparent viscosity, Pa-s, K = consistency coefficient, n = power law index and $\dot{\gamma}_{app}$ = apparent shear rate, s^{-1}. The consistency coefficient (K) is known to be dependent on temperature (T), moisture content (X) as well as process parameters like specific mechanical energy (SME) (Parker and others 1989):

$$K = 80.2 \cdot \exp\left[\frac{4820}{T} - 26.8X - 0.00124(SME)\right] Pa \cdot s^n \tag{4.2}$$

Viscosity can be related to phase transition properties of certain polymers (e.g. glass transition temperature, T_g) through the William-Landel-Ferry (WLF) equation:

$$\log a_T = \log \frac{\eta}{\eta_{T_g}} = \frac{-C_1(T - T_g)}{C_2 + (T - T_g)} \tag{4.3}$$

For most materials, C_1 and C_2 are given as 17.4 and 51.6, respectively.

The WLF equation describes the temperature dependence of all mechanical and electrical relaxation processes. The equation describes the kinetics of glass transition and has been shown to be applicable to any glass-forming polymer, oligomer or monomer.

In most cases, biopolymer foams are heterogeneous. Recent developments in instrumentation have the ability to overcome challenges in measuring raw material properties for these complex, heterogeneous biopolymers. One such innovation is the phase transition analyzer (PTA). The PTA greatly facilitates analysis of composite mixtures such as protein and starch-containing extrudates to give valuable information about the phase transition properties of the mixture (Strahm and Plattner, 2003). Moreover, the PTA has advantages over previous techniques, like differential scanning calorimetry, including the ability to handle relatively large sample size (~1.5 g). The PTA measures phase transition properties similar to glass transition and melt temperatures such as the softening temperature (T_s) of materials at elevated pressures similar to those encountered during extrusion processing (~1-10 MPa). Moreover, the PTA determines the temperature required to lower viscosity sufficiently allowing a material to be forced through a small orifice (flow temperature, T_f) at similar elevated pressures. The PTA, therefore, has the potential to help understand the role material properties play in extrusion processing (Strahm 1998; Strahm and others 2000).

In this study, native and extruded cornstarch was investigated at a variety of moisture contents by DSC, PTA and on-line viscometry for providing an insight into the phase transitions experienced by starch during processing.

MATERIALS AND METHODS

Materials

Unmodified cornstarch (~25% amylose and 75% amylopectin; Cargill Gel 03457, Cargill, Inc., Minneapolis, MN) was used as the only ingredient for all extrusion runs.

Differential Scanning Calorimetry

Extruded cornstarch was freeze-dried (FTS Systems Inc., Stone Ridge, NY) for 48 hours then ground using a Ross roller mill. Moisture contents of ground samples were elevated to their original in-barrel moisture contents (18, 21, 24, 27 and 30%) by humidification using a Model 532 Controlled Environment System (Electro-Tech Systems, Inc., Glenside, PA). A Q100 Differential Scanning Calorimeter (DSC) (TA Instruments, New Castle, DE) was used to determine T_g of extruded cornstarch. Approximately 15 mg sample was placed in a hermetically sealed aluminum pan. The sample and reference pans were placed inside the heating chamber of

the DSC. The chamber was closed and a heating-cooling-heating profile was set. Temperature in the chamber was decreased to -20°C. After reaching the starting temperature, heat was applied elevating the temperature to 200°C. This temperature was held for about 5 minutes before cooling the chamber to -20°C again. A second heating was performed to a temperature of 200°C. All heating and cooling rates were accomplished at 10°C per minute.

On-Line Viscometry

A temperature block, in-line-slit-die viscometer (3 mm height, 50 mm width, 300 mm length slit), pressure valve, pressure transducers (Model GT76/12-5K, Gentran, Fremont, CA) and holder with approximately 3.3 mm die were installed after the last barrel of the extruder. Cornstarch was extruded using a Wenger TX-52 twin-screw extruder (Wenger Manufacturing, Sabetha, KS) with screw diameters of 52 mm and L/D ratio of 16:1, a circular die opening of 3.3 mm, and a medium-shear profile (Figure 4.1). materials. Corn starch was extruded at five in-barrel moisture contents (18, 21, 24, 27 and 30%). The feed rate of raw material was 60 kg/hr. Approximately 5.8 kg/hr of water was added during preconditioning. Water added at the extruder was 0.1, 2.6, 4.9, 7.7 and 10.7 kg/hr for achieving 18, 21, 24, 27 and 30% in-barrel moistures, respectively. Barrel temperatures were set at 40, 40, 90, 120 and 140°C for heads 2 to 6, respectively. Slit die barrel temperature was set at 140°C (using circulating hot oil in the jacket). Extruder conditions were allowed to stabilize for approximately 10 min before samples were collected. A valve was mounted at the start of the slit-die to regulate flow from the extruder to the slit die (for changing shear rate). The two pressure transducers were flush mounted towards the exit end of the slit-die. An 8-channel, 12-bit analog input, USB-based Personal Measurement Device (Model PMD-1208LS, Measurement Computing Corporation, Middleboro, MA) was connected to the two pressure transducers and pressure data (read as mV) were acquired from the transducers during extrusion. The mV data were converted to pressure data. The differences in pressure ΔP were calculated. The ΔP and dimensions of the slit (height H and length L) were used to compute for shear stress. Shear rate was computed from the volume flow rate Q and dimensions of the slit (width W and height H).

Wall shear stress, apparent shear rate and apparent viscosity were calculated as follows (Li et al 2004):

$$\tau_w = \frac{H}{2}\left(\frac{\partial P}{\partial x}\right) = \frac{H}{2}\frac{\Delta P}{L} \tag{4.4}$$

Where τ_w = (slit) wall shear stress, Pa, H = height of slit, mm, ΔP = pressure difference ($P_2 - P_3$), Pa and L = length of the slit, mm.

$$\dot{\gamma}_{app} = \frac{6Q}{WH^2} \tag{4.5}$$

Where $\dot{\gamma}_{app}$ = apparent shear rate, s^{-1}, Q = volume flow rate, mm^3/s, W = width of the slit, mm and H = height of the slit, mm.

$$\eta = \frac{\tau_w}{\dot{\gamma}_{app}} \tag{4.6}$$

Where η = apparent viscosity, Pa-s, τ_w = shear stress at the slit wall, Pa and $\dot{\gamma}_{app}$ = apparent shear rate, s^{-1}.

The viscosity of the melt was governed by the power law model (equation 4.1).

Phase Transition Analysis

Moisture contents of unmodified cornstarch were adjusted to 18, 21, 24, 27 and 30% by mixing approximately 5 g of cornstarch (~10% moisture) with the appropriate amounts of water (using an air displacement micropipette) in a small resealable plastic bag. The bag was sealed and the mixture thoroughly mixed. The different treatments were allowed to equilibrate for 12 hours under refrigerated conditions (≈ 4°C). Softening temperature (T_s) and flow temperature (T_f) were determined using a Phase Transition Analyzer (PTA, Wenger Manufacturing, Inc., Sabetha, KS). The PTA cooling system was allowed to circulate for approximately 30 minutes. Chamber temperature was allowed to reach -5°C before each run. Approximately 1.85 g of sample was loaded unto the chamber. After installing the plunger and locking the system, a pressure of 10.0 MPa was applied initially to compact the sample. An operating pressure of 8.0 MPa was applied subsequently throughout the remainder of the testing. Temperature was increased at a rate of 8°C/min until sample T_s (point of maximum sample compaction) was reached. Subsequently, pressure was temporarily released to allow the insertion of a 2 mm orifice beneath the sample. Once in place, the pressure was resumed and heating was continued

(approximately 10°C below the T_s and 5°C above T_f) at the same rate until the material flowed through the orifice (T_f).

Statistical Analysis

Two sample replications were analyzed using each of the measurement techniques. Standard deviations for replicated parameters were computed. Pair-wise comparison using least significant difference (LSD) was used to determine statistical difference among pooled values. The 'PEARSON' function of EXCEL™ software (2002 edition, Microsoft Corporation, Seattle, WA) was used for finding the Pearson's coefficient of correlation (r) between any two data sets. To provide descriptive terms to the degree of correlation, criteria outlined by Franzblau (1958) were used ($|r| < 0.20$, negligible; $|r| = 0.20$ to 0.40, low; $|r| = 0.40$ to 0.60, moderate; $|r| = 0.60$ - 0.80, marked; and $|r| > 0.80$, high).

RESULTS AND DISCUSSION

Glass Transition Temperature (DSC)

Figure 4.2 shows a heat flow scan at 21% moisture content indicating glass transition. At phase transition, heat capacity (specific heat x sample weight) changes in slope. The inflection point at which the slope changes might be deemed as a change from rubbery to glassy state. Glass transition temperatures of extruded cornstarch decreased from 57.55 to 31.20°C as moisture contents increased from 18 to 30%. Figure 4.3 shows the relationship between moisture content and T_g for extruded cornstarch. Results show that as the water content of the extrudates increases their glass transition temperature decreases. This effect of plasticization of biopolymers by water is well documented (Slade and Levine 1993). The range of glass transition temperatures was 30 to 60°C for moisture contents 18 to 20%. Glass transition values from the work of Bindzus and others (2002) showed that glass transition temperatures ranged from 60 to 160°C for moisture contents 4 to 14%. Kalichevsky et al. (1992) showed glass transition temperatures ranging from 14 to 110°C for moisture contents 10 to 25%. Based on previous studies, results from this study were similar and within the range of glass transition temperature values. Glass transition temperatures in all these studies exhibited linearity from 10 to <20% moisture. However beyond 20% moisture content, glass transition temperature change tended to decrease (decrease in slope). This was exhibited by results from this study as well. This shows

that glass transition temperatures at the higher range were very dependent on moisture content while that of the lower transition temperatures were much less so. Also, the dependence of T_g on molecular weight could be seen in this aspect. The higher the moisture content during extrusion induced lower molecular degradation of the biopolymer, hence, slower decrease in glass transition temperatures.

Softening and Flow Temperatures (PTA)

Results from PTA generated softening temperatures (T_s) ranging from 85.6 to 42.5°C for moisture contents 18 to 30%. Flow temperatures (T_f) ranged from 136 to 109°C for moisture contents 18 to 30%. Figures 4.3 shows the relationship between moisture content and softening (T_s) and flow (T_f) temperatures for native cornstarch. In both cases, T_s and T_f decreased slightly with an increase in moisture content from 18 to 24%. A rapid decrease in temperatures was observed as moisture content increased >24%. At T_s, the bulk of the cornstarch had been softened which indicated a change in phase. Based on the data, softening process seemed to be slower at moisture contents <24%. Consequently, higher moisture (>24%) enhances softening process at a faster rate. At T_f, sufficient portion of the cornstarch had been melted allowing it to flow through a small orifice. This indicated another change in phase of the material. Similarly, the flowing process seemed to be slower at moisture contents <24%.

Strahm et al. (2000) explained the use of PTA as a means of measuring the 'controlling' glass transition temperatures for a complex blend of raw materials. They defined the controlling glass transition temperature as the temperature at which the bulk of the individual ingredients had been softened (T_s). Comparison of T_g and T_s in Figure 4.3 shows that T_g and T_s operate at different ranges (40 to 90°C and 30 to 60°C, respectively). Kalichevsky et al (1992) indicated that various techniques indicate significant changes in molecular mobility and state, all of which might reasonably be referred to as a glass transition. This did not indicate a multiplicity of transitions rather the techniques were sensitive to different degrees of molecular mobility. Although the temperature range and heating rates were approximately the same for both methods, the results reflect the fact that the glass transition was not observed at a unique temperature, but was related to the frequency and nature of the measurement technique. In most glass transition measurement using conventional DSC, there is the possibility of overlapping thermal events such as glass transition and melting of crystals (Liu and Shi 2006). This could

have posed a problem creating the notion that the detected stepwise change in heat flow might not be glass transition but something else. This might also explain the difference between glass transition and softening temperatures.

Upon comparison of T_g and T_s, and T_g and T_f, a high correlation could be seen between parameters (r of 0.94 and 0.93, respectively). This clearly shows that T_s and T_f could be used to approximate T_g behavior of biopolymers. In the case of biopolymer mixes wherein having more than one constituent could lead to complicated phase transition mechanisms, this technique would prove valuable in providing insights into food processing particularly extrusion.

Rheological Behavior Using Slit Die Viscometry

Figure 4.4 shows shear stress-shear rate flow behavior of extruded cornstarch at different in-barrel moistures. Figure 4.5 shows apparent viscosity-shear rate behavior of extruded cornstarch at different in-barrel moistures. Table 6 shows the flow behavior indices (n), consistency coefficients (K) and apparent viscosities at maximum shear rate (η) at different in-barrel moistures. Flow behavior indices (n) ranged from 0.0438 to 0.304. Consistency coefficients (K) ranged from 10,500 to 45,700 Pa-s^{n-1}. Apparent viscosities at maximum shear rate (η) ranged from 183 to 265 Pa-s. Flow behavior indices (n) results from this study compared well with previous studies done by Lengerich 1990 (0.310 to 1.010 for a moisture regime of 25 to 40%). Parker and others (1989) showed flow behavior index ranged from 0.31 to 0.68 for moistures 0.21 to 0.35. Drozdek and Faller (2002) showed flow behavior indices of 0.40 to 0.43 for corn starches for higher moisture contents of 30 to 35%. Differences in the results might have reflected inherent differences in cornstarch (particle size) as well as possible effects of different techniques employed in the measurement. However, the results were still good comparison with results from previous works. Results suggest that at lower moisture contents a significant structural breakdown of the starch granules have taken place. The degree of pseudoplasticity, which was indicated by low values of flow behavior indices (n) was relatively high and resulted in strong shear thinning effect at low moisture contents. At the same time, consistency coefficients (K) were high at low moisture indicating change in molecular structure of cornstarch. With increasing moisture contents, K decreased drastically while n increased. The apparent viscosity decreased with moisture content explaining the inability of the starch at the melt to resist introduction of mechanical energy at high moisture contents. Using

the WLF equation (equation 4.1), reference viscosity (η_{Tg}) at a specific glass transition temperature was computed using η from on-line viscometry experiments and T_g from DSC results. Figure 4.6 shows η_{Tg} (1.7 x 10^7 to 5.5 x 10^7 Pa-s) with increasing T_g (31 to 56°C). Difference in magnitude between η_{Tg} and η was in a the magnitude of 100,000 (10^5). This result indicated a good fit with the WLF equation and provided a good estimate of viscosity at any temperature given η_{Tg} and T_g. This also indicated the validity of both η and T_g measurements from this study. Figure 4.7 shows *K* values from on-line viscometry measurements and *K* values computed using equation 4.2. *K* values from on-line viscometry were higher compared to *K* values using equation 4.2. Discrepancies might be due to differences in SME values since SME seemed to contribute the greatest to the overall *K* value.

Implications With Respect to Processing

Phase transition properties and viscosity of biopolymer melts affect the specific mechanical energy (SME), expansion, collapse and final piece density, all of which are important parameters in understanding foam formation during extrusion. At higher viscosities, SME increases accompanied by greater expansion. At higher viscosities, collapse decreases as well as final piece density. In the presence of high moisture, however, viscosity decreases and, therefore, SME and expansion decreases with increase in collapse and final piece density. Furthermore, at this condition, $T - T_g$ (as well as $T - T_s$ and $T - T_f$) increases due to the moisture depressing T_g, T_s and T_f. In any case, both T_g and apparent viscosity data are very important in understanding extrusion as a process. However, obtaining these data was either time consuming (on-line viscometry) or difficult (DSC) especially for complex raw materials. Therefore, the use of PTA proved to be a good technique for measuring certain material properties (such as T_s and T_f) that could be used to estimate phase transition properties and this melt behavior during extrusion processing.

CONCLUSION

T_g and T_s as well as T_g and T_f were significantly related to each other. This clearly shows that T_s and T_f could be used to approximate T_g behavior of biopolymers. In the case of biopolymer mixes wherein having more than one constituent could lead to complicated phase

transition mechanisms, this technique would prove valuable in providing insights into food processing particularly extrusion.

REFERENCES

Bindzus W, Fayard G, Van Lengerich B, Meuser, F. 2002. Application of an In-line Viscometer to Determine the Shear Stress of Plasticised Wheat Starch. Starch/Stärke 54: 243-51.

Drosdek, K, Faller, J. 2002. Use of dual orifice die for on-line extruder measurement of flow behavior index in starchy foods. Journal of Food Engineering 55(1):79-88.

Franzblau, A. 1958. A Primer of Statistics for Non-Statistician. New York: Harcourt Brace and World.

Kalichevsky MT, Jaroszkiewicz EM, Ablett S, Blanshard JMV, Lillford PJ. 1992. The glass transition of amylopectin measured by DSC, DMTA and NMR. Carbohydrate Polym 18:77-88.

Li PX, Campanella OH, Hardacre AK. 2004. Using an In-Line Slit-Die Viscometer to Study the Effects of Extrusion Parameters on Corn Melt Rheology. Cereal Chem 81(1): 70-6.

Liu H, Lelieve J. 1991. A differential scanning calorimetry study of glass and melting transitions in starch suspensions and gels. Carbohydrate Res 219:23-32.

Parker R, Ollett AL, Lai-Fook R and Smith AC. 1989. The rheology of food melts and its applications in extrusion processing. In: Carter RE. Rheology of Food, Pharmaceutical and Biological materials with General Rheology. NewYork: Elsevier Applied Science. p 57.

Riaz MN. 2000. Extruders in Food Applications. Boca Raton: CRC Press.

Slade L. 1984. Starch properties in processed foods: Staling of starch-based products. Abstract No 112 in Proc. AACC Annual Meeting. Minneapolis: American Association of Cereal Chemists.

Slade L, Levine H. 1987. Recent advances in starch retrogradation. In: Stivala SS, Crescenzi V, Dea ICM. Industrial Polysaccharides: The Impact of Biotechnology and Advanced Methodologies. New York: Gordon and Breach. p 387.

Slade L, Levine H. 1991. Beyond water activity: Recent advances based on an alternative approach to the assessment of food quality and safety. Crit Reviews Food Sci Nutr 30:115-360.

Slade L, Levine H. 1993. Water and the glass transition – dependence of the glass transition on composition and chemical structure: special implication for flour functionality in cookie baking. J Food Eng 24:431-509.

Stevens DJ, Elton GAH. 1971. Thermal properties of the starch/water system: Part 1. Measurement of heat of gelatinization by differential scanning calorimetry. Starch/Stärke 23:8-11.

Strahm B. 1998. Fundamentals of polymer science as an applied extrusion tool. Cereal Foods World 43:621-25.

Strahm B, Plattner B, Huber G, Rokey G. 2000. Application of food polymer science and capillary rheometry in evaluating complex extruded products. Cereal Foods World 45(7): 300-302.

Strahm B, Plattner B. 2003. Phase Transition Analyzer. United States Patent, Patent No. US 6,534,005 B1.

Van Lengerich B. 1990. Influence of extrusion processing on In-Line Rheological Behavior, Structure and Function of Wheat Starch. In: Faridi H, Faubion JM. Dough Rheology and Baked Product Texture. New York: Van Nostrand Reinhold. p 421.

Yost DA, Hoseney, RC. 1986. Annealing and glass transition of starch. Starch/Stärke, 38:289-92.

Wang S, Casulli, J, Bouvier JM. 1993. Effect of dough ingredients on apparent viscosity and properties of extrudates in twin-screw extrusion cooking. International Journal of Food Science and Technology 28:465-79.

Zeleznak KJ, Hoseney RC. 1987. The glass transition in starch. Cereal Chem 64:121-24.

FIGURES AND TABLES

Figure 4.1 Diagram of screw configuration, injection sites, and barrel temperatures for all treatments.

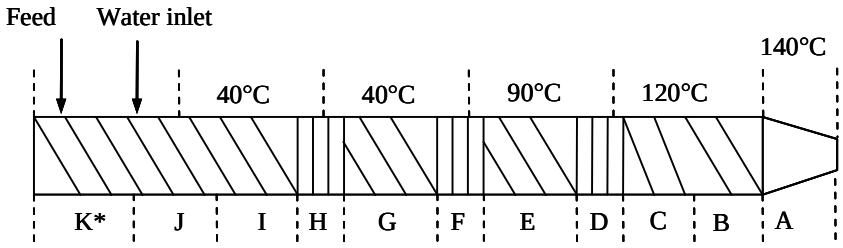

Section	Number of elements	Element length, mm	Element description
A	1	78	¾ pitch, double flighted, conical
B	1	78	¾ pitch, double flighted
C	1	52	½ pitch, double flighted
D	1	26	kneading block, forward
E	1	78	¾ pitch, double flighted
F	1	26	kneading block, forward
G	1	78	¾ pitch, double flighted
H	1	26	kneading block, forward
I	1	78	¾ pitch, double flighted
J	2	78	full pitch, double flighted
K	2	78	¾ pitch, double flighted

*The first two elements of the right shaft at the inlet (K) are ¾ pitch, single flighted.

Figure 4.2 Heat flow scan at 21% moisture content. (I) for inflection point indicating glass transition.

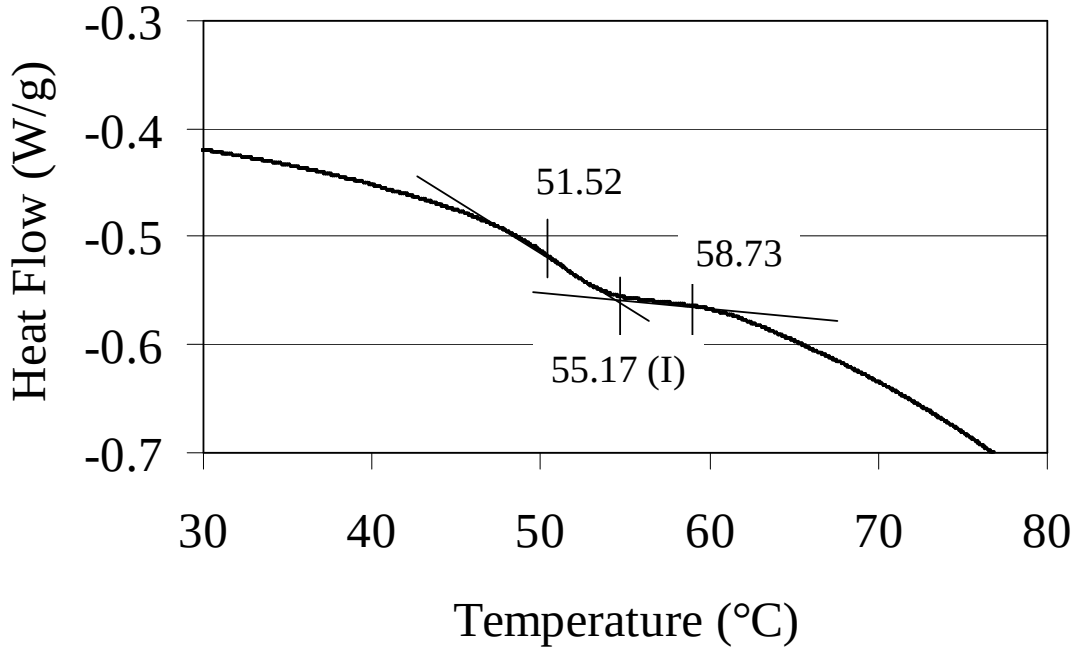

Figure 4.3 Glass transition temperature, T_g (DSC results) of extruded cornstarch, softening (T_s) and flow (T_f) temperatures (PTA results) of raw cornstarch at different moisture contents. Error bars represent least significant differences (LSD).

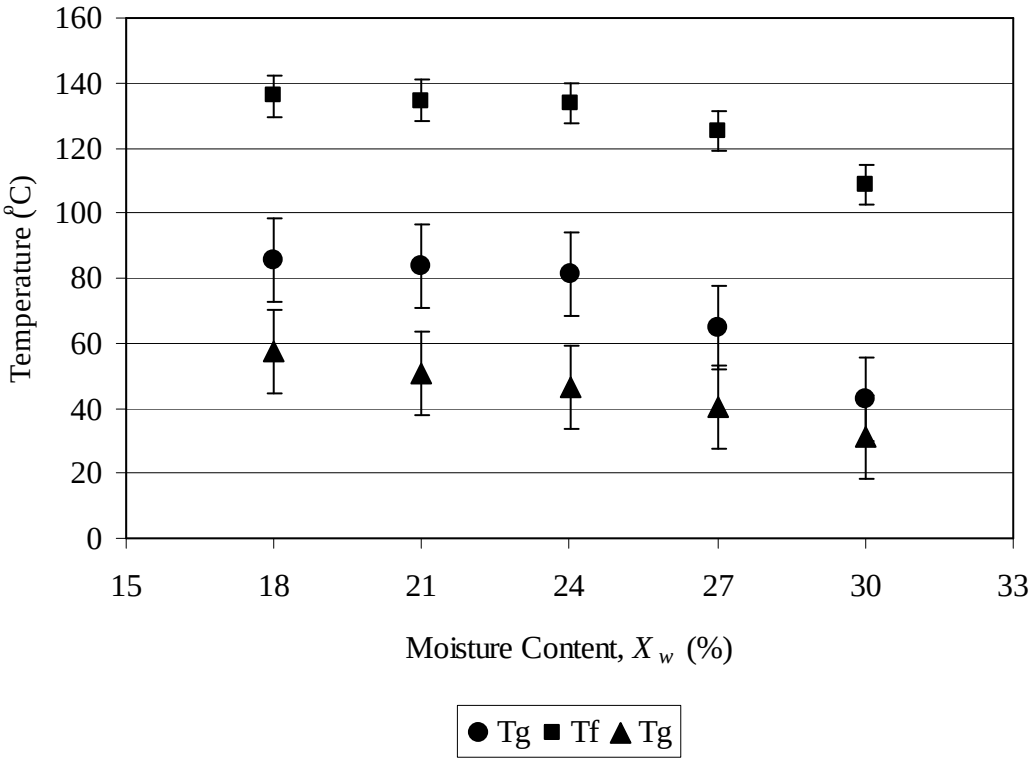

Figure 4.4 Shear stress-shear rate flow behavior from in-line-slit-die experiment of extruded cornstarch at different in-barrel moistures.

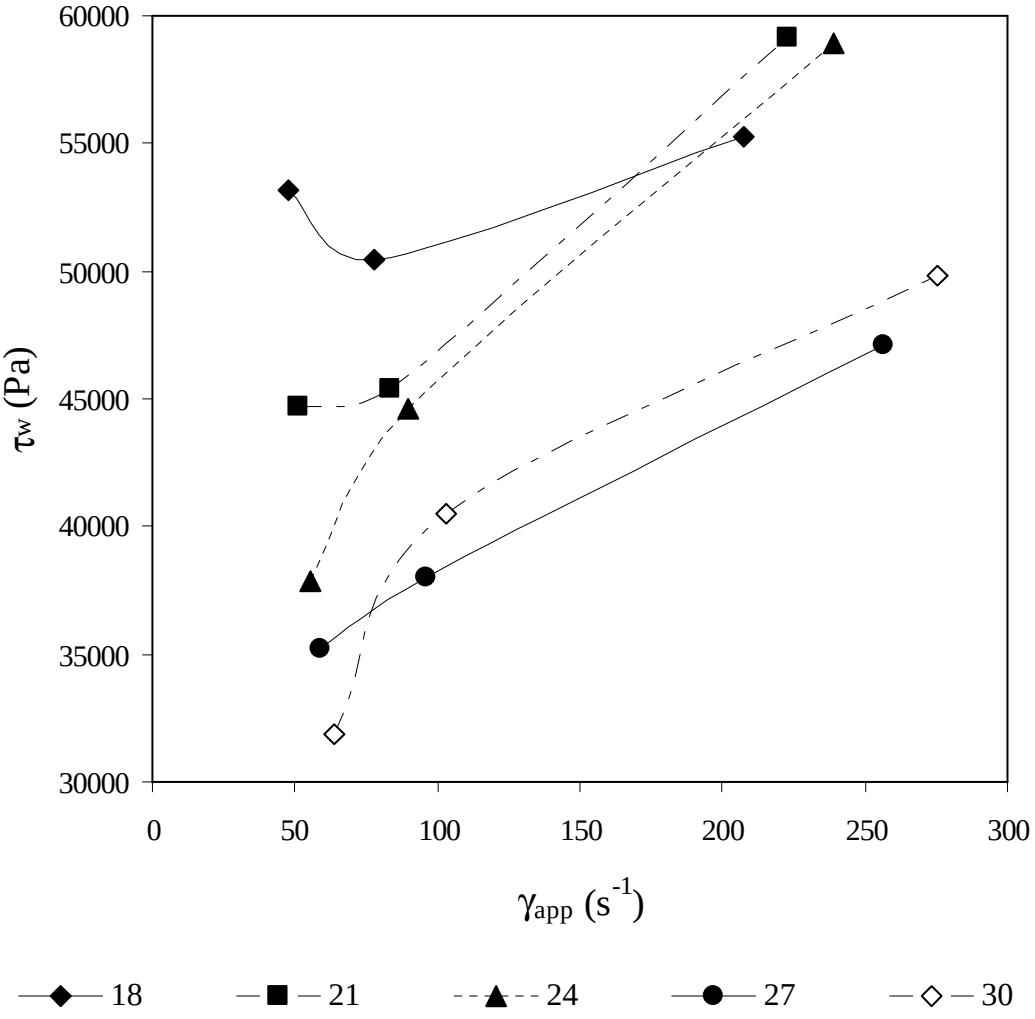

Figure 4.5 Apparent viscosity-shear rate flow behavior from in-line-slit-die experiment of extruded cornstarch at different in-barrel moistures.

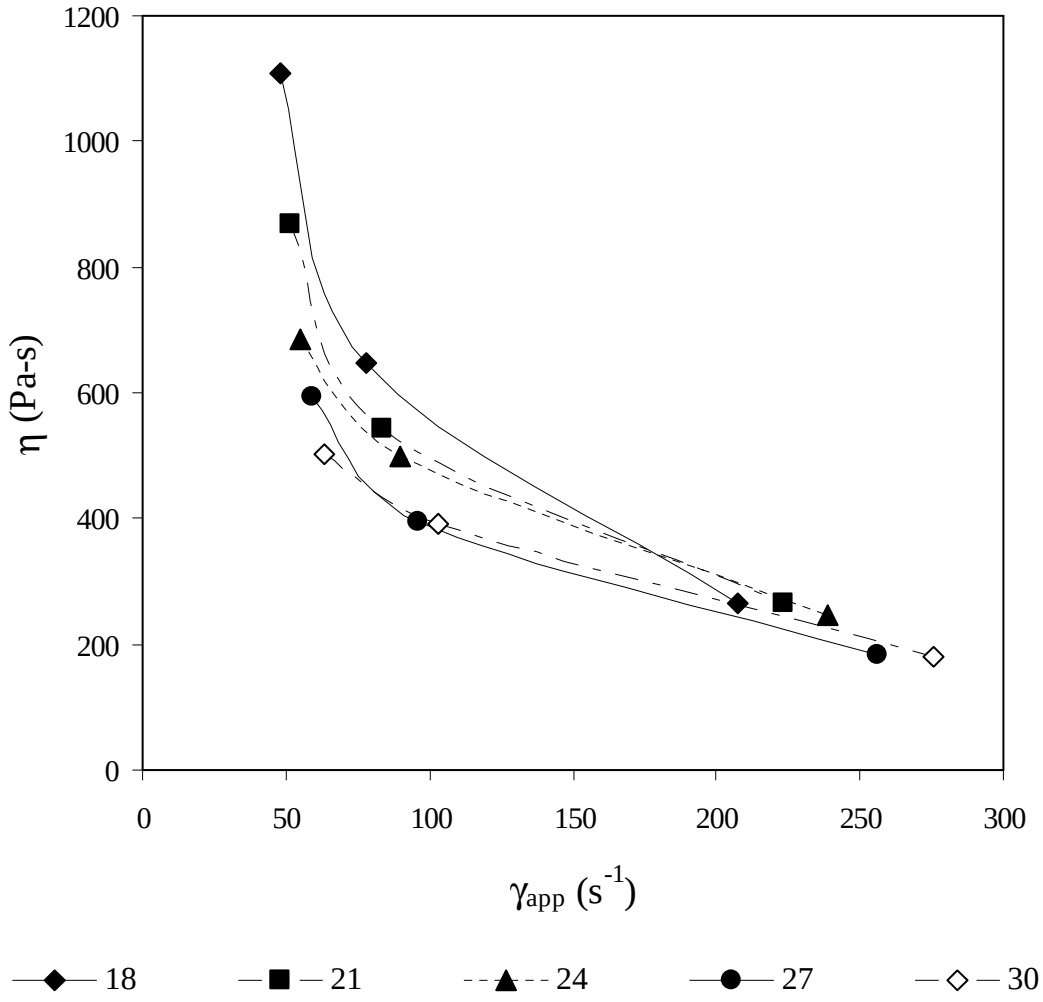

Table 4.1 Die temperature, flow behavior indices, consistency coefficients and apparent viscosities at 275 s^{-1} (maximum shear rate) at different in-barrel moistures.

Moisture Content, x_w	Die Temperature (°C)	Flow Behavior Index, n	Consistency Coefficient, K (Pa-$s^{n-1)}$	Apparent Viscosity, η (Pa-s) at 275 s^{-1} (maximum shear rate)
18	180 ± 2.98^{a}	0.0438 ± 0.0585^{a}	$45{,}700 \pm 20{,}300^{a}$	265 ± 39.4^{a}
21	167 ± 5.40^{b}	0.212 ± 0.0965^{b}	$20{,}400 \pm 12{,}400^{b}$	261 ± 33.4^{a}
24	155 ± 3.57^{c}	0.304 ± 0.0467^{c}	$11{,}600 \pm 4{,}950^{c}$	247 ± 45.3^{a}
27	143 ± 0.33^{d}	0.220 ± 0.152^{b}	$17{,}300 \pm 14{,}900^{c}$	183 ± 28.6^{b}
30	130 ± 3.46^{e}	0.300 ± 0.112^{c}	$10{,}500 \pm 6{,}520^{c}$	185 ± 7.20^{b}
LSD	11.8	0.0614	8,310	19.4

Figure 4.6 Reference viscosity (η_{Tg}) computed using WLF equation at different glass transition temperatures (T_g).

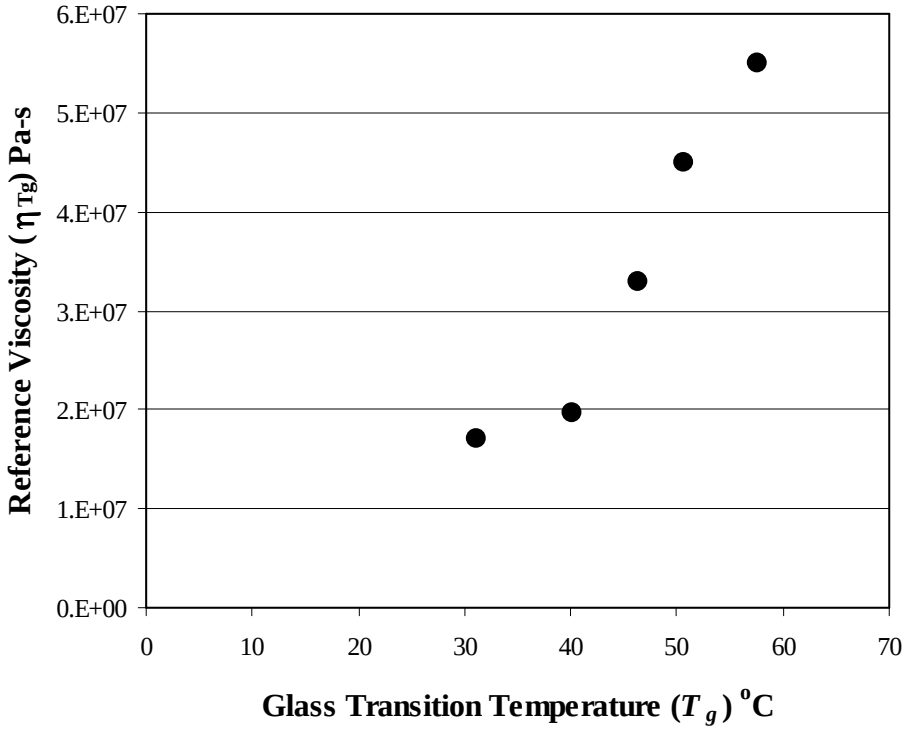

Figure 4.7 Consistency coefficient *K* for different moisture contents: Δ *K* computed using collected data from on-line viscometry and O *K* computed from equation 4.2.